Solution Properties of Polymer Nanostructures Studied by Scattering Techniques

Dissertation

Zur Erlangung des akademischen Grades
eines Doktors der Naturwissenschaften (Dr. rer. nat.)
im Fach Chemie der Fakultät für Biologie, Chemie und Geowissenschaften
der Universität Bayreuth

vorgelegt von
Sreenath Bolisetty
Geboren in Ponugodu, Indien

Bayreuth, 2008

Die vorliegende Arbeit wurde in der Zeit von Oktober 2005 bis November 2008 in Bayreuth am Lehrstuhl Physikalische Chemie I unter Betreuung von Herrn Prof. Dr. Matthias Ballauff angefertigt.

Vollständiger Abdruck der von der Fakultät für Biologie, Chemie und Geowissenschaften der Universität Bayreuth zur Erlangung des akademischen Grades Eines doktors der Naturwissenschaften genehmigten Dissertation.

Dissertation eingereicht am: 23.12.2008

Zulassung durch die Promotionskommission: 14.01.2009

Wissenschaftliches Kolloquium: 06. 05.2009

Amtierender Dekan: Prof. Dr. Axel H. E. Müller

Prüfungsausschuss:

Prof. Dr. Matthias Ballauff (Erstgutachter)

Prof. Dr. Thomas Hellweg (Zweitgutachter)

Prof. Dr. Josef Breu

Prof. Dr. Axel H. E. Müller (Vorsitzender)

.

Table of Contents

Chapter 1 : Introduction **1**

1.1 Cylindrical polymer brushes 2
1.2 Dendronized polymers 4
1.3 Conformational parameters of cylindrical polymer brushes 5
1.4 Microgel 8
1.5 Objective of the thesis 11
1.6 References 12

Chapter 2 : Overview of the Thesis **17**

2.1 Overview 17
2.2 Individual contribution to joint publications 27
2.3 References 29

Chapter 3 : Publications **30**

3.1 Softening of the stiffness of bottle-brush polymers by mutual Interactions 30

3.2 Interaction of the cylindrical bottle brush polymers in dilute and semi dilute solution 35

3.3 Formation of stable mesoglobules by thermosensitive Dendronized polymers 53

3.4 Coupling of rotational motion and shape fluctuations of the microgel with tunable softness 73

Chapter 4 : Summary/Zusammenfassung **94**

List of Publications **97**

Acknowledgement **99**

Erklärung **101**

Chapter 1. Introduction

Nanoscience and technology is the frontier research field since the past decade and rapid developments in nanotechnologies in twenty first century[1] emphasize the miniaturization of the devices into nanometer range and ultimate performance concurrently enhanced.[2,3,4,5] Polymers have naturally been considered as candidates to be used in nanometer scale devices,[6] this close connection added a lot of interest to synthesize[7] and study on nanosized polymer materials[8].

Nanoparticles, nanotubes, and nanoscale films along with nanofabrication technologies will allow for continued advancements in a wide range of applications.[9,10,11,12] In addition nanowires[13] play a vital role in nanodevices[14] for example nano robots,[15] nano electronics,[16] solar cells[17,18] and semiconductors[19,20]. Some nanowires are very good conductors or semiconductors and their miniscule size means that manufactures could fit millions more transistors on a single micro processor. As a result computer speed would increase dramatically. Cylindrical polymer brushes[21] are used as template for the synthesis of these nanowires having magnetic[22] and semi-conducting nanoparticles.[23] The first part of this dissertation will focus on the structural characterization of the cylindrical polymer brushes. Recent developments and advancements of the polymer physics helped to understand in detail the structural characterization of these complex structures.

Polymer brushes are formed when long chain molecules are grafted by one end either to a surface, interface or to another polymer molecule.[24,25] The density of grafting is high enough so that chains stretch away from the attachment much further than the equilibrium size of the free chain. In case when several side chains are densely drafted to a cylindrical backbone, resulting polymer brushes are called as the comb brush polymers or bottle brush polymer.[26] In these kinds of polymer brushes the excluded volume interaction of the side chains are causing the stretching of the main chain to adopt a cylindrical brush structure. Depending on the length, density of the side chains and also the interaction between the side chains causes to attain high stiffness for the cylindrical brushes. These cylindrical polymer brushes have potential application as hydrogels, thermoplastic elastomers, compatibilizers in polymer blends, dispersants and

many more. Another potential application of brush structures relies on their ability to respond to the external stimuli such as pH change,[27] temperature change,[28] light, heat, etc, thereby creating a separate class of materials known as responsive polymer brushes. Due to these specific applications, the tailor made cylindrical brushes have been synthesized by varying the parameters of the type of the main chain, side chains and grafting density using the controlled polymerization techniques.

1.1. Cylindrical Polymer brushes

The cylindrical macromonomer was first successfully synthesized by Tsukahara[29] and coworkers using anionic radical polymerization. These cylindrical polymer brushes consists of oligostyrenes macromonomer processing with methacryloyl end groups. Synthesis and investigation of these comb copolymers having long side chains and high grafting density were reported.[29,30,31,32] Besides these polymerization techniques recently some advanced techniques developed for the synthesis of cylindrical comb polymers. Most cylindrical polymer brushes investigated so far were synthesized by using the "grafting through" method,[33,34] where the macromonomers carrying the polymerizable double bond end groups are grafted together. The selection of the macromonomer and rather stiff, bulky side chains based on Polystyrene (PS), Poly (methyl methacrylate)(PMMA), Poly(2- vinyl peridine) allows us the synthesis of the cylindrical polymer brushes with high and uniform branching density but it have limitation with broad molecular weight distribution.

In addition "grafting onto" technique where the backbone and side chains are prepared separately[35,36] and grafted by using the coupling reaction. The polymer brushes prepared by this technique have the very narrow size distribution, but it has the restriction with the grafting density and efficiency. Other than "grafting to" method there is one more technique of "grafting from",[37,38] in this method a narrowly distributed long backbone is first prepared via living polymerization techniques, followed by functionalization to attach initiating groups to the backbone for the further grafting polymerizations methods.[39,40] With this method well defined cylindrical polymer brushes with the narrow size distribution of the both backbone and side chains

having the high grafting density were prepared. Schematic representation of these three different ways of the cylindrical polymer brushes is shown in figure 1.

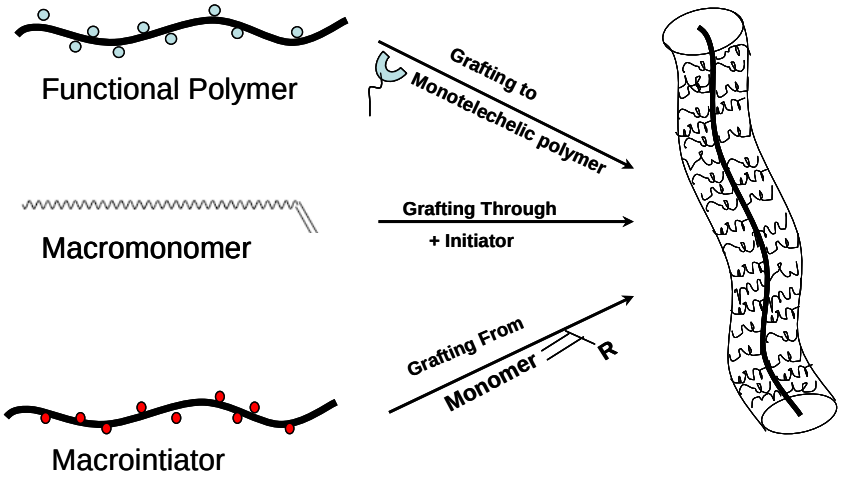

Figure 1. Schematic representation of the synthesis of the cylindrical polymer brushes via three different methods.

The cylindrical polymer brushes examined in this dissertation is composed of a poly(2-hydroxyethyl methacrylate) (poly(HEMA)) backbone grafted with poly(t-butyl acrylate) (PtBu) chains[21]. It has been synthesized using a "grafting from" approach composed of two main steps. First of all, the backbone is prepared by living anionic polymerization of the first monomer which has been silyl protected: 2-(trimethylsilyloxyethyl methacrylate (TMS-HEMA). Then, after deprotection, the pending groups are functionalized in order to obtain the polyinitiator. In an ideal case, at this state, each monomer unit of the backbone must wear a side-group able to initiate the polymerization of the second monomer: t-butyl acrylate (tBu). This last step is here performed by atom-transfer radical polymerization (ATRP) and results in the formation of identical chains which remain attached to the backbone[21]. The polymerizations involved in this synthesis are controlled. Therefore the prepared macromolecule is expected to be well-defined and the polymerization degrees of the backbone and the side chains can be tuned directly by selecting the conditions of reaction. For the studied system, the backbone is composed of about 1600 units and side-chains contain approximately 60 monomer units.

1.2. Dendronized polymers

Depending on the type of the side chains grafting to the backbone resulting the different cylindrical polymer brushes. The side chains of the type homo polymer, block copolymers, hetero side chains resulting to prepare the bottle brush polymer,[41] core shell cylinder[42] and janus structures[43] respectively.

Other than above mentioned cylindrical brushes there are some other cylindrical brushes which are called as dendronized polymers. Dendronized polymers, originally termed 'rod-shaped dendrimers', made their first appearance in a patent filed by Tomalia et al[44] at Dow in 1987. Schlüter et al. had synthesized rod-like polymers with a conjugated backbone first recognized the significance of dendron decoration for the backbone conformation and the overall shape of the obtained macromolecules rendering them shape persistent cylindrical nanoscopic objects[45]. In this context, the term 'dendronized polymers' was coined.

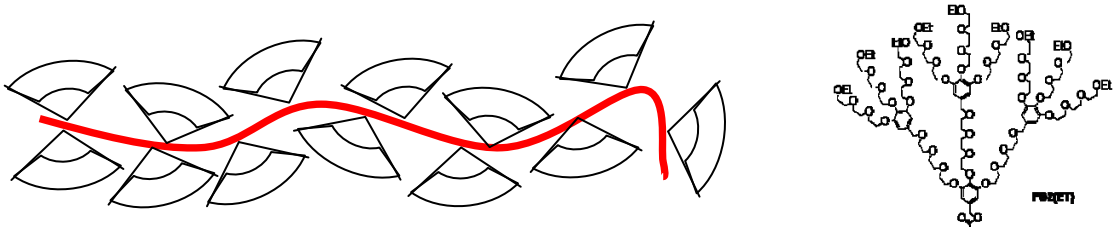

Figure 2. Schematic representation of the second generation dendronized polymers and the chemical structure of second generation of ethoxy-terminated dendronized polymethacrylate

In these polymer brushes the dendrons are grafted to the backbone. i.e the side chains exhibits branching points at which the chain splits up into the several others. This type of dendronized polymer brushes having the single and multiple generation of branching were reported by Schlüter and Rabe.[46]. Figure 2 shows the schematic representation of the second generation dendronized polymer and the chemical structure of the second generation of the etoxy terminated dendronized polymethacrylates. It is obvious, that the number of generations will effect on the overall shape or anisotropy of

the dendronized polymer due to the local motions tend to get hindered with increasing number of generations.

Dendronized polymer properties are fascinating compare to the conventional polymers. The first issue to mention here is their shape and its dependence on the substitution with dendrons. Depending on the dendrons' structure, size, and attachment density along the backbone, conventional polymer backbones such as polyacrylate or polystyrene can attain conformations all the way from random-coil to fully stretched linear: A flexible, cooked spaghetti-like polymer can be converted into a rigid (high bending modulus) rod just by proper substitution with large dendrons. This stiffening of the backbone is caused by steric repulsion between the pendent dendrons. For this reason the whole matter is referred to as shape-control by implementation of steric strain if sequence of dense dendrons grafted to backbone with maximum space then dendronized polymers will attain the shape of cylindrical brushes.

Thermoresponsive polymer have been attained much interest due to their promising applications[47,48] and these polymers collapse above then lower critical solution temperature due to the dehydration of the polymer chains and form the aggregates. Their heating causes to sharp transition where as upon cooling, considerable hystereses are observed. So that great challenges have attained for synthesis of the novel thermoresponsive dendronized polymers having no hystereses at heating and cooling cycles.

1.3. Conformational parameters of cylindrical polymer brushes

The work presented in this dissertation will mainly focus on the solution structure properties of the cylindrical polymer brushes at the different concentration regimes. So far experimental and theoretical studies on the cylindrical polymer brushes have proved that the densely grafted side chains force the main chain into an extended worm like conformation. This conformational effect is caused by the competition of the entropic restoring force on the extended backbone and the repulsive, steric interaction forces between the side chains. The excluded volume interaction of the side chains causes the

stretching of the main chain from its equilibrium conformation to adopt a cylindrical brush structure.

So far, there have been intensive studies on the properties of cylindrical polymer brushes, induced by their peculiar structure, in solution and also in bulk. Most investigations were performed in dilute solutions with emphasis on their molecular shape and dimensions. Cylindrical polymer brushes have certain parameters to define the conformation of the flexible cylindrical chain.[50] Most important defined parameters are contour length (L)[49], radius of cross section (R_{cs}) , end to end distance $<R^2>$ and finally the stiffness of cylindrical polymer brush system traditionally described by the Kuhn length l_K.

In addition to the Kuhn length there is another characteristic length that is often used to describe chain flexibility, the persistence length l_p. This is based on the worm-like chain (WLC) model that considers the chain to be a continuous backbone with a correlation between chain sections that decays exponentially with distance separating them. That is, if we define $<cos\theta(s)>$ as the mean cosine of the angle between the chain segments separated by the length (S), the following relationship holds[50]

$$\langle \cos\theta(s) \rangle = \exp(-\frac{s}{l_p})$$

The constant l_p is the length above which the segment orientations are uncorrelated and it is of the similar magnitude as the Kuhn's length. In fact, for worm like chain with fixed valence angle and free internal rotation, the persistence length and Kuhn's length are related as $l_K = 2\ l_p$

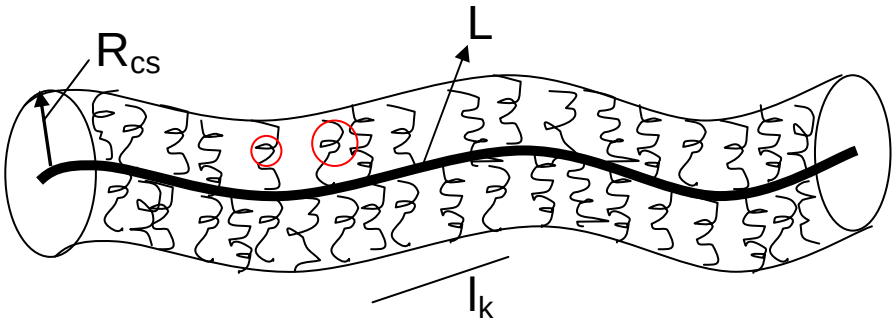

Figure 3. Schematic representation of the flexible cylindrical polymer brush. L is the contour length, l_K is the Kuhn length, R_{cs} is the cross sectional radius.

The cylindrical brushes have certain internal density fluctuations on the small length scale of correlation length ξ (mesh size of entangled polymer network). The correlation length ξ of the density fluctuations defines a spherical volume called "blob"[51]. Below then this correlation length the chains of the cylindrical polymer brushes are self avoiding walk and above the correlation length the chains random walk and the excluded volume interactions have to be considered. The blob contribution from the backbone and side chains to the shape of cylindrical brushes is generally small but the consideration is required for the structural analysis.

The characterization of the cylindrical brushes at the dilute solution concentration was analyzed by using the experimental approaches of the small angle neutron scattering,[52] small angle X-ray scattering and the small angle light scattering.[53] The scattering spectra obtained by these techniques were further analyzed to obtain the form factor[54]. The experimentally obtained form factor were compared with the theoretical modeling and distinguished with the stiff cylinders[55], prolate ellipsoids[56] and flexible cylinders[49]. The form factors of the flexible cylinders were modeled as worm like chain model with the infinite small cross section such as Koyama[57] for the form factor and the models of the Kratky-Porod[58] and Benoit-Doty[49]. By using the MonteCarlo simulation approach Pötschke [59] *et al.* compared the form factor of the wormlike chain described by various theoretical models.[60,61,62,63,64] and concluded that the empirical equations given by Pederson model[64] is the most suitable model for both with and without

excluded volume interactions. The Kholendenko model[63] is also suited to describe the worm like flexible cylindrical model but it does not include the excluded volume interactions[1]. Using these worm like chain models the Kuhn length, the contour length and the radius of cross section are calculated. In addition Nemoto[65] *et al.* discussed the cylindrical brushes diffusion coefficient calculated by dynamic light scattering. They modelled the diffusion coefficient with the prolate ellipsoids where the length of the semi axes are calculated assuming either coiled or fully stretched conformation for the backbone and the side chains.

By combing gel permeation chromatography (GPC) with multi-angle light scattering and viscosity detectors, Schmidt *et al.* reported a structural characterization of cylindrical polymer brushes with fixed side chain length in terms of absolute molar mass, M, the radius of gyration, R_g, and intrinsic viscosity $[\eta]$[66]. Besides the investigations on the solution properties, there are also studies on the bulk state of polymer brushes, about the glass transition and film-forming properties, as well as the presence of liquid-crystalline mesophases resulting from the molecular anisotropy of polymer brushes[67,68,69,70]. Tsukahara *et al.* found that the polymer brushes with PMA main chain and long PS side chains and without any mesogenic groups, formed a mesomorphic phase.[69] The formation of the liquid-crystalline phase indicates that these polymer brushes, possessing large branch number and sufficient branch length, behave as rod-like molecules.

1.4. Microgels

Microgels are cross linked sub-micrometer sized particles made of hydrophilic polymers. In recent years, many investigations of microgels have been carried out.[71,72] Of the many kinds of microgels, one of the most interesting observed is the spherical microgel with a core-shell morphology (the core-shell microgel), because it is composed of two different chemical components and it has the microphase separated structure. Generally, the microgels showed a lot of interesting properties.[73,74,75] Especially, strong dependence has been observed between the swelling behaviour and the diameter of the partic1e. This dependence was usually observed on the microgel without microphase separation.

Microgels can be synthesized by combined polymerization and cross linking, usually in emulsion[76]. They are soluble in water, but have properties different from linear macromolecules of similar molecular weight. Such structures, along with their bigger analogues, microgels have a number of practical applications, mostly in medicine, pharmacy (stimuli-sensitive drug delivery systems), nanocatalysts and water purification systems.

The studied core-shell particles consist of a poly (styrene)-core onto which a thermosensitive shell of poly (N-isopropylacrylamide) (PS-NIPA) has been affixed in a seeded emulsion polymerization. It undergoes completely swollen by the solvent water at the temperature below than the lower critical solution temperature of 32° C and above this temperature the water will be expelled from the shell. The study of coupling, shape fluctuations and rotational motion is extremely interesting with the thermosensitive microgel of poly(N-isopropylacrylamide) (P-NIPA) network[77]. Figure 4 represent the scheme of the thermosenitive core shell microgel system and their response and change in the volume transition with the temperature.

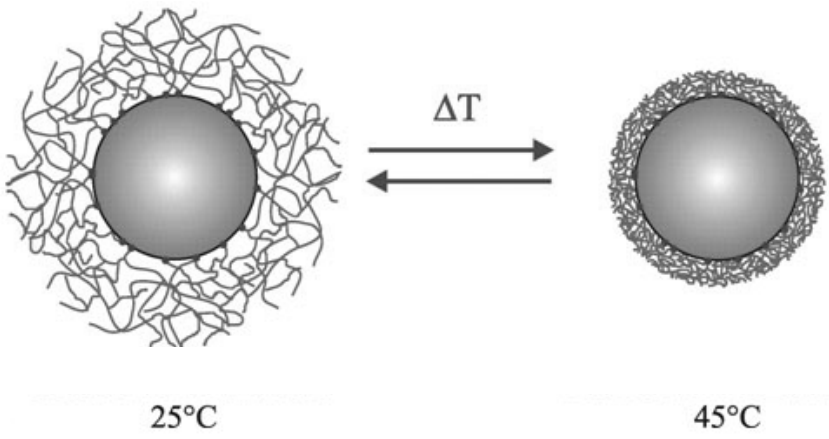

Figure 4. Schematic representation of the thermosensitive core shell microgel system and the change in volume transition at different temperature conditions.

This dissertation focuses on the translational and rotational dynamics of the well defined thermosensitive microgel systems studied by using the polarized and the depolarized dynamic light scattering techniques. The motivation for this study is microgel plays major role in many potential applications.[78,79] Understanding the Brownian motion[80] includes the translational motion, rotational motion and internal

deformation is an important prerequisite to explain the stability of suspensions, their transport mechanism and flow property. These fundamental studies help to solve the application oriented problems for the particles suspensions like pigment dispersion particles (inks, paints), silver bromide grains (photographic films), clays, ceramics and cells. Besides their applications these thermosensitive microgels are very interesting model systems in basic science research [81] with the aim to improve the understanding on the colloidal stability and Brownian dynamics of the shape fluctuation systems.

1.5. Objectives of this thesis

The main aim of this thesis is to understand the solution properties of flexible cylindrical polymer brushes, dendronized polymers and the thermosensitive microgel systems. The work comprises of different polymer nanostructured systems mainly studied by using the scattering techniques at the solution state . The importance of the studying the solution properties of the polymer systems can be related to the solution related applications. In this context the solution properties of the flexible cylindrical brushes and spherical microgels are studied at dilute and semi dilute concentration regime by using scattering techniques. The structure of the cylindrical polymer brushes and understanding the conformational changes of the flexible cylinders with the concentration was especially studied by using the small angle neutron scattering (SANS) and small angle light scattering (SLS). The change in dynamics of the cylindrical polymer brushes at the dilute and semi-dilute concentration regimes was studied by using the dynamic light scattering.

The thermodynamic transition and kinetics of the cylindrical thermosensitive dendronized polymers to fully reversible mesoglobule structure formation at high temperature conditions (above than lower critical solution temperature) was studied by using the dynamic light scattering. The kinetics of the mesoglobule formation is carefully examined by using the time resolved dynamic light scattering measurements.

The aim of this thesis is not only the study of the cylindrical brushes but also to understand the dynamics of the spherical microgel system. The last part of the thesis is focused on the solution dynamics (translational and the rotational dynamics) of the thermosensitive core shell microgel characterized by using the polarized and depolarized dynamic light scattering. In order to understand the shape fluctuations, the coupling phenomenon of the microgel and the influence in the rotational dynamics by embedding the nanoparticles within the thermosensitive shell is studied by the light scattering technique.

1.6. References

[1] Pikna, L.; Stefanova, S. *Transactions of the Universities of Kosice* **2007**, *3*, 27.

[2] Templin, M.; Franck, A.; Du Chesne, A.; Leist, H.; Zhang, Y.; Ulrich, R.; Schädler, V.; Wiesner, U. *Science* **1997**, *278*, 1795.

[3] Alivisatos, A. P. *Science* **1996,** *271*, 933.

[4] Ahmadi, T.; Wang, Z. L.; Green, T. C.; Henglein, A.; El-Sayed, M. A. *Science* **1996,** *272*, 1924.

[5] Weller, H. *Angew.Chem.Int.Ed.Engl.* **1998,** *37*, 1658.

[6] Paul, D. R.; Robeson, L. M. *Polymer* **2008**, *49*, 3187.

[7] Yuan, J.; Xu, Y.; Walther, A.; Bolisetty, S.; Schumacher, M.; Schmalz, H.; Ballauff, M.; Muller, A.H.E.; *Nature materials***, 2008**, *7*, 679.

[8] Wang, G.; Si, L.; Yang, H.; Cai, F.; Wang, Z.; Duan, X. *Journal of Nanoscience and Nanotechnology*, **2005**, *5*, 917.

[9] Fendler, J. H. *Membrane Mimetic Chemistry Approach to Advanced Materials*; Springer-Verlag : Berlin, **1992.**

[10] Lee, J.; Orilall, M. C. Warren, S. C. Kamperman, M. Disalvo, F. J.; Wiesner, U. *Nature Mater.* **2008**, *7*, 222.

[11]. Brinker, C. J.; Lu, Y.; Sellinger, A.; Fan, H. *Adv. Mater.* **1999**, *11*, 579.

[12] Huo, Q.; Margolese, D. I.; Ciesla, U.; Feng, P.; Gier, T. E.; Sieger, P.; Leon, R.; Petroff, P. M.; Schüth, F.; Stucky, G. D. *Nature* **1994**, *368*, 317.

[13] Lauhon, L. J.; Gudiksen, M. S.; Wang, D.; Lieber, C. M. *Nature* **2002**, 420, 57.

[14] Chen, Z. H.; Jie, J. S.; Luo, L. B.; Wang, H.; Lee, C. S.; Lee, S. T. *Nanotechnology*, **2007**, *18*, 345502.

[15] Lee, A. S.; Peteu, S. F.; Ly, J. V.; Requicha, A. A. G.; Thompson, M. E.; Zhou, C. *Nanotechnology,* **2008**, 19, 165501.

[16] Fuhrmann, B.; Leipner, H. S.; Hoeche, H-R.; Schubert, L.; Werner, P.; Goesele, U. *Nano Letters* **2005**, *5*, 2524.

[17] Hu, L.; Chen, G. *Nano Letters* **2007**, *7*, 3249.

[18] Xin, H.; Ren, G.; Kim, F. S.; Jenekhe, S. A. *Chem. Mater.* **2008**, *20*, 6199.

[19] Wang, G.; Gou, X.; Horvat, J.; Park, J. *Journal of Physical Chemistry C*, **2008**, *112*, 15220.

[20] Doh, Y-J; van Dam, J. A.; Roest, A. L.; Bakkers, E. P. A. M.; Kouwenhoven, L. P.; De Franceschi, S. *Science,* **2005**, *309*, 272.

[21] Zhang, M.; Mueller, A. H. E. *J. Poly. Sci., Part A: Poly. Chem.* **2005**, *43*, 3461.

[22] Zhang, M.; Estournes, C,; Bietsch, W.; Mueller, A. H. E. *Adv. Funct. Mat.* **2004,** *14*, 871.

[23] Yuan, J.; Drechsler, M.; Xu, Y.; Zhang, M.; Mueller, A. H. E *Polymer* **2008**, *49*, 1547.

[24] Milner, S. T. Science, **1991**, *251*, 905.

[25] Advincula, R. C.; Brittain, W. J.; Caster, K. C.; Rühe, J., Polymer Brushes. Wiley VCH: Weinheim, **2004.**

[26] Sheiko, S. S.; Sumerlin, B. S.; Matyjaszewski, K. *Prog. Polym. Sci.* **2008,** 33, 759.

[27] Xu, Y.; Bolisetty, S.; Drechsler, M.; Fang, B.; Yuan, J.; Ballauff, M.; Mueller, A. H. E. *Polymer*, **2008**, *49*, 3957.

[28] Li, W.; Zhang, A.; Feldman, K.; Walde, P.; Schlüter, A.D. *Macromolecules*, **2008**, *41*,3659.

[29] Tsukahara, Y.; Mizuno, K.; Segawa, A.; Yamashita, Y. *Macromolecules* **1989**, *22*, 1546.

[30] Tsukahara, Y.; Tsutsumi, K.; Yamashita, Y. *Macromolecules* **1989**, *22*, 2869.

[31] Tsukahara, Y.; Tsutsumi, K.; Yamashita, Y.; Shimada, S. *Macromolecules* **1990**, *23*, 5201.

[32] Tsukahara, Y. in: *Macromolecular design: concept and practice*, M. Misra, ed., Polymer Frontiers International Inc., New York **1993**, pp. 161.

[33] Wintermantel, M.; Gerle, M.; Fischer, K.; Schmidt, M.; Wataoka, I.; Urakawa, H.; Kajiwara, K.; Tsukahara, Y. *Macromolecules* **1996,** *29*, 978.

[34] Dziezok, P.; Sheiko, S. S.; Fischer, K.; Schmidt, M.; Möller, M. *Angew. Chem. Int. Ed.* **1997,** *36*, 2812.

[35] Deffieux, A.; Schappacher, M. *Macromolecules* **1999,** *32*, 1797.

[36] Gao, H.; Matyjaszewski, K. *J. Am. Chem. Soc.* **2007,** *129*, 6633.

[37] Börner, H. G.; Beers, K.; Matyjaszewski, K.; Sheiko, S. S.; Möller, M. *Macromolecules* **2001,** 34, 4375.

[38] Cheng, G.; Böker, A.; Zhang, M.; Krausch, G.; Müller, A. H. E. *Macromolecules,* **2001,** 34, 6883.

[39] Beers, K.; Scott, G.; Mattyjaszewski, K.; Sheiko, S.; Möller, M. *Macromolecules* **1998**, *31*, 9413.

[40] Schappacher, M.; Billaud, C.; Paulo, C.; Deffieux, A. *Macromol. Chem. Phys.* **1999**, *200*, 2377.

[41] Bastardo, L. A.; Iruthayaraj, J.; Lundin, M.; Dedinaite, A.; Vareikis, A.;Makuska, R.; van der Wal, A.; Furo, I.; Garamus, V. M.; Claesson, P. M., *J. Colloid Interface Sci* **2007**, *312*, 21.

[42] Djalali, R.; Hugenberg, N.; Fischer, K.; Schmidt, M. *Macromol.Rapid Commun* **1999**, *20*, 444.

[43] Tsubaki, K.; Kobayashi, H.; Sato, J.; Ishizu, K., *J. colloid and interface Sci.* 2001, 241, 275.

[44] Tomalia D.A.; Kirchhoff, P.M.Rod-shaped dendrimers. 694.Midland, MI, USA: The Dow Chemical Company; 1987. US Patent 4, 694,064.

[45] Freudenberger, R.; Claussen, W.; Schlüter, A.D.; Wallmeier, H. *Polymer* **1994**; *35 ,* 4496.

[46] Schlüter, A. D.; Rabe, J. P. *Angew. Chem. Int.Ed.* **2000**, *39*, 864.

[47] Schmaljohann, D. *Adv. Drug Delivery Rev.* **2006**, *58*, 1655.

[48] Hoffman, A. S.; Stayton, P. S. *Prog. Polym. Sci.* **2007**, *32*, 922.

[49] Benoit, H.; Doty, P. *J. Phys. Chem.* **1953**, *57*, 958.

[50] Grosberg, A.Y.; Khokhlov, A. R.; Statistical Physics of Macromolecules, AIP Press: New York **1994.**

[51] Rathgeber, S.; Pakula, T.; Wilk, A.; Matyjaszewski, K.; Beers, K.L. *J. Chem. Phys.* **2005,** *122*, 124904.

[52] Zhang, B.; Gröhn, F.; Pedersen, J .S.; Fischer, K.; Schmidt, M. *Macromolecules*, **2006,** *39*, 8440.

[53] Rathgeber, S.; Pakula, T.; Wilk, A.; Matyjaszewski, K.; Lee, H.I.; Beers, K.L. *Polymer*, **2006**, *47*, 7318.

[54] Kratky, O., in "Small Angle X-ray Scattering", **1982**, Academic Press.

[55] Guinier, A and Fournet, G., "Small Angle Scattering of X-Rays", Wiley, New York, **1955.**

[56] Wataoka, I.; Urakawa, H.; Kajiwara, K.; Schmidt, M.; Wintermantel, M. *Polym. Int.* **1997**, *44,* 365.

[57] Koyama, R. *J. Phys. Soc. Jpn.* **1974**, *36*, 1409.

[58] Kratky, O.; Porod, G., *Rec. Trav. Chim. Pays.-Bas* **1949**, *68*, 1106.

[59] Pötscke, D.; Hickl, P.; Ballauff, M.; Astrand, P.; Pedersdon; J. *Macromol. Theory Simul*. **2000**, *9*, 345.

[60] Hermans, J.; *J. Phys. Chem* **1958**, 62, 1543.

[61] Cloiseaux J. des, *Macromolecules*, **1973**, 6, 403.

[62] Norisye, T.Murakama , Fujita, *Macromolecules*, **1978**, 11 , 966.

[63] Kolodenko, A. *Macromolecules* , **1993**, 26, 4179.

[64] Pederson, J.; Schrtenburger, P. *Macromolecules*, **1996**, 29, 7602.

[65] Nemoto, N.; Nagai, M.; Koike, A.; Okada, S. *Macromolecules* **1995**, *28*, 3854.

[66] Wintermantel, M.; Schmidt, M.; Tsukahara, Y.; Kajiwara, K.; Kohjiya, S. *Macromol. Rapid Commun.* **1994**, *15*, 279.

[67] Sheiko, S. S.; Gerle, M.; Moller, M. *Langmuir* **1997**, *13*, 5368.

[68] Tsukahara, Y.; Tsutsumi, K.; Okamoto, Y. *Macromol. Chem., Rapid Commun* **1992**, *13*, 409.

[69] Tsukahara, Y.; Ohta, Y.; Senoo, K. *Polymer* **1995**, *36*, 3413.

[70] Namba, S.; Tsukahara, Y.; Kaeriyama, K.; Okamoto, K.; Takahashi, M. *Polymer* **2000**, *41*, 5165.

[71] Kawaguchi, H.; Amagasa, H.; Hagiya, T.; Kimura, N.; Otsuka, Y. *Colloids surface,* **1985** *, 13*, 295.

[72] Furusawa, K.; Kimura, Y.; Tagawa, T. *.J. Colloid Interface sci.,* **1986,** *109*, 69.

[73] Basset, D.R.; Hoy, K. L. *Polymer Colloids, Vol. 2,* Plenum, New York, 1980.

[74] Yamazaki, Kobunshi Ronbunshu, S. *Engl. Ed.,***1980***,* 5,893.

[75] Morgan, L.W. *Ame. Chem. SOC. Div. Org. Coat. Plast. Chem. Pap*. **1981,** *44*, 90.

[76] Makino, K.; Yamanoto, S.; Fujimoto, K.; Kawaguchi, H.; Oshima, H. *J. Colloid Interface Sci.* **1994**, *166*, 251.

[77] Wu, J. Z.; Zhou B.; Hu, Z. B. *Phys. Rev. Lett.* **2003**, *90*, 048304.

[78] Nayak, S.; Lyon, L.A. *Angew. Chem. Int. Ed. Engl.* **2005**, *44*, 7686.

[79] Lu, Y.; Mei, Y.; Ballauff, M.; Drechsler, M. *Angewandte Chemie Int. Ed. Engl.* **2006**, *45*, 813.

[80] Einstein, A. Investigations on the theory of the Brownian movement. Dover, New York, *1956.*

[81] Crassous, J.; Siebenbürger, M.; Ballauff, M.; Drechsler, M.; Hajnal, D.; Henrich, O.; Fuchs, M. *J. Chem. Phys.* **2008**, *128*, 204902.

Chapter 2

2.1 Overview of the thesis

In chapter 3.1 we measured the full formfactor of the cylindrical polymer brushes by the combination of small angle neutron scattering (SANS)[1,2,3] and the static light scattering[4] (SLS) of the cylindrical brushes synthesized by using the "grafting from" route via atom transfer radical polymerization (ATRP) method. The polymer brush consists of poly (tetrabutyl acrylate) side chains, which are grafted to the backbone of the poly (2-hydroxy ethylmethacrylate)[5]. The measured scattering intensities (SANS, SLS) at different polymer concentrations are extrapolated to vanishing concentration were done for all q values. The scattering intensity measured at different techniques of static light scattering and the small angle neutron scattering are normalized with the contrast for calculating the form factor at the wide range of the q-region.

The interpretation of the form factor determined by SANS data we used the empirical equations derived by Pederson and Schurtenberger model[6]. The polymer brushes are not all in same size and have some dissimilarity in sizes so that for modeling the form factor the polydispersity of the cross section is taken into the consideration and it is included using the Schulz-Zimm distribution. In addition to these structural parameters the cylindrical polymer side chains exhibit certain internal density fluctuations (blob scattering) contribute effectively at the large q region. The scattering intensity aroused from these internal density fluctuations was approximated by using the Dozier approach[7].

Comparison of the measured scattering intensity was done with the theoretical model of the Pederson Schurtenberger model for semiflexible polymer chains having the excluded volume interactions. The parameters used for the fit are with the contour length of the 380 nm, persistence length of the 17.5 nm and the radius of cross section of the 5 nm. These fit parameters are comparable with the degree of polymerization and the length of the repeating unit.

The determined structure factors were analyzed by the theoretical approach to understand the interaction between polymer conformations at different concentration of

the solutions. The structure factor at different concentration is calculated by using the determined form factor. The quantitative theoretical approach was done by using the integral equation theory of polymer reference interaction site model (PRISM), which has been already successfully applied to explain the interactions between the polymer species. Figure 5 shows the structure factor determined for the various concentration regimes. The experimental structure factors are compared with the result of integral equation theory of polymer reference interaction site model[8]. For the comparison of the experimental structure factor with the theory we have used the form factor as input.

The dashed lines in figure 5 are the theoretical structure factor calculated with the persistence length of the 17.5 nm. The pronounced deviations from the experimental and the theoretical data were obtained at the concentration above 2.5 g/l and it demonstrates the concentration dependent conformation change was observed. The solid lines represent the modeling of the data with the concentration dependent persistence length of polymer brush. Alternative persistence lengths were used for the solid lines in the figure 5 is as follows at different concentration of the solution. The used persistence lengths for the solid lines at different concentration were as follows (6.45 g/l-13 nm; 14.45 g/l-9 nm; 40.59 g/l- 5 nm). Increase in concentration above 2.5 g/l leads to the decreasing of the persistence length from the 17.5 nm to the 5 nm. It is due to the increase of the concentration leads to the softening of the stiffness of flexible cylindrical brushes[5] due to the excluded volume interaction with the other polymer brushes.

Chapter 3.1 and 3.2 shows the dynamic properties of the polymer brushes are calculated by using the dynamic light scattering and depolarized dynamic light scattering. No contributions from the rotation, bending and stretching to the dynamics have been found. The slow mode and fast modes in translation diffusion were observed at high concentration regime. Moreover at the dilute concentration regime we have determined the hydrodynamic radius of 39 nm calculated from the measured translational diffusion coefficient using the Stokes Einstein relation.

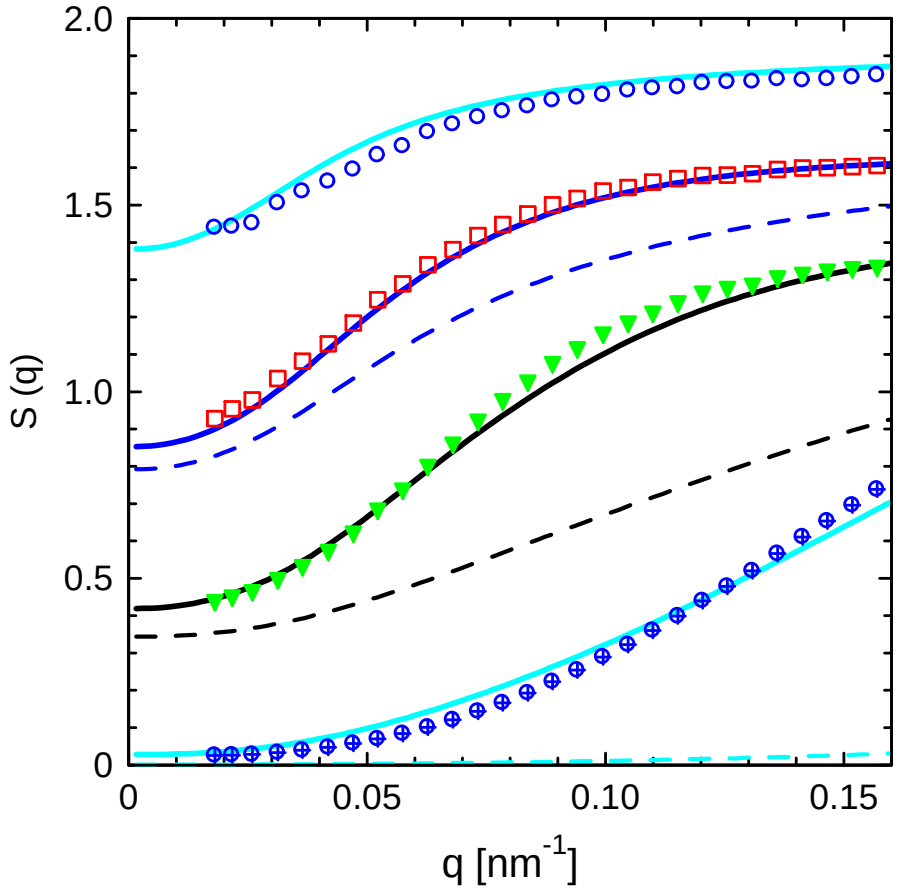

Figure 5. The structure factor S(q) calculated experimentally for four different concentrations of (circles – 2.5 g/l, squares- 6.45 g/l, triangles 14.45 g/l, filled circles 40.59 g/l). The dashed lines represent the structure factors as obtained from the PRISM integral equation theory with the counter length of the 380 nm and persistence length of 17.5 nm). The solid lines represent the structure factors as obtained from the PRISM integral equation theory and using the concentration-dependent persistence lengths.

Kinetics of formation of mesoglobules by thermosensitive dendronized polymers.

Chapter 3.3 shows the thermodynamic transition of the dendrons from coil to globule due to thermosensitive etoxy terminated oligoethyleneoxide (OEO) second generation dendrons[9]. The transition was investigated by using the dynamic light scattering. Also we calculated the kinetics of formation of the mesoglobule with the time and compared with the theoretical models[10,11] .

The change in hydrodynamic radius at different heating and cooling cycles measured with the solution concentration of 0.016 wt-% of the dendronized polymer was shown in figure 4. Initially at the room temperature the particles are having the hydrodynamic radius of the 18 nm. The chains shrink with increase in temperature before reaching the LCST temperature of 35 °C with the small change of the hydrodynamic radius from 18 nm to 16 nm. Further increase of the solution temperature with the rate of 0.1° C/min leads to sudden jump of the hydrodynamic radius from 16 nm to 317 nm. The size of the mesoglobule is constantly increased with increase in temperature till the solution temperature of 40 °C. At all the temperatures the local equilibrium state was found with steady hydrodynamic radius. But after 40 °C further increase in solution temperature lead to shrinkage of the mesoglobule hydrodynamic radius from 600 nm to 450 nm result to form the well defined monodisperse aggregates. Cooling the solution temperature follow on the dissociation of the mesoglobule to the individual chains. Apparently no hysteresis was found. The inset of the figure 7 shows the particles size distribution at different temperature conditions calculated by CONTIN 2DP program. The higher heating rate of 1° C/min also leads to the well defined mesoglobule however size of the mesoglobule is smaller in size compare to the 0.1 °C/min.

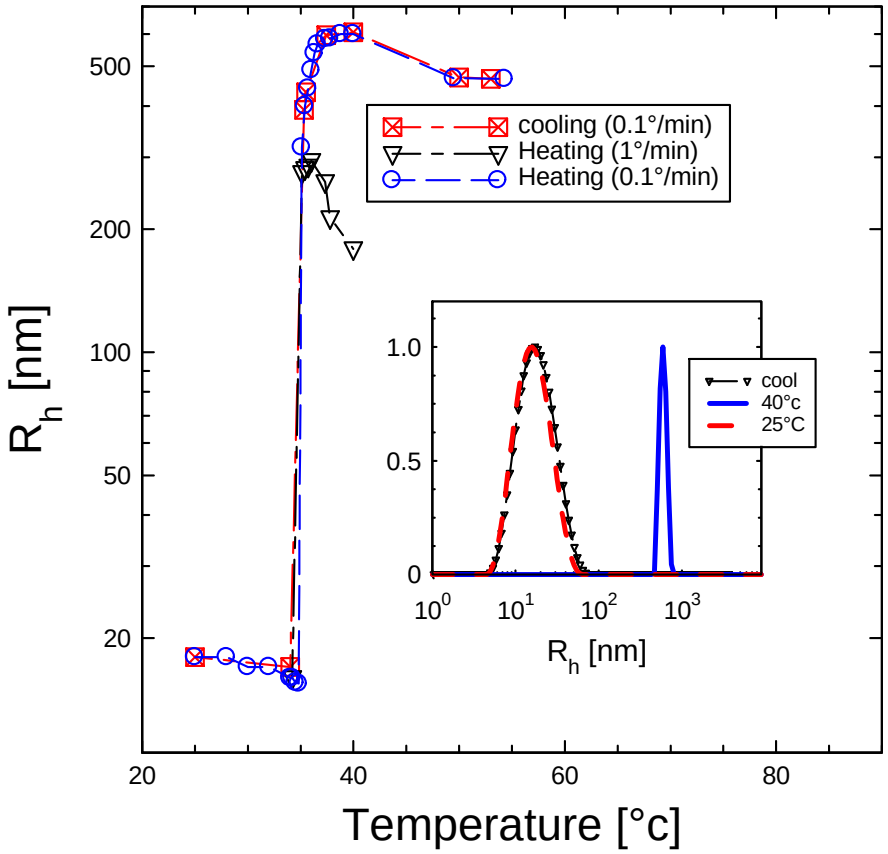

Figure 7. Hydrodynamic radius R_h of the dendronized polymer ***PG2(ET)*** *as a function of temperature. The solution (0.016 wt-%) was heated from 20 °C to the temperature indicated in the graph. Heating and cooling was done using rates of 0.1 °C/min and 1 °C/min, respectively. The inset shows the corresponding particles size distribution at the heating and cooling rate of 0.1 °C/min calculated from CONTIN fits at 25 °C and 40 °C and again at 25 °C after cooling to the respective temperature. Higher concentration leads to the increase of the aggregate size at 40°C. However the size merges to common size of the 500 nm at 50 °C. Also the LCST depends slightly on the solution concentration.*

Further the kinetics of the formation of the mesoglobule investigated by using the time resolved dynamic light scattering measurements. The analysis of the complete coagulation aggregation kinetics was done with the approach followed up by Wagner and coworker[10]. The change of the hydrodynamic radius with time at different temperature above then LCST temperature was measured and normalized with initial hydrodynamic radius. At different temperature conditions reducing the time *t* using the characteristic time for Brownian aggregation t_p as a fit parameter yields a master curve.

For $t/t_p \leq 10$ the early stage single polymer chains begin to merge into clusters. At $10 \leq t/t_p \leq 100$, all data points measured at different temperatures fall onto one master curve. Obviously, the mesoglobule formation can be accurately described by this cluster-cluster aggregation approach in this intermediate stage. The slope is related to the fractal dimension of the aggregates d_f. In our case the slope is compatible with the established value 1.86 for the DLCA. Beyond $t/t_p \geq 100$, however, the growth rate of the aggregates rapidly slows down as the globules become stable. The Brownian aggregation time t_p for the formation of the mesoglobules in this intermediate stage is decreasing with increasing temperature. This clearly indicates that the formation of aggregates at high temperatures is much faster compared to low temperature conditions.

Solution dynamics of thermosensitive microgel

Chapter 3.4 shows the solution dynamics of the thermosensitive microgel and their shape fluctuations studied by using the polarized and depolarized dynamic light scattering.[12,13] The studied microgel consists of polystyrene solid core and the thermosensitive shell of poly(N-isopropylacrylamide) (P-NIPA) with and without palladium nanoparticles[14]. The solution dynamics mainly translational and rotational dynamics are investigated to understand the shape fluctuations of the microgel with and without embedded metal nanoparticles at the different temperature conditions.

With increase in the temperature the thermosensitive shell undergoes volume transition at the temperature of 32 °C resulting to decreasing the hydrodynamic radius[15]. These shape fluctuations of the core shell microgel lead to a significant optical anisotropy to give finite depolarized signal. We found out that embedding the nanoparticles to the microgel network only weakly influences the dynamics of these core shell microgel particles.

The auto correlation function of depolarized dynamic light scattering[16] $g^{(2)}_{VH}(q,t)$ is sum of two discrete exponentially decay functions. Where the slow relaxation mode characterizes the translational diffusion coefficient and the faster relaxation is correspond to the rotational diffusion and shape fluctuations. Whereas for the polarized dynamic light scattering autocorrelation function have the slow mode single exponential

decay. The corresponding translational (D_T) and rotational diffusion (D_R) coefficient of the spherical particles given by

$$D_T(a) = \frac{K_B T}{\eta} \frac{1}{6\pi a}$$
$$D_R(a,\alpha) = \frac{K_B T}{\eta} \frac{1}{8\pi a^3} \alpha \qquad (7)$$

Where T is the temperature, K_B is the Boltzmann constant, a is the particle hydrodynamic radius, η is the viscosity and α =1 for the hard sphere.

At the temperature above than the 45 °C the shell is completely collapsed and the microgel behaves like as hard sphere. Depolarized dynamic light scattering (DDLS)[17] measurements given very good photon counts (I_{VH}) and also results the good intensity auto correlation. From the determined translational diffusion coefficient and rotational diffusion coefficient the hydrodynamic radius is calculated with α=1. The full agreement between the experimental and the theoretical approach was obtained with the hydrodynamic radius of 78 nm. But at the room temperature conditions of 25 °C the shell is completely swollen and it is not perfect hard sphere and the additional dynamics results from the shape fluctuations. In figure 8 shows the depolarized dynamic light scattering intensity (I_{VH}) autocorrelation function as the function of time at the temperature of 25 °C. The corresponding auto correlation function was analyzed by using CONTIN regularization algorithms to determine the decay time.

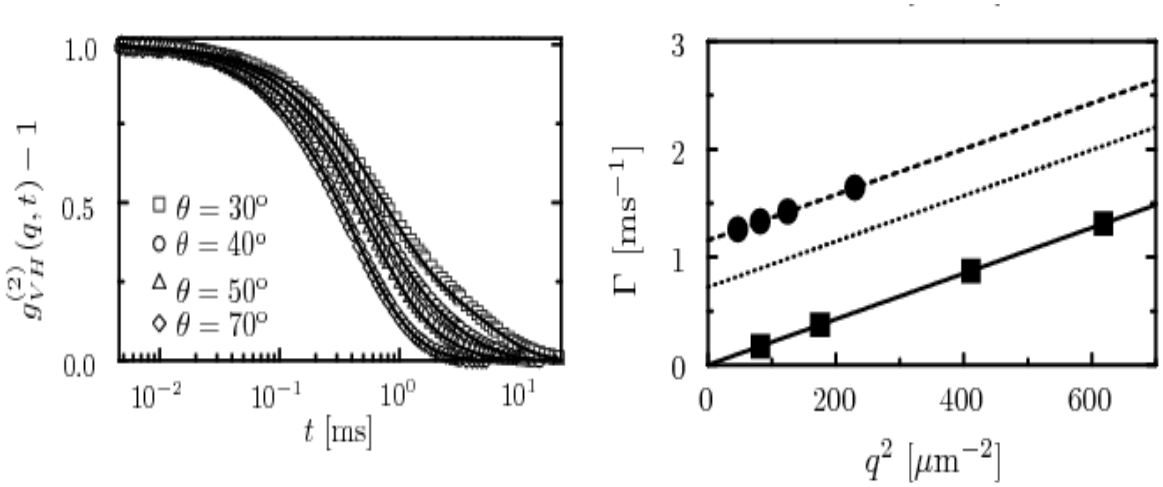

Figure 8. Intensity autocorrelation functions obtained by DDLS for the microgel having Pd nanoparticles at 30°(O) to 60°(Δ) at 25 °C. And the corresponding distribution function analyzed by using CONTIN fit. For the sake of clarity only two autocorrelations are displayed.

At room temperature the DDLS intensity correlation functions fit well only at α=1.6 with the hydrodynamic radius of the 115 nm. The pronounced deviations from the theoretical model of the fast mode (dotted line) with α =1 is clearly visible in fig 8b. This clearly indicates that swollen microgel at 25 °C exhibit the additional dynamics resulting from the shape fluctuations. The value of α (deviations from hard sphere model) was increasing with decreasing the temperature. At the 15 °C the value of the α parameter is of 2.5 with the hydrodynamic radius of the 128 nm and rotational diffusion coefficient of 168 s^{-1}. It clearly explains the interplay between the shape fluctuations and rotational motion of the deformable objects which profoundly affects their dynamics.

The following publications and manuscripts are enclosed in this Ph.D. thesis:

- **"Softening of the Bottle brush polymers by mutual Interaction"**
  Bolisetty, S.; Airaud, C.; Xu, Y.; Müller, A.H.E.; Harnau, L.; Rosenfeldt, S.; Lindner, P.; Ballauff, M.; ***Phys. Rev. E.,*** 2007, *75*, 040803.

- **"Interaction of the Cylindrical Bottlebrush polymers in dilute and semidilute solution"**
  Bolisetty, S.; Rosenfeldt, S.; Rochette, C.; Harnau, L ; Lindner, P.; Xu, Y.; Müller, A.H.E.; Ballauff, M.: has been accepted at ***Colloid and Polymer science,*** **2009,** *287*, 129

- **"Formation of the stable Mesoglobules by thermosensitive Dendronized polymers"**
  Bolisetty, S.; Schneider, C.; Zhang, A.; Li, W.; Schlüter, D.; Ballauff, M.;
  Written in the form of a manuscript and to be submitted under this title

- **"Coupling of the rotational motion and the shape fluctuations of the tunable core-shell microgels"**
  Bolisetty, S.; Hoffmann, M.; Hellweg, T.; Harnau, L.; Ballauff, M. has been accepted ***Macromolecules, 2009,*** *42,* 1264 .

The following publications have been additionally published within the scope of my Ph.D. thesis:

- **"Manipulating cylindrical polyelectrolyte brushes on the nanoscale by counterions Collapse transition to helical structures"**
  Xu, Y.; Bolisetty, S.; Dreschler, M.; Yuan, J.; Ballauff, M.; Müller, A.H.E.; **Softmatter**, 2009, *5*, 379.

- **"Water-Soluble Organo-Silica Hybrid nanowires"**
  Yuan, J.; Xu, Y.; Walther, A.; Bolisetty, S.; Schumacher, M.; Schmalz, H.; Ballauff, M.; Muller, A.H.E.; **Nature materials,** 2008, *7*, 679

- **"pH and Salt Responsive Poly(N,N-dimethylaminoethyl methacrylate) Cylindrical Brushes and their Quaternized Derivatives "**
  Xu, Y.; Bolisetty, S.; Dreschler, M.; Yuan, J.; Ballauff, M.; Müller, A.H.E,; **Polymer**, 2008, *49*, 3957.

- **"Double Grafted Cylindrical Brushes: Synthesis and Characterization of Poly(lauryl methacrylate) Brushes "**
  Xu, Y;Becker, H; Yuan, J; Burkhardt, M; Zhang, Y; Walther, A; Bolisetty, S; Ballauff, M; Müller, AHE,: **Macromol. Chem. Phys.,** 2007, 208, 1666.

- **"Interparticle spacing for the surface modified gold nanoparticle aggregates"**
  Basu, S.; Pande, S.; Jana, S.; Bolisetty, S. ; Pal, T. ; **Langmuir** , 2008**,** *24***,** 5562**.**

- **"Switching the Morphologies of cylindrical Polycataion brushes by Ionic and Supramolecular Inclusion Complexs"**
  Xu, Y.; Bolisetty, S.; Ballauff, M.; Müller, A.H.E.; Submitted to **J. Am. Chem. Soc.,2009,** *131***, 1640**

- **"Salt –induced Aggregation of Polyelectrolyte-amphiphilic Dendron Complexes in THF Solutions"**
  Zhang, X.; Bolisetty, S.; Wang, Y.; Lu, Y.; Ballauff, M.; Wang. W.; Accepted **Langmuir** 2009, *25*, 2075.

2.2 Individual Contribution to Joint Publications

The publications/manuscripts, which are presented in the dissertation, were obtained in cooperation with other co-workers in different departments. My contributions to each publication are specified below.

Chapter 3.1.

This work has been published with the title **"Softening of the Bottle brush polymers by mutual Interaction"**by Bolisetty, S.; Airaud, C.; Xu, Y.; Müller, A.H.E.; Harnau, L.; Rosenfeldt, S.; Lindner, P.; Ballauff, M.; in *Phys. Rev. E***.,** (2007), *75*, 040803.

- I have performed all the scattering experiments (SLS, DLS, SANS, SAXS) and analysis of the formfactor and structure factor characterization.
- Youyong Xu from Macromolecular Chemistry II, synthesized TBA bottle brush.
- Dr. Ludger Harnau performed the theoretical analysis of the structure factors by using PRISM model.
- Airaud Cedric and Dr. Sabine Rosenfeldt helped me for the interpretation of scattering data.
- Prof. Matthias Ballauff and Prof. Axel H. E. Mueller contributed to the discussion.

Chapter 3.2.

This work with the title "**Interaction of the Cylindrical Bottlebrush polymers in dilute and semidilute solution**" by Bolisetty, S.; Rosenfeldt, S.; Rochette, C.; Harnau, L ; Lindner, P.; Xu, Y.; Müller, A.H.E.; Ballauff, M.: has been accepted ***Colloid and Polymer science*** (DOI: 10.1007/s00396-008-1962-3)

- I have performed all the scattering experiments (SLS, DLS, SANS, SAXS) and analysis of the scattering data.
- Youyong Xu from Macromolecular Chemistry II, synthesized TBA bottle brush.
- Dr. Ludger Harnau performed the theoretical analysis of the structure factors by using PRISM model.
- Christope Rochette and Dr. Sabine Rosenfeldt helped me for the interpretation of scattering data.

- Prof. Matthias Ballauff and Prof. Axel H. E. Mueller contributed to the discussion.

Chapter 3.3.

This work with the title "**Formation of the stable Mesoglobules by thermosensitive Dendronized polymers**" by Bolisetty, S.; Schneider, C.; Zhang, A.; Li, W.; Schlüter, D.; Ballauff, M: to be submitted

- I have performed all the dynamic light scattering measurements and kinetic measurements.
- Dr. Afang Zhang from ETH, Zurich synthesized dendronized polymer brush.
- Christian Schneider helped me for interpretation of the kinetic measurement data.
- Prof. Matthias Ballauff and Prof. Dieter Schlüter contributed to the discussion

Chapter 3.4.

This work with the title "**Coupling of the rotational motion and the shape fluctuations of the tunable core-shell microgels"** by Bolisetty, S.; Hoffmann, M.; Hellweg, T.; Harnau, L.; Ballauff, M. ***Macromolecules,* 2009,** *42***, 1264.**

- I have performed all the depolarized and polarized dynamic light scattering measurements.
- Dr. Ludger Harnau performed the theoretical analysis of the light scattering autocorrelation functions
- Prof. Matthias Ballauff, Martin Hoffmann and Prof. Thomas Hellweg contributed to the discussion.

References

[1] Wataoka, I.; Urakawa, H.; Kajiwara, K.; Schmidt, M.; Wintermantel, M. *Polymer* **1997,** *44*, 365

[2] Rathgeber, S.; Pakula, T.; Wilk, A.; Matyjaszewski, K.; Beers, K.L. *J. Chem. Phys.* **2005,** *122*, 124904.

[3] Zhang, B.; Gröhn, F.; Pedersen, J. S.; Fischer, K.; Schmidt, M. *Macromolecules* **2006**, *39*, 8440.

[4] Rathgeber, S.; Pakula, T.; Wilk, A.; Matyjaszewski, K.; Lee, H.I.; Beers, K.L. *Polymer,* **2006,** *47*, 7318.

[5] Bolisetty, S.; Airaud, C.; Xu, Y.; Müller ,A.H.E.; Harnau, L.; Rosenfeldt, S.; Lindner, P.; Ballauff, M. *Phys. Rev. E*. **2007**, *75*, 040803.

[6] Pederson, J.; Schrtenburger, P.; Macromolecules, 1996, 29, 7602.

[7] Dozier, W.; Huang, J.; Fetters,,L.: Macromolecules, 1991, 24, 2810 .

[8] Bolisetty, S.; Rosenfeldt, S.; Rochette, C.N.; Harnau, L.; Lindner, P.; Xu, Y.; Müller,A.H.E.;; Ballauff, M. *Coll. Poly. Sci.* **2008** ((DOI: 10.1007/s00396-008-1962-3).

[9] Li, W.; Zhang, A.; Feldman, K.; Walde, P.; Schlüter, A.D. *Macromolecules*, **2008**, *41*,3659.

[10] Hanus, L. H.; Hartzler, R. U.; Wagner, N. J. *Langmuir* **2001**, *17*, 3136.

[11] Lin, M. Y.; Lindsay, H. M.; Weitz, D. A.; Ball, R. C.; Klein, R.; Meakin, P. *Nature* **1989**, *339*, 360.

[12] Berne, B.; Pecora, R. Dynamic Light Scattering, Wiley: New York, **1976**.

[13] Koenderink, G. H.; Philipse, A. P. Langmuir **2000**, *16*, 5631.

[14] Mei, Y.; Lu, Y.; Polzer, F.; Ballauff, M.; Drechsler, M. *Chem. Mater.* **2007**, *19*, 1062.
[15] Crassous, J.; Ballauff, M.; Drechsler, M.; Schmidt, J.; Talmon, Y. *Langmuir* **2006**, *22*, 2403.

[16] Pecora R. *J. Chem. Phys.* **1968**, *49*, 1036.

[17] Schmitz, K. S. An Introduction to Dynamic Light Scattering by Macromolecules, Academic Press: London, **1990**.

Chapter 3. Publications

Chapter 3.1

Softening of the stiffness of the bottle brush polymers by mutual interaction

Sreenath Bolisetty [a)], Cédric Airaud [a)] ,Youyong Xu [b),] Ludger Harnau [c)], Sabine Rosenfeldt [a)], Peter Lindner [d)],, Axel H. E. Müller [b)], Matthias Ballauff [a),]*

[a)]Physikalische Chemie I, University of Bayreuth, 95440 Bayreuth, Germany

[b)]Makromolekulare Chemie II, University of Bayreuth, 95440 Bayreuth, Germany

[c)] Max-Planck-Institut für Metallforschung, Heisenbergstrasse 3, 70569 Stuttgart, Germany, and Institut für Theoretische und Angewandte Physik, Universität Stuttgart, Pfaffenwaldring 57, 70569 Stuttgart, Germany

[d)] Institut Laue-Langevin, Grenoble Cedex, France

Published in *Physical review E.* 2007, *75*, 040803.

PHYSICAL REVIEW E **75**, 040803(R) (2007)

Softening of the stiffness of bottle-brush polymers by mutual interaction

S. Bolisetty,[1] C. Airaud,[1] Y. Xu,[2] A. H. E. Müller,[2] L. Harnau,[3] S. Rosenfeldt,[1] P. Lindner,[4] and M. Ballauff[1,*]

[1]*Physikalische Chemie I, University of Bayreuth, D-95440 Bayreuth, Germany*

[2]*Makromolekulare Chemie II, University of Bayreuth, D-95440 Bayreuth, Germany*

[3]*Max-Planck-Institut für Metallforschung, Heisenbergstraße 3, D-70569 Stuttgart, Germany and Institut für Theoretische und Angewandte Physik, Universität Stuttgart, Pfaffenwaldring 57, D-70569 Stuttgart, Germany*

[4]*Institut Laue-Langevin, B. P. 156X, 38042 Grenoble CEDEX 9, France*

(Received 21 December 2006; published 30 April 2007)

We study bottle-brush macromolecules in a good solvent by small-angle neutron scattering (SANS), static light scattering (SLS), and dynamic light scattering (DLS). These polymers consist of a linear backbone to which long side chains are chemically grafted. The backbone contains about 1600 monomer units (weight average) and every second monomer unit carries side chains with approximately 60 monomer units. The SLS and SANS data extrapolated to infinite dilution lead to the form factor of the polymer that can be described in terms of a wormlike chain with a contour length of 380 nm and a persistence length of 17.5 nm. An analysis of the DLS data confirms these model parameters. The scattering intensities taken at finite concentration can be modeled using the polymer reference interaction site model. It reveals a softening of the bottle-brush polymers caused by their mutual interaction. We demonstrate that the persistence decreases from 17.5 nm down to 5 nm upon increasing the concentration from dilute solution to the highest concentration (40.59 g/l) under consideration. The observed softening of the chains is comparable to the theoretically predicted decrease of the electrostatic persistence length of linear polyelectrolyte chains at finite concentrations.

DOI: 10.1103/PhysRevE.75.040803 PACS number(s): 61.25.Hq, 61.12.−q, 61.41.+e

If polymeric side chains are grafted to a flexible or rigid polymer backbone, a cylindrical bottle-brush polymer results [1–7]. The main feature of these polymers is a marked stiffening of the main chains (see, e.g., the discussion in Refs. [5–7]). It has been demonstrated theoretically and by computer simulations that this stiffening is due to a balance of the repulsive forces originating from a steric overcrowding of the side chains and the entropic restoring force of the main chain [8]. The analysis of bottle-brush polymers by small-angle neutron scattering (SANS), small-angle x-ray scattering (SAXS), and static light scattering (SLS) in dilute solution has supported this picture by showing that these macromolecules exhibit a wormlike conformation [5–7]. However, up to now most studies on bottle-brush polymers in solution have focused on the dilute regime and *conformational ideality* has been assumed. That is, the intramolecular pair correlations are presumed to be independent of polymer concentration and can be computed based on a chain model that only accounts for intramolecular interactions between monomers. However, this assumption can fail upon increasing the polymer concentration because the polymers begin to interpenetrate leading to a medium-induced interaction between two monomers of individual polymers. As a result the persistence length is expected to decrease with increasing polymer concentration in the semidilute solution regime. Such concentration-dependent conformational changes of chain molecules have been investigated theoretically for semidilute solutions of bottle-brush polymers [9], dense polymer solutions and melts (see, e.g., [10–14]), and semiflexible chain polyelectrolyte solutions (see, e.g., [15–21]). Here we present a systematic experimental and theoretical study of concentration-dependent conformational changes of bottle-brush polymers which elucidates the importance of the medium-induced interaction on soft materials such as polymers. We demonstrate that mutual interaction between the bottle-brush polymers leads to a significant reduction of their stiffness in solution.

Figure 1 displays the repeating unit of the polymer under consideration. This polymer has been synthesized by a "grafting form" method and composed of poly(2-hydroxyethylmethacrylate) backbone grafted with poly(*t*-butyl acrylate) chains. Details of the synthesis and the characterization have been reported in Ref. [22]. SANS measurements of dilute solutions of the bottle-brush polymer in deuterated tetrahydrofurane (THF) were performed at the beamline D11 of the Institut Laue-Langevin in Grenoble, France. The incoherent contribution to the measured intensities has been determined at the highest scattering angles and subtracted in order to obtain the coherent part. In all cases absolute intensities have been obtained. Details of the data evaluation may be found in Refs. [23,24].

Without loss of generality, the measured scattering intensity $I(q,\phi)$ as a function of the magnitude of the scattering vector $q=|\vec{q}|$ and the volume fraction of the solute ϕ can be rendered as the product of a form factor $P(q)$ and a structure factor $S(q,\phi)$ according to

$$I(q,\phi) = \phi(\Delta\rho)^2 V_p P(q) S(q,\phi), \tag{1}$$

where V_p is the volume of the solute per particle and $\Delta\rho = \bar{\rho} - \rho_m$ is the contrast of the solute resulting from the difference of the average scattering length density $\bar{\rho}$ and the scat-

*Electronic address: Matthias.Ballauff@uni-bayreuth.de; harnau@fluids.mpi-stuttgart.mpg.de

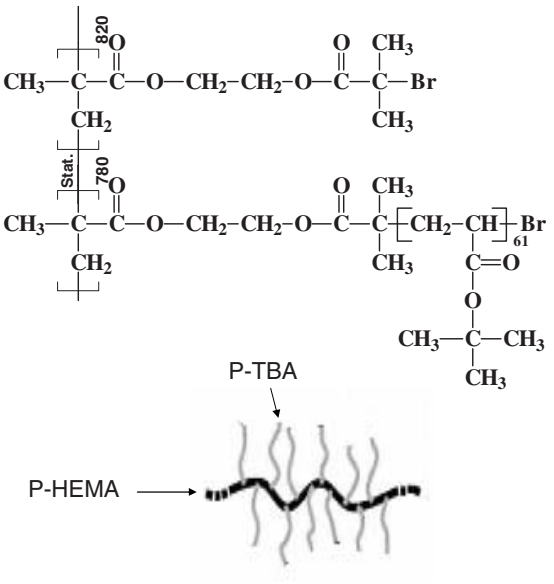

FIG. 1. Chemical structure of the investigated bottle-brush polymer consisting of a poly(2-hydroxyethylmethacrylate) (*p*-HEMA) backbone and poly(*t*-butyl acrylate) (*p*-TBA) side chains. The repeating units carrying the side chains alternate statistically with unsubstituted repeating units. The average number of repeating units per side chain is 61.

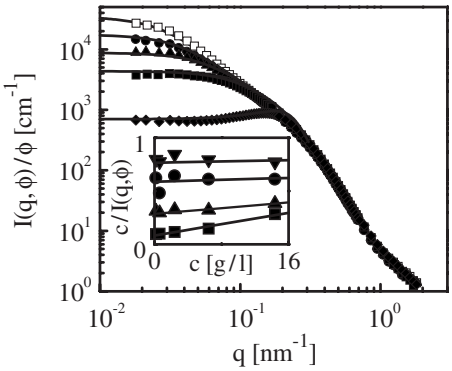

FIG. 2. Absolute scattering intensities $I(q,\phi)$ of bottle-brush polymer solutions normalized to their volume fraction ϕ. The open squares and the upper line represent the intensity extrapolated to vanishing concentration and the calculated form factor of a wormlike chain, respectively. The solid symbols denote the measured intensities for four bottle-brush polymer concentrations (circles, $c=2.40$ g/l; triangles, $c=6.45$ g/l; squares, $c=14.35$ g/l; diamonds, $c=40.59$ g/l). The four lower lines represent the corresponding intensities as obtained from the polymer reference interaction site model (PRISM) integral equation theory [Eqs. (3) and (4)] and taking into account the softening of the bottle-brush polymers [see Figs. 3(a) and 3(b)]. The inset shows the extrapolation of the measured intensities to vanishing concentration according to Eqs. (1) and (2) for four scattering vectors: down triangles, $q=0.15$ nm^{-1}; circles, $q=0.12$ nm^{-1}; up triangles, $q=0.08$ nm^{-1}; squares, $q=0.04$ nm^{-1}.

tering length density ρ_m of the solvent (see Refs. [23,24] and further citations given there). From these definitions the volume fraction ϕ follows as $\phi=c\bar{v}$, where c is the weight concentration of the dissolved polymer and $\bar{v}$ is its specific volume in the respective solvent. The latter quantity can be obtained precisely from density measurements of dilute solutions ($\bar{v}=1.10\pm0.02$ cm^3/g). These data also serve for the calculation of $\Delta\rho=-5.67\times10^{10}$ cm^{-2}. Figure 2 displays SANS data obtained for various concentrations of the bottle-brush polymer dissolved in deuterated tetrahydrofurane. Additional investigations were done by static light scattering in order to explore the region of smaller q values. These data have been used to obtain the molecular weight of the bottle-brush polymer.

For sufficiently small volume fractions ϕ, the structure factor $S(q,\phi)$ can be expanded according to [24]

$$1/S(q,\phi) = 1 + 2B_{app}\phi + O(\phi^2), \tag{2}$$

where B_{app} is the apparent second virial coefficient. Hence Eq. (2) suggests to plot $\phi/I(q,\phi)$ vs ϕ for all q values under consideration. The inset of Fig. 2 displays such a plot using the concentration c instead of the volume fraction ϕ. Straight lines are obtained allowing us to extrapolate the measured intensity to vanishing concentration. The open squares in Fig. 2 show the data obtained from this extrapolation together with the form factor obtained from the Pedersen-Schurtenberger model 3 [25] which includes the effect of excluded volume (see also the discussion of this problem in Ref. [7]). The scattering intensity extrapolated to vanishing concentration is well described by the model of the wormlike chain. We obtain the contour length $L=380$ nm and the persistence length $l_p=17.5$ nm. The radius of cross section of the chains follows as 5 nm. Static light scattering leads to a weight-average molecular weight of 7.41×10^6 g/mol. Together with the weight-average degree of polymerization determined from the precursor polymer a molecular weight $M_0=4600$ g/mol of the repeating unit results. Assuming a length of the repeating unit of 0.25 nm this would lead to a mass per unit length M_L of 18.400 g/mol/nm. Estimates of M_L using the Holtzer plot (see, e.g., Ref. [7] and further literature given there) lead to a value of approximately 19.000 g/mol/nm. Hence the length of the repeating unit is approximately 0.24 nm which is slightly smaller than the calculated value of 0.25 nm. A similar finding was reported recently by Zhang and co-workers [7]. Moreover, we have determined the contribution to the scattering intensity due to thermal fluctuations of the side chains.

We now turn our attention to the analysis of the scattering intensities taken at finite concentration. The form factor $P(q)$ determined by extrapolating $I(q,\phi)$ to vanishing concentration is used to calculate $S(q,\phi)$ according to Eq. (1). Figure 3(a) displays the experimental data obtained for four different concentrations. A quantitative understanding of correlations and interactions between various colloidal and polymeric species can be achieved using the well-established techniques of liquid-state theory. The polymer reference interaction site model (PRISM) integral equation theory has been successfully applied to various systems, such as rodlike viruses [26], platelike colloids [27] and dendrimers [23], flexible polymers [28], and mixtures of spherical colloids and semiflexible polymers [29]. Within the PRISM theory the structure factor $S(q,\phi)$ reads

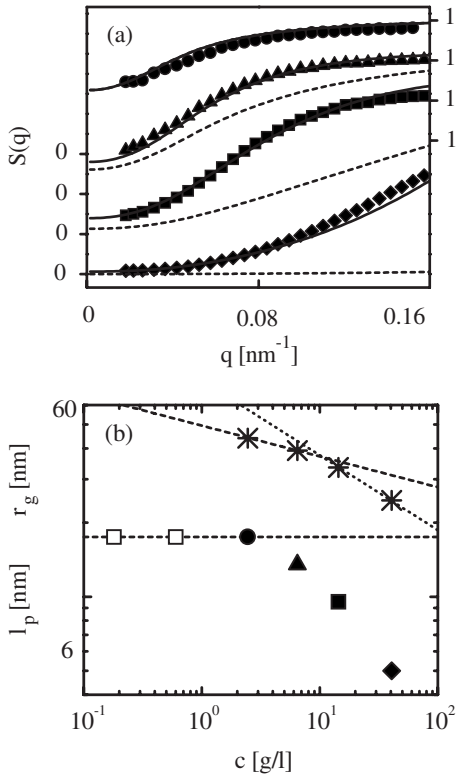

FIG. 3. (a) The structure factor $S(q,\phi)$ determined experimentally according to Eq. (1) for four concentrations (with the same symbol code as in Fig. 2). The dashed lines represent the structure factors as obtained from the PRISM integral equation theory [Eqs. (3) and (4)] and assuming a *concentration-independent* shape of the bottle-brush polymers. The solid lines represent the structure factors as obtained from the PRISM integral equation theory and using the *concentration-dependent* persistence lengths shown in (b) with the same symbol code (solid circle, triangle, square, and diamond). For reasons of clarity, the upper three data sets in (a) have been shifted up. For $c=2.40$ g/l the dashed and solid curve coincide because the same persistence is used for both curves. The open squares in (b) denote two low concentrations which have been used for the extrapolation to infinite dilution as mentioned above. The radii of gyration as obtained from Eq. (5) are indicated in (b) by the stars. The upper dashed and dotted lines of slopes $c^{-1/8}$ and $c^{-17/56}$, respectively, represent two asymptotic scaling regimes [9].

$$S(q,\phi) = 1 + \phi h(q,\phi)/(V_p P(q,\phi)), \tag{3}$$

where $P(q,\phi)$ is the Fourier transform of the sum of the intramolecular two-point correlation functions for a given volume fraction ϕ. In the limit $\phi \to 0$ this function reduces to the form factor $P(q) \equiv P(q,\phi \to 0)$. The total correlation function $h(q,\phi)$ describes correlations between different bottle-brush polymers, and is given by the generalized Ornstein-Zernike equation

$$h(q,\phi) = P^2(q,\phi)c(q,\phi)/(1 - \phi c(q,\phi)P(q,\phi)/V_p), \tag{4}$$

where $c(q,\phi)$ is the direct correlation function. This equation is solved numerically together with the Percus-Yevick closure taking steric interactions into account [27].

In Fig. 3(a) the experimental structure factor $S(q,\phi)$ is compared to the results of the integral equation theory for the PRISM. We have used the form factor $P(q)$ (see the upper curve in Fig. 2) as input into the generalized Ornstein-Zernike equation, i.e., $P(q,\phi)=P(q)$ in Eqs. (3) and (4). With increasing bottle-brush polymer concentration the integral equation results (dashed lines) and the experimental data (symbols) deviate. The comparison of the calculated structure factors with the experimental data demonstrates that the *concentration-independent* persistence length $l_p=17.5$ nm and the form factor $P(q)$ may be used as input into the generalized Ornstein-Zernike equation only for very low concentrations of the bottle-brush polymers ($c \lesssim 2.5$ g/l). For higher concentrations marked deviations are found indicating that this approach is no longer valid.

An alternative way of modeling these data is to consider a *concentration-dependent* persistence length of bottle-brush polymers and hence a concentration-dependent intramolecular correlation function $P(q,\phi)$ as input into Eqs. (3) and (4). The results for the structure factors as obtained from the PRISM integral equation theory and using concentration-dependent persistence lengths are in agreement with the experimental data both for $S(q,\phi)$ [solid lines in Fig. 3(a)] and $I(q,\phi)$ (four lower solid lines in Fig. 2). The dependence of the persistence length on concentration shown in Fig. 3(b) is reminiscent of the behavior of the predicted persistence length of polyelectrolytes (see Fig. 3 in Ref. [15] and Fig. 4 in Ref. [20]). Although the bottle-brush polymer solutions under consideration and the theoretically investigated polyelectrolyte solutions distinctly differ from each other, there is a significant overlap between them, namely the change of the shape of the polymers upon varying the concentration. Moreover, Fig. 3(b) demonstrates that the concentration dependence of the calculated radii of gyration [30]

$$r_g = \sqrt{Ll_p/3 - l_p^2 + 2l_p^3/L - 2(1 - e^{-L/l_p})l_p^4/L^2} \tag{5}$$

is in agreement with scaling considerations.

In addition to static properties we have investigated dynamic properties of the bottle-brush polymers using dynamic light scattering (DLS). The measured time-dependent scattering intensity is a single exponential function of time for concentrations $c \lesssim 2.5$ g/l signaling pure translational diffusion of the polymers. No contributions of internal modes such a rotation, bending, or stretching to the dynamics have been found. We have determined the hydrodynamic radius $R_h = 39 \pm 2$ nm from the measured translational diffusion coefficient. In order to understand the dynamic properties of the bottle-brush polymers at low concentrations it is instructive to compare the measured hydrodynamic radius with the results for a semiflexible chain model which has been used to interpret quasielastic neutron and dynamic light scattering measurements on various natural and synthetic macromolecules [30] and wormlike micelles [31]. The numerical evaluation yields $R_h=38.5$ nm which is comparable with the experimentally determined value. Moreover, we have calcu-

lated the dynamic form factor and we have found that internal modes do not contribute to the dynamic form factor for the scattering vectors used in the light scattering experiments. However, internal modes do contribute for stiffer polymers confirming our findings concerning the stiffness of the bottle-brush polymers.

Figure 4 demonstrates that the measured cooperative diffusion coefficient $D(\phi)$ (solid circles) increases upon increasing the bottle-brush polymer concentration due to an increasing restoring force for concentration fluctuations. We have solved the equation $dI(q,\phi,t)/dt=-\Omega(q,\phi)I(q,\phi,t)$ for the time-dependent scattering intensity $I(q,\phi,t)$, where the decay rate $\Omega(q,\phi)$ depends on the solvent of the viscosity and the static scattering intensity $I(q,\phi)$ (see Ref. [28] for further details). As before in the case of the static correlation functions we have found that the cooperative diffusion coefficients $D(\phi)=\lim_{q\to 0}\Omega(q,\phi)/q^2$ as obtained from the equation for the time-dependent scattering intensity and using concentration-dependent persistence lengths (solid line in Fig. 4) are in better agreement with the experimental data than the corresponding ones using the concentration-independent persistence length $l_p=17.5$ nm (dashed line in Fig. 4). In addition we have observed experimentally a slow diffusive process at higher concentrations (open circles in Fig. 4) which might be associated with long-range concentration fluctuations.

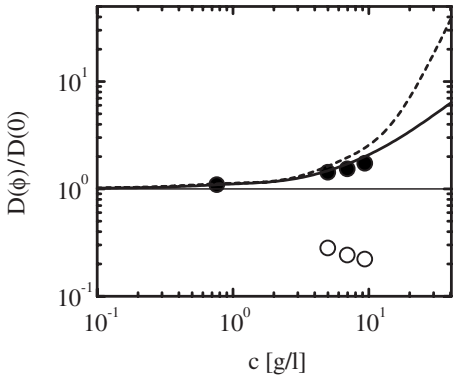

FIG. 4. Normalized cooperative diffusion coefficients $D(\phi)$ (solid circles) together with theoretical calculations using a concentration-independent (dashed line) [-dependent (solid line)] shape of the bottle-brush polymers. The open circles denote the measured diffusion coefficients of an additional slow diffusive process for concentrations $c \gtrsim 5$ g/l.

We wish to acknowledge financial support by the Deutsche Forschungsgemeinschaft, SFB 481, Bayreuth.

[1] M. Wintermantel *et al.*, Macromol. Rapid Commun. **15**, 279 (1994).
[2] M. Wintermantel *et al.*, Angew. Chem., Int. Ed. Engl. **34**, 1472 (1995).
[3] M. Gerle *et al.*, Macromolecules **32**, 2629 (1999).
[4] M. Zhang and A. H. E. Müller, J. Polym. Sci., Part A: Polym. Chem. **43**, 3461 (2005).
[5] S. Rathgeber *et al.*, J. Chem. Phys. **122**, 12904 (2005), and further references therein.
[6] S. Rathgeber *et al.*, Polymer **47**, 7318 (2006).
[7] B. Zhang, F. Gröhn *et al.*, Macromolecules **39**, 8440 (2006).
[8] S. Elli *et al.*, J. Chem. Phys. **120**, 6257 (2004).
[9] O. V. Borisov, T. M. Birshtein, and Y. B. Zhulina, Polym. Sci. U.S.S.R. **29**, 1413 (1987).
[10] K. S. Schweizer *et al.*, J. Chem. Phys. **96**, 3211 (1992).
[11] A. Yethiraj and K. S. Schweizer, J. Chem. Phys. **97**, 1455 (1992).
[12] J. Melenkevitz *et al.*, Macromolecules **26**, 6190 (1993).
[13] K. S. Schweizer and J. G. Curro, Adv. Chem. Phys. **XCVIII**, 1 (1997).
[14] B. J. Sung and A. Yethiraj, J. Chem. Phys. **122**, 234904 (2005).
[15] M. J. Stevens and K. Kremer, Phys. Rev. Lett. **71**, 2228 (1993).
[16] M. J. Stevens and K. Kremer, J. Chem. Phys. **103**, 1669 (1995).
[17] A. Yethiraj, Phys. Rev. Lett. **78**, 3789 (1997).
[18] A. Yethiraj, J. Chem. Phys. **108**, 1184 (1998).
[19] C.-Y. Shew and A. Yethiraj, J. Chem. Phys. **110**, 5437 (1999).
[20] C.-Y. Shew and A. Yethiraj, J. Chem. Phys. **113**, 8841 (2000).
[21] T. Hofmann *et al.*, J. Chem. Phys. **118**, 6624 (2003).
[22] M. Zhang *et al.*, Polymer **44**, 1449 (2003).
[23] S. Rosenfeldt *et al.*, ChemPhysChem **7**, 2097 (2006).
[24] L. Li *et al.*, Phys. Rev. E **72**, 051504 (2005).
[25] S. Pedersen and P. Schurtenberger, Macromolecules **29**, 7602 (1996).
[26] L. Harnau and P. Reineker, J. Chem. Phys. **112**, 437 (2000).
[27] L. Harnau *et al.*, Europhys. Lett. **53**, 729 (2001).
[28] L. Harnau, J. Chem. Phys. **115**, 1943 (2001).
[29] L. Harnau and J.-P. Hansen, J. Chem. Phys. **116**, 9051 (2002).
[30] L. Harnau *et al.*, J. Chem. Phys. **104**, 6355 (1996); **109**, 5160 (1998); Macromolecules **30**, 6974 (1997); **32**, 5956 (1999).
[31] H. von Berlepsch *et al.*, J. Phys. Chem. B **102**, 7518 (1998).

Chapter 3.2

Interaction of Cylindrical Polymer Brushes in Dilute and Semi-dilute Solution

Sreenath Bolisetty [a)], Sabine Rosenfeldt [a) *], Christophe N. Rochette [a)], Ludger Harnau [b) *], Peter Lindner [c)], Youyong Xu [d)], Axel H. E. Müller [d)], Matthias Ballauff [a)]

[a)] *Physikalische Chemie I, University of Bayreuth, 95440 Bayreuth, Germany*

[b)] *Max-Planck-Institut für Metallforschung, Heisenbergstrasse 3, 70569 Stuttgart, Germany, and Institut für Theoretische und Angewandte Physik, Universität Stuttgart, Pfaffenwaldring 57, 70569 Stuttgart, Germany*

[c)] *Institut Laue-Langevin, Grenoble Cedex, France*

[d)] *Makromolekulare Chemie II, University of Bayreuth, 95440 Bayreuth, Germany*

Sabine.Rosenfeldt@uni-bayreuth.de, harnau@fluids.mpi-stuttgart.mpg.de

Published in Colloid .and Polymer Science **2009**, *287*, 129

Colloid Polym Sci
DOI 10.1007/s00396-008-1962-3

ORIGINAL CONTRIBUTION

Interaction of cylindrical polymer brushes in dilute and semi-dilute solution

Sreenath Bolisetty · Sabine Rosenfeldt · Christophe N. Rochette · Ludger Harnau · Peter Lindner · Youyong Xu · Axel H. E. Müller · Matthias Ballauff

Received: 3 September 2008 / Revised: 24 October 2008 / Accepted: 29 October 2008

Abstract We present a systematic study of flexible cylindrical brush-shaped macromolecules in a good solvent by small-angle neutron scattering (SANS), static light scattering (SLS), and by dynamic light scattering (DLS) in dilute and semi-dilute solution. The SLS and SANS data extrapolated to infinite dilution lead to the shape of the polymer that can be modeled in terms of a worm-like chain with a contour length of 380 nm and a persistence length of 17.5 nm. SANS data taken at higher polymer concentration were evaluated by using the polymer reference interaction site model (PRISM). We find that the persistence length reduce from 17.5 nm at infinite dilution to 5.3 nm at the highest concentration (volume fraction 0.038). This is comparable with the decrease of the persistence length in semi-dilute concentration predicted theoretically for polyelectrolytes. This finding reveals a softening of stiffness of the polymer brushes caused by their mutual interaction.

Keywords Cylindrical polymer brushes · Softening of polymers · SANS · DLS · PRISM

S. Bolisetty · S. Rosenfeldt (✉) · C. N. Rochette · M. Ballauff
Physikalische Chemie I, University of Bayreuth,
95440 Bayreuth, Germany
e-mail: Sabine.Rosenfeldt@uni-bayreuth.de

L. Harnau
Max-Planck-Institut für Metallforschung,
Heisenbergstrasse 3,
70569 Stuttgart, Germany
e-mail: harnau@fluids.mpi-stuttgart.mpg.de

L. Harnau
Institut für Theoretische und Angewandte Physik,
Universität Stuttgart,
Pfaffenwaldring 57,
70569 Stuttgart, Germany

P. Lindner
Institut Laue-Langevin,
Grenoble Cedex, France

Y. Xu · A. H. E. Müller
Makromolekulare Chemie II, University of Bayreuth,
95440 Bayreuth, Germany

Introduction

If polymeric side chains are grafted to a polymer backbone, a cylindrical polymer brush results [1–3]. In recent years, these polymers have become the subject of intense experimental and theoretical research interest by a broad variety of methods [4, 5]. The main feature of cylindrical brushes is a marked stiffening of the main chains. It has been shown theoretically and by computer simulations [6] that this stiffening is due to a balance of repulsive forces originating from a steric overcrowding of the side chains and the entropic restoring forces of the main chain. The analysis of cylindrical brushes by small-angle neutron scattering (SANS) [7, 8], small-angle X-ray scattering (SAXS) [9] and static light scattering (SLS) [10] in dilute solution has demonstrated that these macromolecules exhibit a worm-like conformation that may be approximated by a cylinder if the length of the brush is not too large. This is in qualitative agreement with studies of the contour length and end to end distance of individual brush molecules in the dried state by atomic force microscopy (AFM) [11]. Up to now, most studies on cylindrical brushes in solution have been conducted in the dilute regime. Recently, Rathgeber et al. [10] reported the formation of ordered structures of dissolved brushes at intermediate concentrations. However, still higher concentrations lead to the disappearance of the ordered phase and thus to a

reentrant isotropic phase. The authors explained this by a screening of the excluded volume interaction when the polymers start to overlap. However, no quantitative explanation was given.

The central question of this investigation is the interplay between the interaction and the stiffness of the brushes in dilute and semi-dilute solution. Following the decrease of the persistence length by mutual interaction, we aim at a general discussion of concentration-dependent conformational changes of chain molecules. The decrease of the persistence length by mutual interaction has first been discussed for cylindrical brushes by Borisov et al. in 1987 [12]. For polyelectrolytes in solution, Stevens and Kremer demonstrates that an increase of the concentration must lead to a decrease of the persistence length [13]. Cylindrical polymer brushes offer the possibility to study the softening of the stiffness in a neutral system. Scattering methods allows in situ studies and therefore give access to this important problem related to polymer solutions. A quantitative understanding of the correlations and interaction of polymeric species can be achieved using the polymer reference interaction site model (PRISM) integral equation theory. Here we use the PRISM theory to model the interaction of cylinder brushes at finite concentrations.

Recently, we investigated a worm-like polymer brush near the overlap concentration and detected a softening of the bottle-brush at high concentrations due to mutual interaction with the other brushes [14]. Here we give a full account of this work.

Figure 1 displays the chemical structure of the polymer studied here. The brush was synthesized by a "grafting from" method and composed of poly(2-hydroxyethylmethacrylate) (P-HEMA) backbone grafted with poly(t-butyl acrylate)(P-TBA) chains. The weight average number of repeating units in the main chain is 1,600 with a polydispersity index of M_W/M_n=1.06. Due to the initiator efficiency of approximately 0.5 only every second repeating unit carries a side chain containing ca. 61 units. Thus, the brush is a statistical copolymer of units with side chains (ca. 780) and units without side chains (ca. 820). Hence, we deal with a rather sparse brush system as opposed to dense brushes in which each repeating unit carries a side chain. The details of the synthesis have been reported in reference [4].

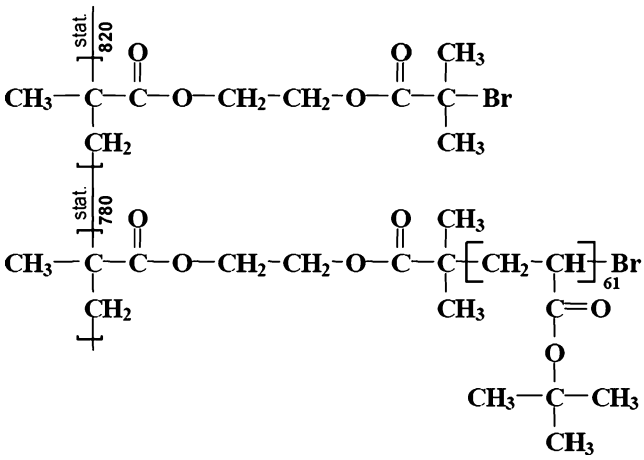

Fig. 1 Chemical structure of the investigated cylindrical polymer brush consisting of a poly(2-hydroxy-ethylmethacrylate) (P-HEMA) backbone grafted with poly(t-butyl acrylate)(P-TBA) chains. The repeating units carrying side chains (ca. 780) alternate statistically with unsubstituted repeating units (ca. 820). The weight average number of repeating units per side chain is 61

The article is organized as follows: first we present a characterization of the brush macromolecules in dilute solution in order to characterize its molecular structure and bare persistence length measured at infinite dilution. Next, more concentrated solutions will be analyzed. The interaction between the brushes will be modeled using the PRISM integral equation theory. In the third section the dynamic properties of the polymer brushes will be considered.

Experiment

Small-angle neutron scattering

The poly(t-butyl acrylate) brush was synthesized by "grafting from" route via atom transfer radical polymerization leading to a (poly 2-hydroxyethylmethacrylate) backbone partially grafted with poly(t-butylacrylate) (P-TBA) side chains. Details have been reported before [3–5, 14]. Deuterated tetrahydrofuran (THF-d_8, Fluka, deuteration degree 99.9%) was used as received. The partial specific volume of the polymer was determined using a DMA-60-densitometer (Paar, Graz, Austria) to $\overline{v} = 1.10$ (±0.02) cm^3/g. All SANS data were obtained using the instrument D11 of the Institute Laue-Langevin (ILL) in Grenoble (France). The wavelength of the incident neutrons was 0.6 nm and the sample-detector distances were set to 1.1, 5, and 20 m. In order to obtain the radial averaged intensities in absolute scale, the data were treated by the use of the software provided at the instrument. For all data sets, the rates of incoherent scattering caused mainly by the protons were determined at high scattering angle, set as a constant and subtracted from the crude data. Further treatment was done according to references [15, 16].

Light scattering

The polymer brush was dissolved in THF (Sigma Aldrich) leading to a concentration range of 1.5 g/L to 7.0 g/L. The solutions are filtered into dust-free optical cells using 0.45 μm PTFE filters. The light scattering experiments were carried out by using the ALV/DLS/SLS-5000 compact goniometer system equipped with a He-Ne laser (λ=

632.8 nm). For each solution simultaneous dynamic light scattering (DLS) and static light-scattering (SLS) measurements were performed (three runs of 600 s, angles changing from 30° to 150° with an angular step width of 10°). The refractive increment d*n*/d*c* of the solution was measured using a DnDc2010 device supplied by Polymer Standards Service to 0.063±0.002 ml/g. For depolarized dynamic light scattering (DDLS) measurements a Glan-Thomson polarizer with an extension coefficient better than 10^{-5} was used. The light scattering data were analyzed according to the CONTIN method using standard ALV software.

Theoretical basis

Small-angle neutron scattering and light scattering determine the intensity $I(q,\phi)$ as a function of the scattering vector q and the volume fraction ϕ of the dissolved objects. The absolute value of the scattering vector is given by $q=|q|=(4\pi n/\lambda)\sin(\theta/2)$ in which n is the refractive index of the medium, λ is the incident wavelength, and θ is the scattering angle. For the systems under consideration the scattering intensity may be rendered as [17]

$$I(q,\phi) = \phi(\Delta\rho)^2 V_p P(q) S(q,\phi) + \phi I_{fluc}(q). \quad (1)$$

The form factor $P(q)$ is determined by interference effects between radiation scattered by different parts of the same particle. Consequently, this scattering intensity describes the shape of the particle with volume V_p. The degree of local order in the sample is given by the structure factor $S(q,\phi)$ which is related to the mutual interactions between different particles. $\Delta\rho$ denotes the excess scattering length density between the solute and the solvent. Finally, the contribution to the scattering intensity due to density fluctuations of the polymer chains is denoted by $I_{fluc}(q)$. This contribution becomes only important for high scattering vectors.

For dilute solutions, the dependence of the structure factor $S(q,\phi)$ on the volume fraction ϕ ($\phi=c/\rho_T$, ρ_T is the density of the particle and c is the weight concentration of the dissolved polymer) may be expressed in a virial series by [15, 17–20]

$$\frac{1}{S(q,\phi)} = 1 + 2B_{app}(q)\phi + O(\phi^2). \quad (2)$$

The apparent second virial coefficient $B_{app}(q)$ includes the effective diameter of interaction d_{eff} and the particle volume V_p. The apparent second virial coefficient is an explicit function of q [15, 17–19]

$$B_{app}(q) = \frac{2\pi d_{eff}^3}{3V_p}\left(1 - \frac{1}{10} d_{eff}^2 q^2 + O(q^3)\right). \quad (3)$$

In the limit of vanishing scattering vector $B_{app}(q)$ reduces to its thermodynamic limit, the second virial coefficient. Thus, the effective diameter d_{eff} gives the balance of both repulsive and attractive interactions between the solute molecules [15, 19].

With complete generality, $I(q,\phi)$ may be approximated in the region of small q by Guinier's law [17]

$$I(q,\phi) \xrightarrow{qR_g << 1,\ \phi \to 0} \phi V_p (\Delta\rho)^2 \exp\left(-\frac{R_g^2}{3} q^2\right) \quad (4)$$

where R_g is the radius of gyration. R_g depends on the excess scattering length density $\Delta\rho$.

The scattering intensity of randomly orientated, non-interacting cylindrical objects can be approximated by the product of an infinitely thin rod and a factor which is due to the finite diameter of the chain [17]. At sufficiently high scattering angles this approximation is given by [17]

$$I(q,\phi) - \phi I_{fluc}(q) \xrightarrow{qR_g >> 1} \pi(\Delta\rho)^2 \phi \frac{V_p}{qL} \exp\left(-\frac{1}{2} R_c^2 q^2\right) \quad (5)$$

Here the radius of gyration perpendicular to the chain axis is denoted as R_c. From the particle volume V_p the molecular weight M_W can be obtained by $V_p = M_W/N_A/\rho_T$ (N_A is Avogadro's number). The division of the molecular weight M_W by the total length L leads to the mass per unit length M_L.

Thus, the forgoing consideration suggest the following way to determine the overall structure of the isolated polymer brush: At first, the data measured at finite concentration are extrapolated to vanishing concentration by use of Eqs. 2 and 3. After subtraction of the scattering contribution due to thermal fluctuations of the side chains the scattering intensity of a single particle $P(q)$ results and the worm-like shape of the investigated polymer brushes can be confirmed. Finally, the structure factor $S(q,\phi)$ obtained according to Eq. 1 can be compared to calculations done within the frame of the PRISM approach.

Results and discussion

Analysis of the particles in dilute solution

The present analysis rests on precise measurements of $I(q,\phi)$ at different concentrations. The set of data obtained for different concentrations are displayed in Fig. 2 together with the result of the extrapolation to vanishing concentration which includes SANS and SLS data.

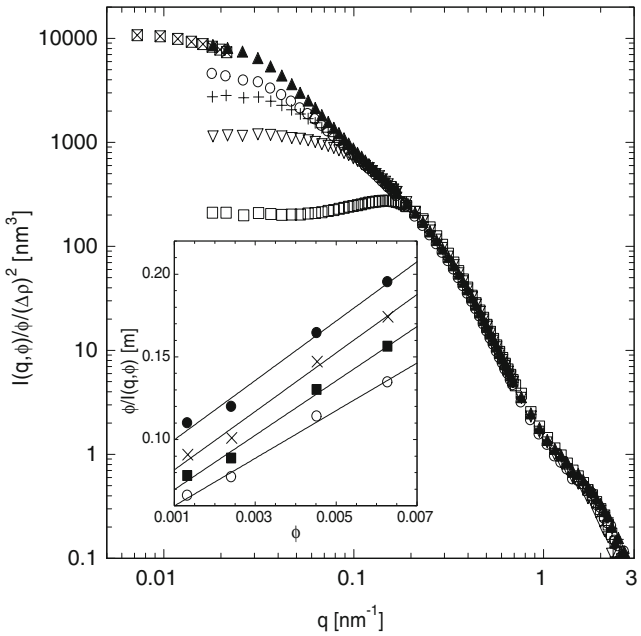

Fig. 2 Influence of concentration on the absolute scattering intensities $I(q,\phi)/\phi$. a: $I(q,\phi)/\phi$ as function of q. Parameter of the different SANS curves is the volume fraction (*top to bottom* ϕ =0.000, 0.002, 0.006, 0.013, and 0.038). The extrapolation to ϕ=0.000 includes the SLS data (*filled squares*). *Inset* Determination of $S(q,\phi)$ from the dilute regime by extrapolation for different q values (*top to bottom*: q=0.027 nm^{-1}, 0.021 nm^{-1}, 0.016 nm^{-1}, and 0.010 nm^{-1}). Here SLS data are shown

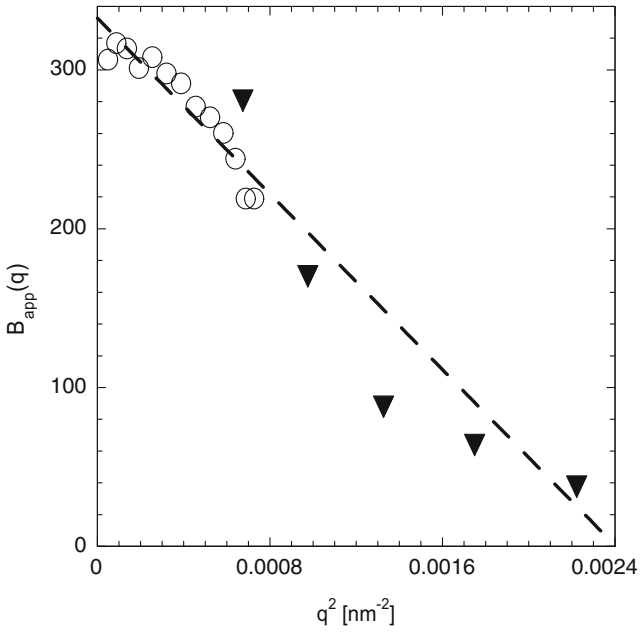

Fig. 3 Apparent second viral coefficient $B_{app}(q)$ of the polymer brush in the dilute regime as determined by SLS (*circles*) and SANS (*inverted triangles*). The effective diameter d_{eff} deriving from the linear regression results as ca. 64 nm

For the sake of clarity not all data taken at low concentration are shown in the graph. As expected, all measured SANS intensities as the function of concentration differ strongly at low q but superimpose at intermediate and high q values. The suppression of the intensity near q=0 (correlation hole effect) affects more than one order of magnitude. This point directly to the effect of mutual interaction of the polymer brushes. Evidently, non-negligible interaction starts at much lower volume concentrations than measured, e.g. below ϕ=0.001. The extrapolation to vanishing concentration is done separately for each q value as suggested by Eq. 2 (see Fig. 2 inset). Due to statistical problems and low concentrations a linear extrapolation is used. Since we aim at the limits of vanishing q values, the q range accessible by SANS was not sufficient. Hence, static light scattering was used to obtain data at smallest q values possible in order to supplement the analysis by SANS.

Having extrapolated $I(q,\phi)/\phi$ to ϕ =0, Eq. 3 may be used to determine the effective diameter d_{eff} of interaction. Figure 3 shows the apparent virial coefficient $B_{app}(q)$ in the dilute regime as obtained by SLS and SANS as function of q^2. The data agree within the given limits of error. Figure 3 clearly demonstrates that $B_{app}(q)$ strongly depends on the scattering angle as expected. The effective diameter d_{eff} can be calculated from the slope of the linear regression to d_{eff}=64±10 nm.

Figure 4 displays the intensity, extrapolated to vanishing concentration for the entire q range available by the combination of SLS and SANS. In general, the side chains of the polymer brushes exhibit density fluctuations that will give an additional scattering contribution at large q values (cf. Eq. 1). The rather flat region at small q in Fig. 3 is due to the fact that the intensity must follow Guinier's law (Eq. 4) in this regime. The radius of gyration resulting from Guinier's law follows as R_g=53 nm and the molecular weight M_W is found to be 7.41×10^6 g/mol. Together with the weight-average degree of polymerization P_w=1,600 of the main chain this leads to an average molecular weight of the repeating unit of M_0=4,600 g/mol. Note that this is the average of all repeating units of which only ca. 50% carry side chains (cf. Fig. 1).

Further, Fig. 4 demonstrates that the scattering intensity is dominated by an additional contribution at q>0.8 nm^{-1}. The contribution due to internal density fluctuations may be approximated by [7]

$$I_{fluc}(q) = a_b \frac{\sin[\mu \tan^{-1}(q_b^*)]}{\mu q_b^* \left[1 + q_b^{*2}\right]^{\mu/2}} \tag{6}$$

with

$$q_b^* = \frac{q\xi}{\left[\mathrm{erf}\left(qR_c/\sqrt{6}\right)\right]^3} \text{ and } \mu = \frac{1}{\upsilon_b} - 1 \tag{7}$$

where υ_b is the Flory exponent, a measure of the fractal dimension, erf denotes the error function. The amplitude a_b

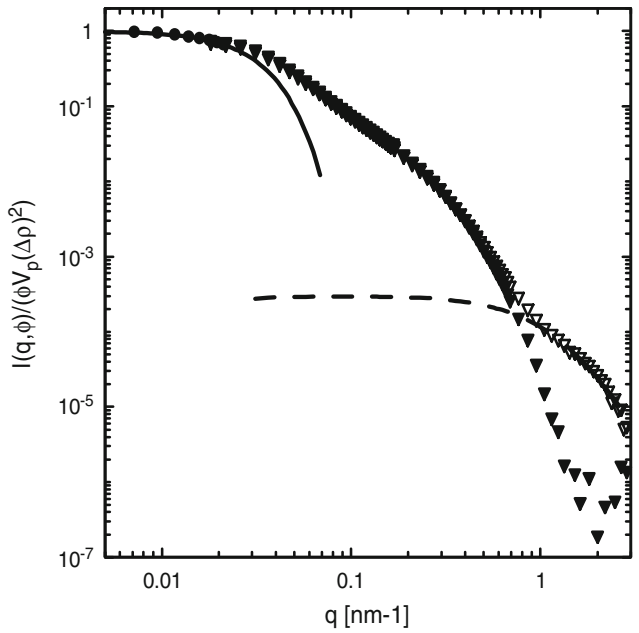

Fig. 4 Scattering intensity $I(q,\phi)\Big/\left(\phi V_p(\Delta\rho)^2\right)$ in the limit of vanishing concentration before (*open symbols*) and after (*filled symbols*) subtraction of scattering contributions due to fluctuations (blob scattering). The *circles* denotes the values obtained by SLS and the *inverted triangles* the ones obtained from SANS. The *dashed line* corresponds to the blob scattering (Eq. 6). The forward scattering according to Guinier's law (Eq. 4) is given by the *full line*

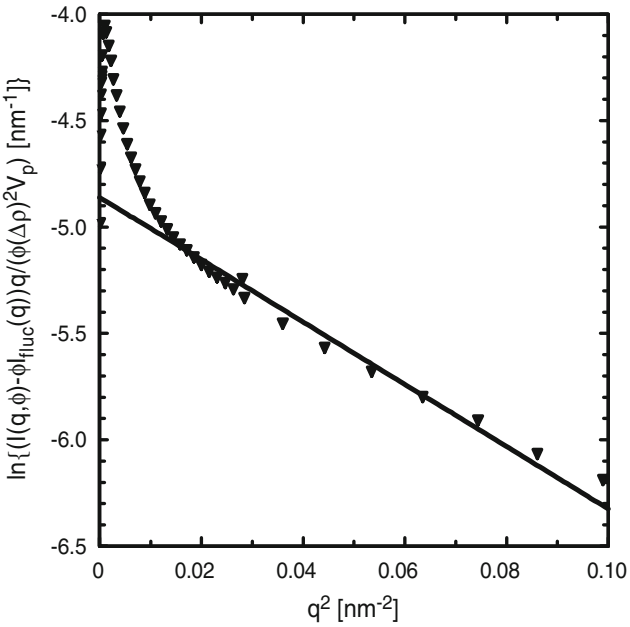

Fig. 5 Plot of the normalized scattering intensity scattering according to Eq. 5 for the determination of the mass per unit length M_L and the cross-sectional radius of gyration R_c. The measured intensity is corrected to the blob scattering. From the linear relationship V_p and thus M_L and R_c are obtained

is the scattering due to thermal fluctuations relative to the amplitude of the contribution resulting from the overall shape. $I_{\mathrm{fluc}}(q)$ is also called blob scattering [7]. The dashed line in Fig. 4 displays the fit according to Eq. 6. The best description fitting Eq. 6 to the experimental data base on a radius of gyration of the cross section R_c of 5.0 nm, a correlation length (blob size) ξ of 1.0 nm and the Flory exponent υ_b of 0.6. The value υ_b is very close to the theoretical result expected from perturbation calculations for flexible cylinders with excluded volume interactions, which is 0.588.

The corrected intensity thus obtained can now be used to estimate the mass per unit length M_L and the cross-sectional radius of gyration R_c (see discussion of Eq. 5). Figure 5 displays the respective plot. The q range in which Eq. 5 can be applied safely is rather small. However, the accuracy is sufficient to estimate M_L to 19000 g/Mol/nm. If the length of the repeating unit would be 0.25 nm as expected for vinylic chains, M_L follows from the degree of polymerization of 1,600 and the molecular weight of the repeating unit M_0 (see above) to 18400 g/Mol/nm. The slightly higher value of M_L (19000 g/Mol/nm), however, points to a length of the repeating unit of ca. 0.24 nm. We admit that this value is affected by a significant error. Nevertheless a similar shortening of the repeating unit was found recently by Zhang and coworkers [8]. Up to now, the origins of this effect are not fully clear. The cross-section radius of gyration R_c of ca. 5.4 nm is afflicted by a big error around 15% (cf. Fig. 5).

The investigated polymers can be described as flexible cylinders with a circular cross-section and a uniform scattering length density. Thus, for the interpretation of the scattering intensity at vanishing concentration, we used the empirical equations for semiflexible polymer chains with excluded volume interaction derived by Petersen and Schurtenberger (model 3 of reference [21]). The model is a parameterization of Monte Carlo simulations of a discrete representation of the worm-like chain model of Kratky and Porod applied to the pseudo-continuous limit. For details see Eqs. 3, 26, and 27 in the original reference [21]. The parameters of the model are the cross-sectional radius R_c, the contour length L (total length) and the persistence length l_p. The contour length is described as a chain of some number of locally stiff segments of length l_p. Hence, this value is a measure for the stiffness of the chain. Polydispersity of the cross-section is included using a Schulz–Zimm distribution. The comparison of the experimental data to the model is shown in Fig. 6.

The scattering intensity extrapolated to vanishing concentration is well-described by this model using 5.0 nm as radius of the cross-section as suggested by the fit of the blob scattering. The contour length results as 380 nm and the persistence length as 17.5 nm. The contour length is comparable with the contour length of 384 nm calculated

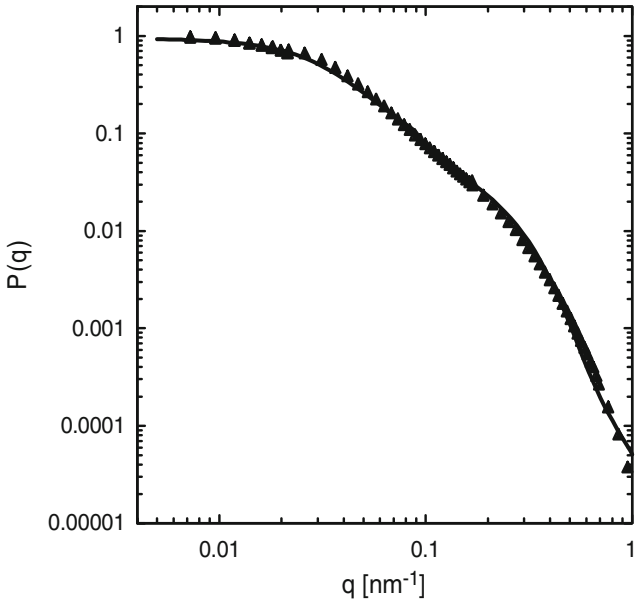

Fig. 6 Comparison of the experimental data extrapolated to zero concentration to the model of flexible cylinder with a circular cross section. The measured scattering intensity is corrected to the blob scattering. Parameters of the fit are: L=380 nm, R_c=5.0 nm (σ =30%), and l_p=17.5 nm

from degree of polymerization and the length of the repeating unit of 0.24 nm.

Intermolecular pair correlation

We now turn our attention to the analysis of the scattering intensities taken at finite concentration. One can calculate structural properties of interacting polymer brushes using generalized Ornstein–Zernike equations of an interaction site integral equation theory. Spatial pair correlations of a polymer brush solution are characterized by a set of intermolecular site–site total correlation functions $h_{ij}(r,\phi)$, where the indices i and j run over interaction sites on each of two brush polymers. These functions are related to a set of intermolecular site–site direct correlation functions $c_{ij}(r,\phi)$ by the generalized Ornstein–Zernike relations of the reference interaction site model [22]. This set of generalized Ornstein–Zernike equations must be supplemented by a set of closure relations. If the interaction sites are simply the centers of exclusion spheres, to account for steric effects, a convenient closure is the Percus–Yevick approximation [22]. The reference interaction site model has been proved to be a successful theory of the pair structure of many molecular fluids [23]. In the case of macromolecular and colloidal systems, with very large numbers of interaction sites, the number of coupled Ornstein–Zernike equations becomes intractable, and a considerable simplification follows from the assumption that the direct correlation functions $c_{ij}(r,\phi)$ are independent of the indices i and j. This leads to the polymer reference interaction site model theory first applied by Schweizer and Curro to long flexible polymers [24]. PRISM neglects end effects in that case. The resulting single generalized Ornstein–Zernike equation of the PRISM reads

$$h(q,\phi) = \frac{P^2(q,\phi)c(q,\phi)}{1 - \frac{\phi}{V_p}c(q,\phi)P(q,\phi)}, \tag{8}$$

where $h(q,\phi)$ and $c(q,\phi)$ are particle-averaged total and direct correlation functions, respectively. $P(q,\phi)$ is the Fourier transform of the sum of the intramolecular two-point correlation functions for a given volume fraction ϕ. In the limit $\phi \to 0$ this function reduces to the form factor $P(q) \equiv P(q,\phi \to 0)$. Eq. 8 is solved numerically together with the Percus–Yevick closure taking steric interactions into account. Within the PRISM theory the structure factor $S(q,\phi)$ reads

$$S(q,\phi) = 1 + \frac{\phi h(q,\phi)}{V_p P(q,\phi)}. \tag{9}$$

The scattering intensity $I(q,\phi)$ is calculated according to Eq. 1 with $S(q,\phi)$ as input. The PRISM integral equation theory has been successfully applied to various systems, such as rod-like viruses [25], plate-like colloids [26], dendrimers [16, 20], and nanoparticles [27], flexible polymers [28], mixtures of spherical colloids and semiflexible polymers [29], polyelectrolyte brushes [30]. Moreover, it has been demonstrated that the simpler PRISM theory yields results in good agreement with the more elaborate reference interaction site model calculations for lamellar colloids [31].

In Fig. 7 the experimental scattering intensity $I(q,\phi)$ is compared to the results of the integral equation theory for the PRISM. We have used the form factor *P(q)* calculated for a worm-like chain of length L=380 nm und persistence length l_p=17.5 nm as input into the generalized Ornstein–Zernike equation, i.e., $P(q,\phi)=P(q)$ in Eqs. 8 and 9. For the sake of clarity the scattering intensities related to different volume fractions have been shifted vertically in Fig. 7. With increasing volume fraction the integral equation results (long dashed lines) and the experimental data (symbols) deviate. The comparison of the calculated scattering intensities with the experimental data demonstrates that the persistence length, l_p=17.5 nm, and the form factor *P(q)* may be used as input into the generalized Ornstein–Zernike equation only for very low volume fractions of the polymer brushes $\phi \leq 0.002$. For higher volume fractions marked deviations are found indicating that this approach is no longer valid.

An alternative way of modeling these data is to consider a volume fraction-dependent persistence length of polymer

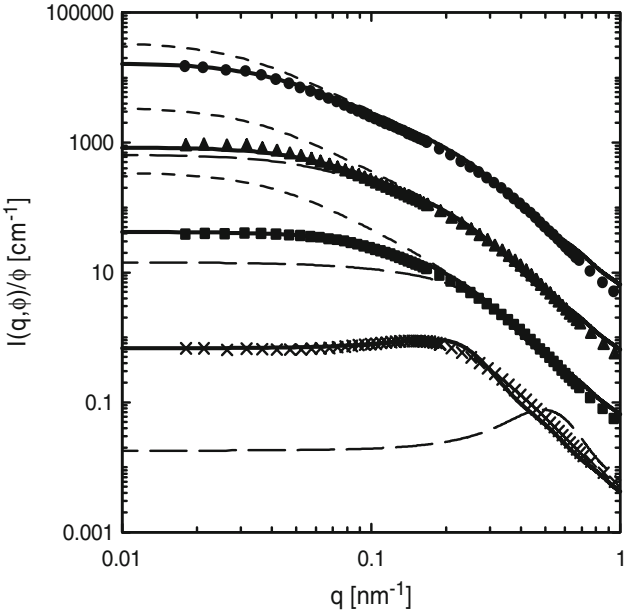

Fig. 7 Measured scattering intensity of $I(q,\phi)$ of polymer brush solutions normalized to their volume fraction ϕ which increases from top to bottom (ϕ =0.002, 0.006, 0.013, 0.038). The three lowermost intensities are shifted down by a factor of 10, 100, and 1,000 respectively. The *dashed lines* represent the corresponding intensities as obtained from the PRISM integral equation theory (Eqs. 8, 9 and 1) and assuming a volume fraction-independent shape of the polymers. The *solid lines* represent the scattering intensities as obtained from the PRISM integral equation theory using the volume fraction-dependent persistence lengths shown in Fig. 8 with the same symbol code (*solid circle*, *triangle*, *square* and *cross*). For ϕ =0.002 the *dashed* and *solid curve* coincide because the same persistence is used for both curves. The *short dashed lines* represent the scattering intensity calculated according to Eq. 1 with $S(q,\phi) = 1$ for ϕ =0.002, 0.006, and 0.013

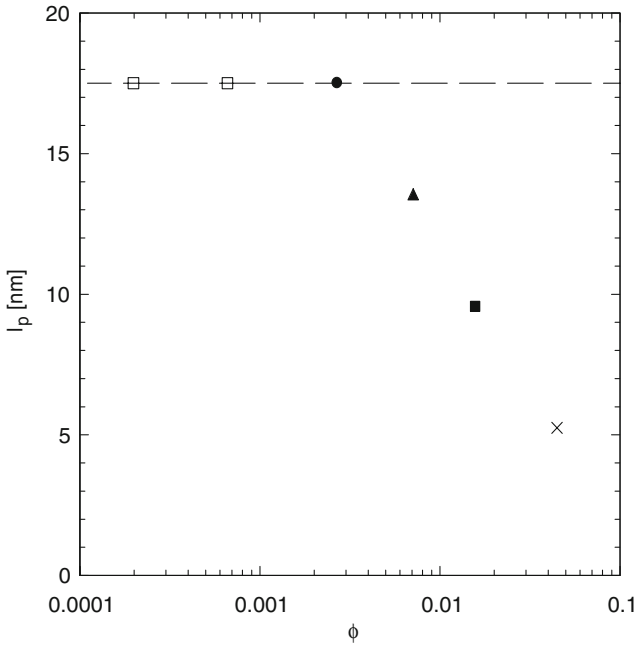

Fig. 8 The volume fraction-dependent persistence lengths used in the calculation of the scattering intensities shown by the *solid lines* in Fig. 7 (with the same symbol code, i.e., *solid circle* l_p=17.5 nm, *triangle* l_p=13.5 nm, *square* l_p=9.55 nm, and *crosses* l_p=5 nm). The *open squares* denote two low volume fractions which have been used for the extrapolation to infinite dilution

brushes and hence a volume fraction-dependent intramolecular correlation function $P(q,\phi)$ as input into Eqs. 8 and 9. Here $P(q,\phi)=P(q,\phi,l_p,L)$ is the form factor of a semi-flexible polymer chain that depends on both the contour length L and the persistence length l_P [21]. The results for the scattering intensities as obtained from the PRISM integral equation theory using volume fraction-dependent persistence lengths are in agreement with the experimental data for $I(q,\phi)$ (solid lines in Fig. 7). For comparison, the short dashed lines in Fig. 7 depict the modeling of the experimental data assuming a solution of noninteracting polymer brushes characterized by $S(q,\phi)=1$ in Eq. 1.

The dependence of the persistence length on the volume fraction shown in Fig. 8 is reminiscent of the behavior of the predicted persistence length of polyelectrolytes [13, 32]. Although the polymer brush solutions under consideration and the theoretically investigated polyelectrolyte solutions distinctly differ from each other, there is a significant overlap between them, namely the change of the shape of the polymers upon varying the volume fraction. The essential features that determine the shape of these macromolecules are the following ones: (1) The bare main chain molecules, i.e., without grafted side chains in the case of the brushes and without charges in the case of the polyelectrolyte chains, are rather flexible coils. (2) In dilute solution, the macromolecules adopt a worm-like configuration due to the steric interaction between the side chains in the case of the polymer brushes and due to the electrostatic repulsion in the case of the polyelectrolyte chains. (3) For both systems the contribution of the intermolecular interactions to the total free energy increases upon increasing the volume fraction. In order to reduce this contribution a softening of the stiffness of the macromolecules occurs because for a flexible macromolecule the excluded volume that is not available for the other macromolecules is smaller than the corresponding one of a rigid macromolecule.

Within a self-consistent integral equation theory [32–39] based on a variational method [39] the volume fraction-dependent persistence length $l_p(\phi)$ can be obtained from the self-consistent equation

$$G\left[\left(l_p(\phi), l_p(0)\right] = \int_0^\infty dq\, q^2 \frac{W(q,\phi)}{k_B T} \int_0^L ds_1 \int_0^L ds_2\, (s_1 - s_2)^2 \exp\left(-\frac{q^2 a(s_1 - s_2, \phi)}{6}\right) \right. \tag{10}$$

with

$$\frac{W(q,\phi)}{k_B T} = -\frac{\phi}{V_p} c^2(q,\phi)\left(P(q,\phi) + \frac{\phi}{V_p} h(q,\phi)\right) \qquad (11)$$

and

$$a(s,\phi) = 2l_P(\phi)|s| - 2l_P(\phi)^2(1 - \exp(-|s|/l_P(\phi))). \qquad (12)$$

The functional $G[l_p(\phi),l_p(0)]$ is discussed in detail in reference [39] and a schematic presentation of the medium-induced interaction $W(q,\phi)$ between two monomers of a polymer due concentration fluctuations of the surrounding polymers is given in Fig. 1 of reference [33]. Although the Fourier transform of the sum of the intramolecular two-point correlation functions $P(q,\phi)$ and the particle-averaged total correlation function $h(q,\phi)$ of polymer brush solutions and polyelectrolyte solutions differ from each other, the persistence length may exhibit a similar volume fraction dependence due to the fact that the term on the right-hand side of Eq. 10 represents an integrated quantity. We have confirmed this hypothesis by performing additional numerical calculations for semi-flexible polyelectrolyte chains within the PRISM integral equation theory.

It is worthwhile to mention that in the case of rather rigid polymer brushes or polyelectrolyte chains an isotropic to nematic phase transition occurs upon increasing the volume fraction. In this case the contribution of the intermolecular interactions to the total free energy is reduced due to orientational order while the contribution of the orientational entropy to the total free energy is increased.

Finally we emphasize that our measurements corroborate the softening of the stiffness of polymer brushes due to mutual interactions predicted by Borisov et al. [12]. We have demonstrated that the volume fraction dependence of the radius of gyration R_g (see Eq. 4) is in agreement with scaling considerations for polymer brush solutions [14]. A similar decrease of the radius of gyration with increasing volume fraction has also been measured for flexible polystyrene chains in solution [40] and calculated for neutral polymer chains modeled as pearl necklaces of freely jointed tangent hard spheres [34, 41].

Dynamic properties

In addition to static properties we have investigated dynamic properties of the polymer brushes using dynamic light scattering and depolarized dynamic light scattering. The measured time-dependent DLS intensity autocorrelation function is a single exponential function of time for volume fractions $\phi \leq 0.002$ signaling pure translational diffusion of the polymers. No contributions of internal modes such as rotation, bending, or stretching to the dynamics have been found. Hence, one may describe the experimental data in terms of a decay rate $\Gamma(q)$ according to $\Gamma(q)=q^2D$, where D is the translational diffusion coefficient of the polymer in dilute solution. Figure 9 shows the measured decay rate (CONTIN analysis) as a function of q^2 for the volume fraction $\phi = 0.002$. The inset shows the CONTIN plots at 90° scattering angle at various concentrations.

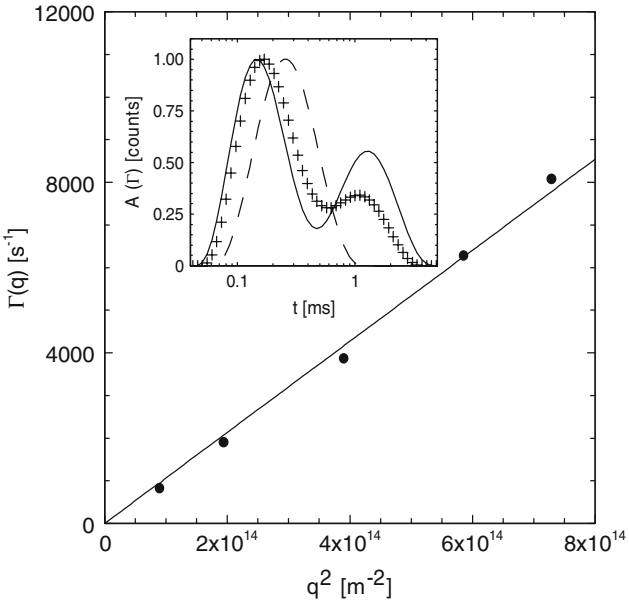

Fig. 9 Measured decay rate $\Gamma(q)=q^2D$ of the time-dependent intensity autocorrelation function of the polymer brush in dilute solution at the volume fraction $\phi=0.002$ as function of the square of the scattering vector q^2 (*symbols*). The resulting translational diffusion coefficient D is given by $D=1.1\cdot10^{-11}$ m^2/s (slope of the *solid line*). *Inset* CONTIN plot at 90° scattering angle for $\phi=0.002$ (*dashed line*), 0.006 (*symbols*), and 0.009 (*solid line*)

Moreover, we have determined the hydrodynamic radius $R_h=39\pm2$ nm from the measured translational diffusion coefficient using the Stokes–Einstein relation $R_h=k_BT/(6\pi\eta D)$, where the temperature T and the viscosity η characterize the solvent. It is instructive to compare the measured hydrodynamic radius with the results for a semiflexible chain model which has been used to interpret quasi-elastic neutron and dynamic light-scattering measurements on various natural and synthetic macromolecules such

Table 1 The experimental normalized diffusion coefficient $D^{(ex)}(\phi)/D(0)$ together with the theoretical calculations $D^{(th)}(\phi)/D(0)$ according to Eq. 13 and using a volume fraction-dependent shape of the polymer brush. An additional measured slow diffusive process is characterized by the normalized diffusion coefficient $D^{(sl)}(\phi)/D(0)$

ϕ	0.006	0.008	0.01
$D^{(ex)}(\phi)/D(0)$	1.42	1.53	1.72
$D^{(th)}(\phi)/D(0)$	1.49	1.64	1.85
$D^{(sl)}(\phi)/D(0)$	0.28	0.24	0.22

as denaturated ovalbumin, DNA, F-actin [42], gellan [43], polystyrene [44], xanthan [45], and worm-like micelles [46]. The numerical evaluation according to [42]

$$\frac{1}{R_h} = 2\left(1 + \frac{\sqrt{3}}{\sqrt{\pi}L}\int_{2R}^{L} ds \frac{L-s}{a(s,\phi)} \exp\left(-\frac{3R^2}{2a(s,\phi)}\right)\right) \quad (13)$$

yields R_h=38.5 nm which is comparable with the experimentally determined value. In the calculations the contour length L=380 nm, the persistence length l_p=17.5 nm, and the radius of the cross-section $R = \sqrt{2}R_c = 7$ nm have been used. Moreover, we have calculated the full time-dependent intensity autocorrelation function and we have found that internal modes do not contribute for the scattering vectors used in the DLS experiments. However, internal modes do contribute for stiffer polymers confirming our findings concerning the stiffness of the polymer brushes. The DDLS intensity signal is too low to measure an intensity autocorrelation function as expected for rather flexible worm-like cylinders in contrast to rigid rods.

Finally, we study dynamic properties of the polymer brushes at higher volume fractions. The time-dependent scattering intensity may be written as

$$I(q,\phi,t) = I(q,\phi,0)\exp(-\Gamma(q,\phi)t) \quad (14)$$

with the decay rate [47]

$$\Gamma(q,\phi) = \frac{k_B T}{4\pi^2\eta}\int_0^\infty dq_1\, q_1^2 \frac{I(q_1,\phi)}{I(q,\phi)}\left(\frac{q_1^2+q^2}{2q_1 q}\log\left|\frac{q_1+q}{q_1-q}\right| - 1\right). \quad (15)$$

The volume fraction-dependent diffusion coefficient $D(\phi)$ can be calculated according to

$$D(\phi) = \lim_{q\to 0}\frac{\Gamma(q,\phi)}{q^2}. \quad (16)$$

This diffusion coefficient increases upon increasing the volume fraction of the cylindrical polymer brushes due to an increasing restoring force for concentration fluctuations as is illustrated in Table 1, where the calculated normalized diffusion coefficient $D^{(th)}(\phi)/D(0)$ is shown together with the corresponding measured diffusion coefficient $D^{(ex)}(\phi)/D(0)$ for three volume fractions.

In the calculations according to Eqs. 15 and 16 the volume fraction-dependent persistence lengths and the corresponding static scattering intensities $I(q,\phi)$ have been used (solid lines in Fig. 7). The deviations between the theoretical and experimental might be due to the fact that the hydrodynamic interaction has been taken into account in terms of the Oseen tensor in order to derive Eq. 15 [47].

Using the Rotne–Prager tensor [48] as a first correction to the Oseen tensor will improve the results. However, we emphasize that using the volume fraction-independent persistence length l_p=17.5 nm and the corresponding static scattering intensities $I(q,\phi)$ as input into Eqs. 15 and 16 does not lead to an agreement with the experimental data. The calculated diffusion coefficients are larger than both the experimental and theoretical values shown in Table 1. In addition we have observed experimentally a slow diffusive process at higher volume fractions $D^{(sl)}(\phi)$ in Table 1 which might be associated with long-range concentration fluctuations. The contribution of the slow mode to the time-dependent intensity autocorrelation function increases upon increasing the volume fraction as it is apparent from the inset of Fig. 9.

Conclusion

We presented the full analysis of a cylindrical polymer brush in the dilute and semi-dilute regime by a combination of small-angle neutron scattering, static and dynamic light scattering. At first, the limit of infinite dilution was established by careful extrapolation to vanishing concentration. The evaluation of the SANS data taken at finite concentration then demonstrated that the persistence length is decreasing from 17.5 nm (infinite dilution) to 5.3 nm at ca. 4 wt.%. This finding is in full agreement with the analysis of the data obtained by dynamic light scattering. The marked decrease of the persistence length with concentration is hence comparable to the decrease of this quantity of linear polyelectrolytes in the same concentration regime.

Acknowledgment Financial support by the Deutsche Forschungsgemeinschaft SFB 481, Bayreuth, is gratefully acknowledged. The authors thanks the Institute Laue-Langevin in Grenoble (France) for providing beamtime at the instrument D11.

References

1. Gerle M, Fischer K, Roos S, Müller AHE, Schmidt M, Sheiko SS, Prokhorova S, Möller M (1999) Macromolecules 32:2629
2. Wang J, Matyjaszewski K (1995) J Am Chem Soc 117:5614
3. Zhang M, Breiner T, Mori H, Müller AHE (2003) Polymer 44:1449
4. Zhang M, Drechsler M, Müller AHE (2004) Chem Mater 16:537
5. Zhang M, Müller AHE (2005) J. Polym. Sci.—Part A: Polym Chem 43:3461
6. Elli S, Ganazzoli F, Timoshenko EG, Kuznetsoy YA, Connolly R (2004) 120:6257
7. Rathgeber S, Pakula T, Wilk A, Matyjaszewski K, Beers KL (2005) J Chem Phys 122:124904
8. Zhang B, Gröhn F, Pedersen JS, Fischer K, Schmidt M (2006) Macromolecules 39:8440

9. Wataoka I, Urakawa H, Kajiwara K, Schmidt M, Wintermantel M (1997) Polymer International 44:365
10. Rathgeber S, Pakula T, Wilk A, Matyjaszewski K, Lee HI, Beers KL (2006) Polymer 47:7318
11. Gunari N, Schmidt M, Janshoff A (2006) Macromolecules 39:2219
12. Borisov OV, Birshtein TM, Zhulina YB (1987) Polym Sci USSR 29:1552
13. Stevens MJ, Kremer K (1993) Phys Rev Lett 71:2228
14. Bolisetty S, Airaud C, Xu Y, Müller AHE, Harnau L, Rosenfeldt S, Lindner P, Ballauff M (2007) Phys Rev E 75:040803
15. Rosenfeldt S, Karpuk E, Lehmann M, Meier H, Lindner P, Harnau L, Ballauff M (2006) Chem Phys Chem 7:2097
16. Rosenfeldt S, Dingenouts N, Ballauff M, Werner N, Vögtle F, Lindner P (2002) Macromolecules 35:8098
17. Guinier A, Fournet G (1955) Small Angle Scattering of X-rays. Wiley, New York
18. Li L, Harnau L, Rosenfeldt S, Ballauff M (2005) Phys Rev E 72: 051504
19. Rosenfeldt S, Dingenouts D, Ballauff M, Lindner P, Likos CN, Werner N, Vögtle F (2002) Macromol Chem Phys 203:1995
20. Harnau L, Rosenfeldt S, Ballauff M (2007) J Chem Phys 127:014901
21. Pedersen J, Schurtenberger P (1996) Macromolecules 29:7602
22. Chandler D, Andersen HC (1972) J Chem Phys 57:1930
23. Monson PA, Morriss GP (1990) Adv Chem Phys 77:451
24. Schweizer KS, Curro JG (1987) Phys Rev Lett 58:246
25. Harnau L, Reineker P (2000) J Chem Phys 112:437
26. Harnau L, Costa D, Hansen JP (2001) Europhys Lett 53:729
27. Weber CHM, Chiche A, Krausch G, Rosenfeldt S, Ballauff M, Harnau L, Schnetmann IG, Tong O, Mecking S (2007) Nano Letters 7:2024
28. Harnau L (2001) J Chem Phys 115:1943
29. Harnau L, Hansen JP (2002) J Chem Phys 116:9051
30. Henzler K, Rosenfeldt S, Wittemann A, Harnau L, Finet S, Narayanan T, Ballauff M (2008) Phys Rev Lett 100:158301
31. Costa D, Hansen JP, Harnau L (2005) Molec Phys 103:1917
32. Shew CY, Yethiraj A (2000) J Chem Phys 113:8841
33. Schweizer KS, Honnell KG, Curro JG (1992) J Chem Phys 96:3211
34. Yethiraj A, Schweizer KS (1992) J Chem Phys. 97:1455
35. Melenkevitz J, Schweizer KS, Curro JG (1993) Macromolecules 26:6190
36. Schweizer KS, Curro JG (1997) Adv Chem Phys 98:1
37. Yethiraj A (1997) Phys Rev Lett 78:3789
38. Shew CY, Yethiraj A (1999) J Chem Phys 110:5437
39. Shew CY, Yethiraj A (1998) J Chem Phys 108:1184
40. Daoud M, Cotton JP, Farnoux B, Jannink G, Sarma G, Benoit H, Duplessix R, Picot C, de Gennes PG (1975) Macromolecules 8:804
41. Yethiraj A, Hall CK (1992) J Chem Phys 96:797
42. Harnau L, Winkler RG, Reineker P (1996) J Chem Phys 104:6355
43. Harnau L, Winkler RG, Reineker P (1997) Macromolecules 30:6974
44. Harnau L, Winkler RG, Reineker P (1998) J Chem Phys 109:5160
45. Harnau L, Winkler RG, Reineker P (1999) Macromolecules 32:5956
46. Berlepsch H, Harnau L, Reineker P (1998) J Phys Chem B 102:7518
47. Doi M, Edwards SF (1986) The Theory of Polymer Dynamics. Clarendon, Oxford
48. Rotne J, Prager S (1969) J Chem Phys 50:4831

Chapter 3.3

Formation of Stable Mesoglobules by Thermosensitive Dendronized Polymers

Sreenath Bolisetty, Christian Schneider, Matthias Ballauff[*]

Physikalische Chemie I, University of Bayreuth, 95440 Bayreuth, Germany

Afang Zhang, Wen Li, A. Dieter Schlüter[*]

Institute of Polymers, Department of Materials, ETH Zürich, Wolfgang-Pauli-Strasse 10, HCI G 525, 8093 Zurich, Switzerland

Manuscript to be submitted

ABSTRACT

We present a study on the formation of stable mesoglobules by a thermosensitive dendronized polymer in aqueous solution. The polymer consists of a poly(methacrylate) backbone (M_n = 0. 34 x 10^6, M_w = 1.1 x 10^6 g/Mol). Onto each repeat unit ethoxy-terminated oligoethyleneoxide (OEO) dendrons of second generation are appended. The collapse of the dendronized chains well as their aggregation with increasing temperature is followed by monitoring the hydrodynamic radius R_h using dynamic light scattering. It is found that for dilute concentrations the size of the mesoglobules at 50° C only weakly depends on concentration. Moreover, no hysteresis of the formation of mesoglobules is found, that is, R_h is solely a function of temperature for both heating and cooling runs. The kinetics of the early stage of mesoglobule formation can be monitored by measurements of R_h as the function of time. It is modeled in terms of diffusion limited colloid aggregation (DLCA). In their final stage, the resulting mesoglobules present stable and well-defined entities. The origin of the stability that prevents further aggregation may be steric stabilization caused by the OEO dendrons located most probably on the surface of the globules.

KEYWORDS; dendron, dendronized polymers, mesoglobule, dynamic light scattering, DLCA

INTRODUCTION

Phase separation of polymers in poor solvents is among the classical subjects of polymer science.[1] Homopolymers dissolved in a poor solvent will undergo phase separation below the theta-temperature leading to the formation of macroscopic phases. In an early stage of this process, the polymer chains will associate and form larger and larger globular structures. The process of association will continue until all globules have been associated to form a macroscopic phase. However, copolymers composed of hydrophilic repeat units together with a certain percentage of hydrophobic units can associate to an intermediate state termed mesoglobule.[2,3] The resulting micelle-like structures have been intensively studied in the last years.[4,5,6,7] It is now well-understood that the more hydrophilic parts will be located preferably at the periphery of the mesoglobule thus providing sufficient steric stabilization. The more hydrophobic parts will be buried inside of the globule thus preventing further aggregation. The formation of mesoglobules can be therefore compared with the folding transition of globular proteins.[8] Given the considerable technological importance of thermoresponsive materials for applications such as sensors, drug delivery and catalysis it was an obvious next step to elucidate the formation of the mesoglobules in more depth. Light scattering[9,10,11], differential scanning calorimetry[12], fluorescence spectroscopy[13,14] and turbidity studies[15] have been successfully used as analytical tools to follow the process of the formation of mesoglobules. The kinetics of the globule formation is fairly well understood in terms of theoretical treatments[16] and by Monte Carlo simulation.[17] Thus, a multi-stage process for mesoglobule formation subdivided into nuclei formation, growth of the nuclei into clusters and cluster-cluster aggregation has been proposed to explain the formation of mesoglobules[16]. Using a stopped flow device and

fluorescence[18], Liu et al. successfully identified the different stages during the formation of mesoglobules as proposed by theory. The influence of temperature on the mesoglobule formation was investigated in these experiments as well.[18,19]

Recently we demonstrated that the thermoresponsive dendronized polymer **PG2** (Figure 1) undergoes a sharp, fast and fully reversible phase transition in aqueous solution at 36 °C.[20] Moreover, it was shown by optical microscopy that this transition leads to the formation of globular structures in a surprisingly narrow size range of 3-4 μm. However, given the techniques used in this study, only the later stage of the mesoglobule formation could be studied. Here we describe the study of the early stage of the coil-to-globule transition of dilute solutions of **PG2**. Using dynamic light scattering (DLS) we demonstrate that the association of the **PG2** in aqueous solution leads to well-defined and stable mesoglobules. The kinetics of the cluster-cluster aggregation resulting in stable mesoglobules are described in terms of the model derived by Wagner and coworkers.[24]

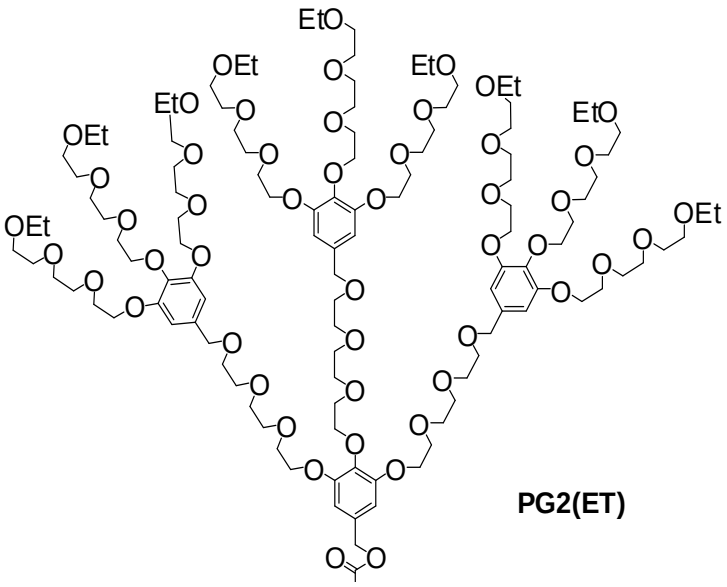

Fig. 1: Chemical structure of ethoxy-terminated dendronized polymethacrylate **PG2.** The polymer's lateral substituent has two consecutive branching points which explains why this polymer is referred to as second generation (G2).

EXPERIMENTAL

Materials: The details of the synthesis of PG2(ET) can be found in Ref.[20] The degree of polymerization of the sample used here was Mn = 0. 34 x 10^6, M_w = 1.1 x 10^6 g/Mol.

Dynamic light scattering: The light scattering experiments were carried out by using the ALV/DLS/SLS-5000 compact goniometer system with multiple tau digital correlator system, equipped with a He-Ne laser (λ = 632.8 nm). The temperature of the sample cell was maintained exactly by using program controlled thermostat within the error of 0.1 °C. The solutions are filtered into dust free optical cells using 0.2 μm nylon syringe filters. The normalized intensity correlation functions were evaluated using the CONTIN 2DP program. The hydrodynamic radius of the thermosensitive dendrons were calculated using the Stokes-Einstein relation at their corresponding temperature.

The time resolved aggregation kinetic measurements were performed at a scattering angle of 90° at regular interval of 10 sec.

Aggregation Kinetics: In order to follow the aggregation in a quantitative manner, we measured the hydrodynamic radius R_h of the aggregates as a function of time. This procedure leads directly to the rate constant of binary collisions between the dissolved polymers if the concentration is low enough.[21] Thus, Borkovec and coworkers were able to study the rate of duplet formation of latex particles with great precision.[22,23] However, we found that the process of aggregation is much to fast for the present system to be able to attain the regime in which aggregation has not proceeded much beyond the stage of dimerization. Hence, we use the approach devised by Wagner and coworkers[24] which is valid at later time as well. It is based on earlier work by Lin and colleagues that considers the aggregation of spherical colloids in dilute suspension.[25,26,27] In short, two limiting cases must be considered: In the Diffusion Limited Colloid Aggregation (DLCA) the particles do not repel each other. They stick to each other once they touch, that is, theory assumes that no disaggregation will occur. In the Reaction-Limited Colloidal Aggregation (RLCA) the particles have a weak but finite repulsive interaction that may be overcome by Brownian motion. In both cases, the aggregates have a fractal structure characterized by a fractal dimension d_f of the aggregates. For DLCA d_f equals 1.86 whereas d_f = 2.1 results for the RLCA regime.[26] The number of particles in an aggregate N is related to the radius of gyration R_g of the aggregates and single particle radius as:[24]

$$N = (R_g / a)^{d_f} \tag{1}$$

In case of DLCA, Wagner et al. have shown that for long aggregation times ($t/t_p >> 1$) we have[24]

$$(R_g / a) = (1 + t/t_p)^{1/d_f} \approx (t/t_p)^{1/d_f} \quad . \tag{2}$$

Here, t_p is the Brownian aggregation time and d_f is the fractal dimension of the aggregate. The relationship between the radius of gyration and the hydrodynamic radius in case of DLCA can be calculated[28] and eq. 2 leads to[24]

$$\frac{R_h(t)}{R_{h,0}} \approx 1.129 \left(\frac{t}{t_p} \right)^{1/d_f} , \tag{3}$$

whereas $R_h(t)$ is the hydrodynamic radius at time t and $R_{h,0}$ the initial particle hydrodynamic radius at time t = 0. In case of diffusion limited coagulation, von Smoluchowski[29] has shown that the Brownian aggregation time t_p is related to the aggregate number concentration C at time t and the initial particle concentration C_0:

$$\frac{C_0}{C(t)} = 1 + \frac{k_{11}}{2} C_0 t = 1 + \frac{t}{t_p} . \tag{4}$$

The initial particle concentration can be calculated using the particle volume fraction Φ and the initial particle radius a with $C_0 = 3\Phi/4\pi a^3$. In a coagulation experiment, we approximate a as the initial hydrodynamic radius of the particles $R_{h,0}$. Following the arguments of von Smoluchowski, the coagulation rate constant for binary collisions in the DLCA regime results to $k_{11,Sm} = 8k_BT/3\eta$, where k_BT denotes the thermal energy of the particles and η the viscosity of the solvent. Approximating k_{11} in eq. 4 by the von Smoluchowski rate constant $k_{11,Sm}$ and substituting C_0 yields a theoretical Brownian aggregation time for DLCA $t_{p,Sm} = \eta\pi {R_{h,0}}^3/\Phi k_BT$.

The foregoing approach suggests the following experiments: For a given polymer concentration, the analysis of the aggregation can be done by precise measurements of the hydrodynamic radius R_h as the function of time at a given temperature T. In the limit

of DLCA the ratio of $R_h/R_{h,0}$ as the function of time should be given by a power law as stated in equation 3. Therefore we can construct a master curve by reducing the aggregation time t with the Brownian aggregation time t_p.[24] However, as is obvious from eq. 4, t_p is a function of the initial particle concentration C_0. Therefore, we normalize the Brownian aggregation time at each temperature T with its characteristic Brownian aggregation time in the DLCA regime $t_{p,Sm}$. This approach thus yields the dimensionless stability parameter $t_p/t_{p,Sm.}$ for different temperatures. This information leads to a quantitative description of the rate of aggregation in the limit of the DLCA.

RESULTS AND DISCUSSION

Dilute solutions containing 0.016 wt-% of the dendronized polymer **PG2** were analyzed by dynamic light scattering at temperature 25 °C. Figure 2 shows the normalized intensity auto-correlation function measured at a scattering angle of 90°. The hydrodynamic radius was calculated using the Stokes-Einstein relation and the particle size distribution was determined using the CONTIN program. The inset of this figure shows the particle size distribution with an average size of 18 nm. Using the relative width of the peak we estimate the polydispersity of the particles which amounts to 1.2. Figure 2 therefore demonstrates that there is no association of polymer chains at lower temperatures and the aggregation starts from a well-defined solution state, that is, from single molecules.

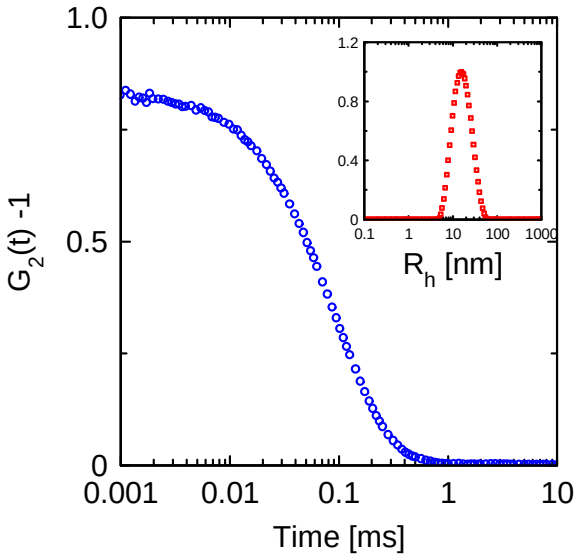

Fig. 2: The intensity auto correlation function measured at 25 °C and 90° angle. The inset shows the particle size distribution calculated by using a CONTIN fit.

Figure 3 displays the increase of the hydrodynamic radius with time if the sample is heated quickly from 25 °C to 35.3 °C (heating rate: 1 °C/min.). There is a strong increase of R_h which points to the rapid formation of aggregates. However, *an Rh level off after ca. 1000 sec and a plateau value is* reached. This situation remains stable for hours. It demonstrates that the polymer under consideration here forms well-defined mesoglobules in the size range of approximately 300 nm in radius.

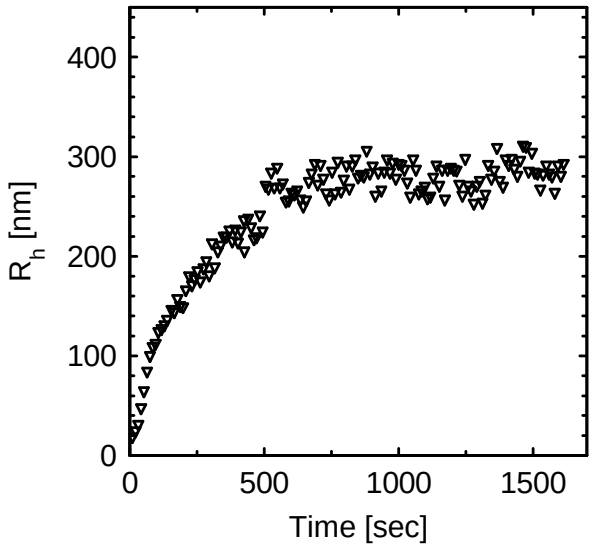

Fig. 3: Hydrodynamic radius of the dendronized polymer after a sudden raise of the temperature from 25 °C to 35.3 °C (heating rate: 1 °C/min) using a polymer solution with a concentration of 0.016 wt-%.

Figure 4 shows the hydrodynamic radius of the dendronized polymer in equilibrated states during several heating and cooling cycles. The solution was first heated slowly with a rate of 0.1 °C/min starting from 24°C until the temperature of 34.9°C was reached. First, the chains shrink as indicated by the small change in the hydrodynamic radius from 18 nm to 16 nm as shown in figure 4a. This is to be expected because the solvent quality deteriorates slowly when going from 24 °C to 34.9°C. However, a further raise of the solution temperature to 35°C results in a sudden increase of the hydrodynamic radius of the polymer particles to approximately 317 nm. This state is found to be stable and may thus be regarded as local equilibrium. The temperature was then raised further in small steps (0.3 °C) which resulted in even larger aggregates. Each state corresponds to a stable mesoglobule at the given temperature. Finally, between 38-40 °C the aggregates reach a hydrodynamic radius of 600 nm, which remains constant

up to 50 °C. Raising the temperature further, the mesoglobules are found to shrink to well-defined, nearly monodisperse aggregates of approximately 450 nm, shown in the inset of fig. 4a.

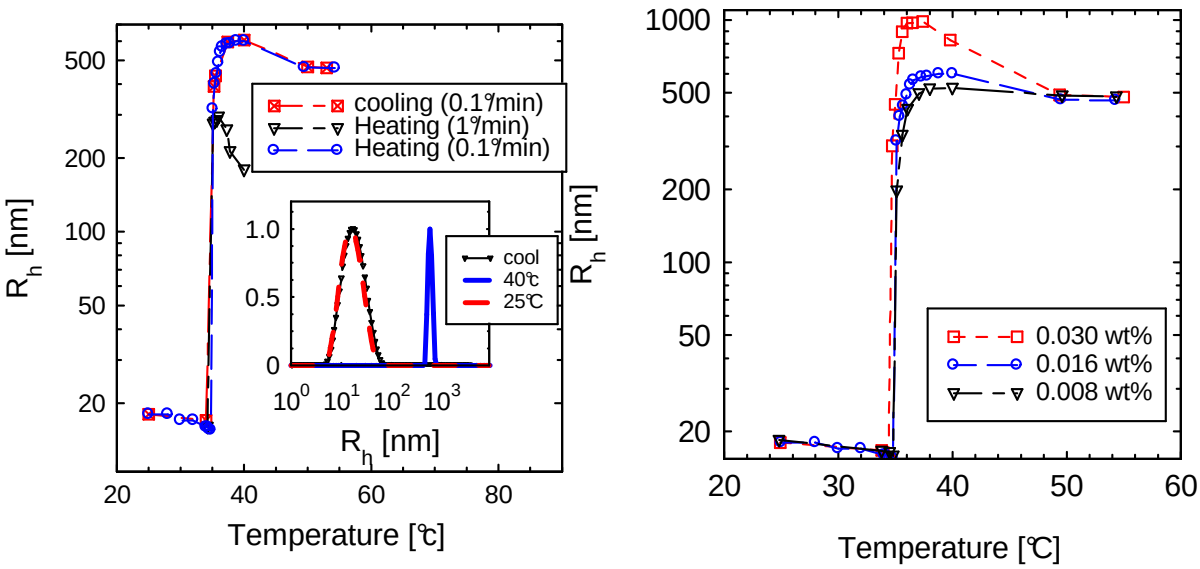

Fig. 4: (a) Hydrodynamic radius R_h of the dendronized polymer **PG2(ET)** as a function of temperature. The solution (0.016 wt-%) was heated from 20 °C to the temperature indicated in the graph. The hydrodynamic radii were measured after equilibrium temperature had been reached at the given temperature. Heating and cooling was done using rates of 0.1 °C/min and 1 °C/min, respectively. The inset shows the corresponding particles size distribution at the heating and cooling rate of 0.1 °C/min calculated from CONTIN fits at 25 °C and 40 °C and again at 25 °C after cooling to the respective temperature. (b) Change of hydrodynamic radius with temperature at three different polymer concentrations.

The cooling is performed in the same way: we decrease the temperature at a rate of 0.1°C/min. to the given temperature and then keep it constant until we reach a stable state of the aggregates. The cooling process was stopped at the same temperatures adjusted in the heating process before. In this way the measured hydrodynamic radii R_h obtained for heating and cooling could directly be compared. Here we find that R_h hardly depends on the process in which the temperature was reached. The heating/cooling cycle was repeated several times leading always to the same results. We also performed the heating experiment by using a higher heating rate of 1 °C/min. The triangles in figure 4a indicate that again well-defined aggregates were formed, size of which, however, was smaller than the size obtained at a slower heating rate (0.1 °C/min).

Figure 4 hence demonstrates that there is virtually no hysteresis between the cooling and heating process. This is remarkable since considerable hystereses is commonly observed for other systems. For example, Kujawa et al. found a marked hysteresis for mesoglobules formed by poly(*N*-isopropylacrylamide).[5] Also Cheng et al. studying the association and dissociation of the same polymer in aqueous solution reported similar findings.[7] They explained the hysteresis by assuming additional hydrogen bonds in the dense globule formed upon packing the chains in the globule. Such additional bonds resemble cross-linking points that render the globules more stable against dissociation. The absence of a hysteresis for the present system thus points to the absence of strong hydrogen bonding within the mesoglobule which is in agreement with the polymer's chemical structure lacking any sites capable of hydrogen bond formation.

The apparent lower critical solution temperature (LCST) depends only slightly on concentration. Figure 4b shows the change of the hydrodynamic radius as a function of temperature depending on the concentration of the solution. For more highly

concentrated solutions, increasingly larger aggregates are formed which at approximately 50 °C merge to a common size of approximately 500 nm. The formation of stable mesoglobules of similar sizes seems to be a robust phenomenon that does not depend strongly on concentration.

Figure 5 gives a schematic representation of the association and dissociation of PG2(ET) at different heating and cooling cycles. The chains contract until the LCST of 35 °C is reached, when the formation of mesoglobules starts. The size of the stable mesoglobules depends on the heating rate. At high temperature conditions, we observe mesoglobules which are monodisperse, but somewhat smaller than at lower temperatures. The mesoglobules formed at a slow heating rate (0.1 °C/min) are larger than those at a fast heating rate (1°C). During the cooling cycle the mesoglobules completely dissociate back into individual polymer chains as is evident from Figure 4a.

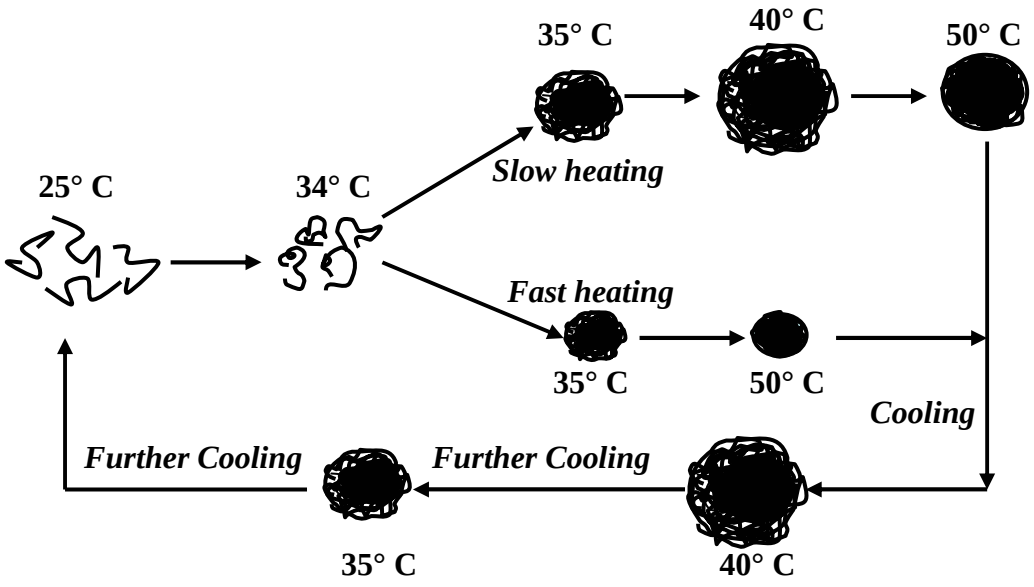

Fig. 5: Schematic representation of temperature dependent PG2(ET) association and dissociation at different heating and cooling cycles using two different heating rates (slow: 0.1 °C/min, fast: 1 °C/min). The PG2(ET) chains shrink up to 34 °C. Then

mesoglobule formation starts at the LCST of 35 °C. During the cooling cycle, the mesoglobules completely disaggregate back into individual polymer chains.

In order to complement the investigation of the equilibrated states of PG2(ET) in solution, we also analyzed the process of mesoglobule formation at different temperatures by time resolved dynamic light scattering measurements.[24] The analysis of the aggregation as the function of temperature was done at a low polymer concentration (0.016 wt-%.). First, the hydrodynamic radius $R_h(t)$ is normalized to its initial value $R_{h,0}$ at time $t = 0$ for different temperatures. Figure 6a displays $R_h(t)/R_{h,0}$ obtained from time-dependent DLS measurements at different temperatures. For the sake of clarity only data for three different temperatures are shown. Obviously, $R_h(t)/R_{h,0}$ is rapidly increasing above the value of 1.38 for dimers.[22,23] In order to apply the analysis of Borkovec and coworkers, aggregation must be restricted to the very early stage of aggregation where mostly dimers are formed, meaning and where $R_h(t)/R_{h,0}$ must remain below 1.38 in the DLS experiments.[22,23] This state cannot be reached for the present system: Lowering the polymer concentration further would certainly lead to a regime where binary collisions prevail. In order to obtain a sufficient scattering intensity, however, the DLS measurements require a certain minimum concentration which is beyond this regime.

Figure 6b focuses on the early time scale. Here we clearly observe that the dependence of $R_h(t)$ on time t differs markedly with increasing temperature. Therefore the rate of aggregate formation differs at different temperatures. For high temperatures the rate of mesoglobule formation is much faster compared to low temperatures. In particular, Fig. 6 demonstrates that the rate of mesoglobule formation does not increase anymore when going from 38 to 40 °C. Hence, the diffusion-limited colloidal

aggregation is reached at 38°C. Below this temperature, not every collision can therefore lead to association. Hence, there must be a finite repulsion between the polymers or the clusters that only vanishes at 38 °C and above. Thus, the observations shown in Fig. 6b clearly demonstrate that there is a transition from the RLCA to the DLCA at 38°C which should be followed by a different fractal dimension d_f (see above). However, the present limits of error do not allow us to analyze a small change of the exponent. Hence, in what is to follow we give a simplified treatment in terms of the RLCA only.

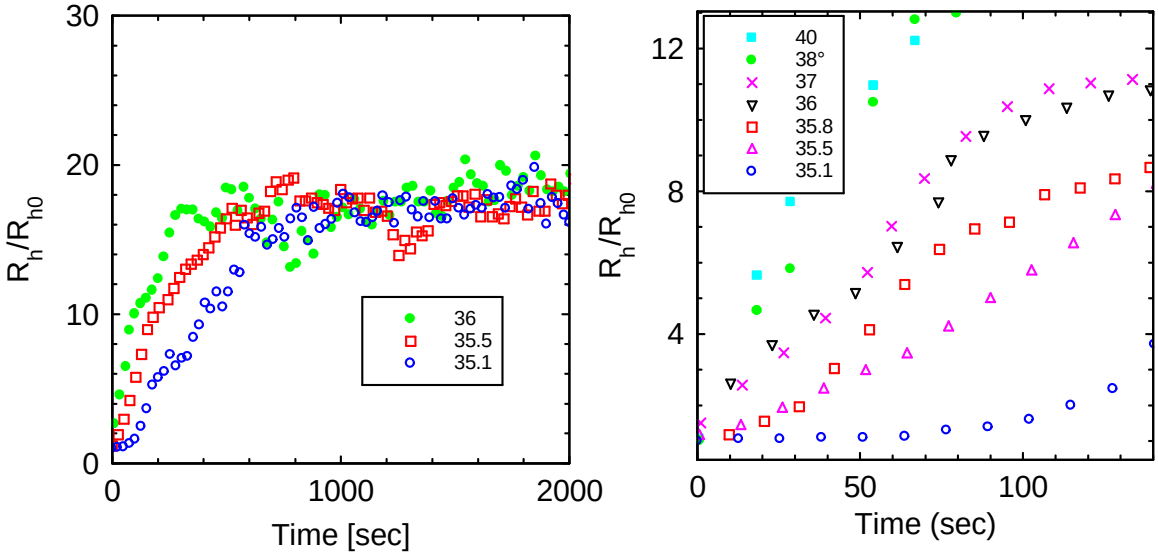

Fig. 6: (a) Change in the hydrodynamic radius normalized with its initial radius as function of the time for the dendronized polymer at different temperature conditions. The concentration of the polymer was 0.016 wt-%. (b) Change in the hydrodynamic radius normalized with its initial radius at the early time scale.

In the approach of Wagner et al.[24] the Brownian aggregation time of the aggregates t_p can be determined out of $R_h(t)/R_{h,0}$ at different temperatures according to eq. 3. Reducing the time t using the characteristic time for Brownian aggregation t_p as a fit parameter yields a master curve for all measurements of $R_h(t)/R_{h,0}$ for a certain time

window as shown in fig. 7a: For $t/t_p \leq 10$ the data points do not fit on the master curve since in this early stage single polymer chains begin to merge into clusters. At $10 \leq t/t_p \leq 100$, all data points measured at different temperatures fall onto one master curve. Obviously, the mesoglobule formation can be described by cluster-cluster aggregation approach in this intermediate stage. The slope of the dashed line in figure 7a is related to the fractal dimension of the aggregates d_f. In our case the slope is compatible with the established value 1.86 for the DLCA. However, the limits of error do not allow a more precise determination of the exponent from the present experimental data.

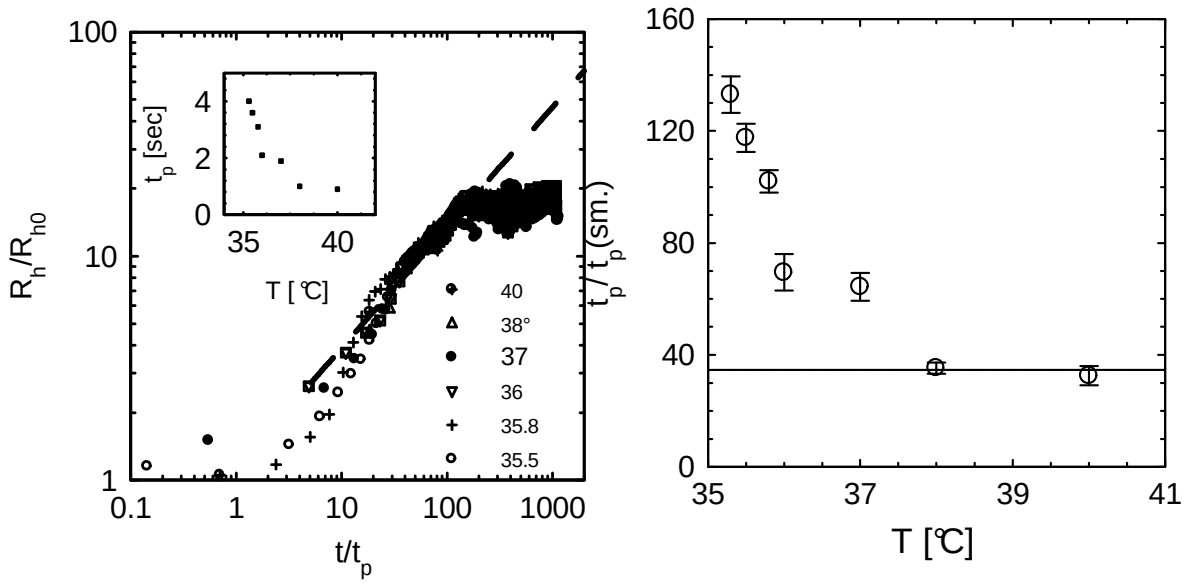

Fig. 7 (a): Master curve of the intermediate stage of aggregation: Here the data presented in fig. 6 are plotted according to eq. 3. The dashed line corresponds to the fractal dimension of the aggregates with d_f = 1.89. The inset of the figure shows the Brownian aggregation time t_p used for the construction of the master curve at different temperatures. (b) The values of t_p normalized with the von Smoluchowski fast coagulation time $t_{p,Sm}$ at the corresponding temperatures using eq 4. Three regimes can be discerned: For temperatures below 35°C, single chains are stable in solution. For temperatures 35°C < T < 38°C there is a cluster-cluster aggregation following the

RLCA. Finally, above 38°C the clusters are instable in the intermediate stage and their aggregation follows the DLCA.

Beyond $t/t_p \geq 100$, however, the growth rate of the aggregates rapidly slows down as the globules become stable. In contrast to the situation encountered in the coagulation of destabilized colloidal particles[22,23,24], aggregation comes to an end if a given size of the mesoglobules is reached. This findings points to an internal structure in which the stabilizing groups are located at the periphery of the globules.

The values of t_p used for the construction of the master curve are shown in the inset of figure 7a. The Brownian aggregation time t_p for the formation of the mesoglobules in this intermediate stage is decreasing with increasing temperature. This clearly indicates that the formation of aggregates at high temperatures is much faster compared to low temperature conditions. Plotting the dimensionless parameter $t_p/t_{p,Smol.}$ as a function of the solution temperature T clearly reveals two coagulation regimes (Fig. 7b): For temperatures $T \geq 38$°C we find the diffusion limited coagulation regime. This indicates that no repulsive forces are left to stabilize the polymer particles and $t_p/t_{p,Sm.}$ stays constant even if the temperature is further increased. For temperatures below 38°C we find that $t_p/t_{p,Sm.}$ is increasing with decreasing temperature. In principle, $t_p/t_{p,Sm}$ should be of the order of unity. However, due to the various approximations this ratio adopts a higher value. As the temperature of the solution is decreasing, the stability of the polymer particles increases until the LCST at 35 °C is reached, where the single chains of the dissolved polymer become thermodynamically stable.

The temperature which separates the fast from the slow aggregation regime may be regarded as the critical aggregation temperature of the dendronized polymers. In case of PG2(ET), we find the critical aggregation temperature at approximately 38 °C. Thus we

have shown that the polymer particles turn from a stable solution to an instable state followed by aggregation in a total temperature range of approximately 3 °C. Moreover, Fig. 7b indicates the transition from the RLCA to the DLCA at 38°C. Hence, in a strict sense (see above), the exponent d_f should be higher when going from 35°C to 38°C. However, as already indicated above the experimental uncertainty of the present experimental data does not allow us to discern between different values of d_f.

CONCLUSION

We investigated the solution behavior of thermosensitive dendronized polymers (OEO) at different temperature conditions using dynamic light scattering. At temperatures higher than the LCST of 35°C, we observed a coil-to-mesoglobule transition of the polymer chains in solution. The resulting mesoglobules are stable and monodisperse. Upon cooling, the mesoglobules completely disassociate back into singular chains without any marked hysteresis. In dilute concentrations the equilibrium size of the mesoglobules is a function of the solution temperature. Also the equilibrium size of the aggregates in high temperature conditions above 50°C weakly depends on the polymer concentration. We showed that the intermediate stage of the formation of mesoglobules can approximately be described by a cluster-cluster aggregation model as devised by Wagner and coworkers.[24] The master curve (see the discussion of eq.(3)) exhibits 3 different stages during the formation of mesoglobules: In a first stage single chains aggregate to form clusters. In the intermediate regime ($5 \leq t/t_p \leq 100$), these cluster aggregate.[24] Finally, aggregation stops when the mesoglobules have reached a certain size. To a certain extend, the formation of mesoglobules is reversible and may be compared to protein folding. Thus, there is a relation of the architecture of the dendronized polymer to its aggregation behavior. We plan to pursue this interesting relation in due course.

ACKNOWLEDGMENT

Financial support by the Deutsche Forschungsgemeinschaft, SFB 481, Bayreuth is gratefully acknowledged.

REFERENCES

[1] Flory, P. J., *Principles of Polymer Chemistry, Cornell University Press*, **1953.**

[2] Siu, M.; Liu, H. Y.; Zhu, X. X.; Wu, C. *Macromolecules* **2003**, *37*, 4989.

[3] Wu, C.; Li, W.; Zhu, X. X., *Macromolecules* **2004**, 37, 4989.

[4] Chen, H.; Zhang, Q.; Li, J.; Ding, Y.; Zhang, G.; Wu, C., *Macromolecules* **2005**, *38*, 8045.

[5] Kujawa, P.; Aseyev, V.; Tenhu, H.; Winnik, F. M. *Macromolecules* **2006**, *39*, 7686.

[6] Kujawa, P.; Tanaka, F.; Winnik, F. M. *Macromolecules* **2006**, *39*, 3048

[7] Cheng, H.; Shen, L.; Wu, C. *Macromolecules* **2006**, *39*, 2325.

[8] Zhang, Q.; Ye, J,.; Nie, Y.; Xie, D.; Song, Q.; Chen, H.; Zhang, Q.; Tang, Y.; Wu, C.; Xie, Z. *Macromolecules* **2008**, *41*, 2228.

[9] Wu, C.; Zhou, S. Q. *Macromolecules* **1995**, *28*, 5388.

[10] Wang, X.; Qiu, X.; Wu. C. *Macromolecules* **1998**, *32*, 2972.

[11] Nakata, M.; Nakumara, Y.; Sasaki, N. *Phys.review. E*, **2007**, *76*, 041805.

[12] Ding, Y. W.; Ye, X.D.; Zhang, G. Z. *Macromolecules*, **2005**, 38, 904.

[13]. Picarra, S.; Gomes, P.T.; Martinho, J. M. G. *Macromolecules*, **2000**, *33*,3947.

[14] Maeda, Y.; Nakamura, T.; Ikeda, I. *Macromolecules*, **2001**, *34*, 1391

[15] Kjoniksen, A.L.; Zhu, K.; Pamies, R.; Nyström,B. *J. Phys. Chem. B.* **2008**, *112*, 3294.

[16] Byrne, A.; Kiernan, P.; Green, D.; Dawson, K.A. *J. Chem. Phys.* **1995**, *102*, 573.

[17] Kuznetsov, Y.A.; Timoshenko; E.G.; *J. Chem. Phys.* **1996**, *104*, 3338.

[18] Xu, J.; Zhu, Z.Y.; Luo, S.Z.; Wu, C.; Liu, S.Y. *Phys. Rev. lett*. **2006**, *96*, 027802.

[19] Chu, B.; Ying, Q.; Macromolecules, 1996, 29,1824.

[20] Li, W.; Zhang, A.; Feldman, K.; Walde, P.; Schlüter, A.D. *Macromolecules*, **2008**, *41*,3659.

[21] Evans, D.F.; Wennerström, H. *The Colloidal Domain*, **1999.**

[22] Holthoff, H.; Egelhaff, S.U.; Borkovec, M.; Schurtenberger, P.; Sticher, H. *Langmuir*, **1996,** *12***,** 5541**.**

[23] Holthoff, H.; Schmitt, A.; Fernandez B.A.; Borkovec, M.; Cabrerizo, V.; Miguel, A.; Schurtenberger, P. Hidalgo, A. R. *J. Colloid. Interface. Sci*. **1997,** *192*, 463.

[24] Hanus, L. H.; Hartzler, R. U.; Wagner, N. J. *Langmuir* **2001**, *17*, 3136.

[25] Lin, M. Y.; Lindsay, H. M.; Weitz, D. A.; Ball, R. C.; Klein, R.; Meakin, P. *Nature* **1989**, *339*, 360.

[26] Lin, M. Y.; Lindsay, H. M.; Weitz, Klein, R.; D. A.; Ball, R. C.; Meakin, P. *J. Phys.: Condens. Matter* **1990**, *2*, 3093.

[27] Lin, M. Y.; Lindsay, H. M.; Weitz, D. A.; Ball, R. C.; Klein, R.; Meakin, P. *Phys. Rev. A* **1990**, *41*, 2005.

[28] Torres, F. E.; Russel, W. B.; Schowalter, W. R. *J. Colloid interface Sci.* **1991**, *142*, 554.

[29] von Smoluchowski, M. *Phys. Z.* **1916**, *17*, 557.

Chapter 3.4

Coupling of Rotational Motion with Shape Fluctuations of Core-shell Microgels Having Tunable Softness

Sreenath Bolisetty [a], Martin Hoffmann [a], Swapna Lekkala [a], Thomas Hellweg [a], Matthias Ballauff [a], and Ludger Harnau[b]

a) Physikalische Chemie I, University of Bayreuth, D-95440 Bayreuth, Germany

b) Max-Planck-Institut f¨ur Metallforschung,
Heisenbergstr. 3, D-70569 Stuttgart, Germany,
and Institut f¨ur Theoretische und Angewandte Physik,
Universit¨at Stuttgart, Pfaffenwaldring 57, D-70569 Stuttgart, Germany

Published in Macromolecules, **2009**, *42*, 1264 .

Coupling of Rotational Motion with Shape Fluctuations of Core-shell Microgels Having Tunable Softness

S. Bolisetty[a], M. Hoffmann[a], S. Lekkala[a], Th. Hellweg[a], M. Ballauff[a], and L. Harnau[b]

[a] *Physikalische Chemie I, University of Bayreuth, D-95440 Bayreuth, Germany*

[b] *Max-Planck-Institut für Metallforschung,*

Heisenbergstr. 3, D-70569 Stuttgart, Germany,

and Institut für Theoretische und Angewandte Physik,

Universität Stuttgart, Pfaffenwaldring 57, D-70569 Stuttgart, Germany

(Dated: December 17, 2008)

Abstract

The influence of shape fluctuations on deformable thermosensitive microgels in aqueous solution is investigated by dynamic light scattering (DLS) and depolarized dynamic light scattering (DDLS). The systems under study consist of a solid core of polystyrene and a thermosensitive shell of cross-linked poly(N-isopropylacrylamide) (PNIPA) without and with embedded palladium nanoparticles. PNIPA is soluble in water, but has a lower critical solution temperature at 32 °C (LCST). Below the LCST the PNIPA shell is swollen. Here we find that besides translational and rotational diffusion, the particles exhibit additional dynamics resulting from shape fluctuations. This leads to a pronounced apparent increase of the rotational diffusion coefficient. Above the transition temperature the shell collapses and provides a rather tight envelope of the core. In this state the dynamics of the shell is frozen and the core-shell particles behave like hard spheres. A simple physical model is presented to capture and explain the essentials of the coupling of rotational motion and shape fluctuations.

I. INTRODUCTION

In recent years, a lot of research has been focused on the preparation and investigation of "smart" microgels consisting of a thermosensitive network of poly(N-isopropylacrylamide) (PNIPA).[1–7] Major incentives for this research were possible applications in catalysis,[6] photonics[8] or for the fabrication of responsive surface coatings.[9] In particular, core-shell particles consisting of a polystyrene core onto which a thermosensitive network is affixed present well-defined model colloids and exhibit polydispersities below ± 6%.[10–14] Hence, besides their potential for applications these core-shell microgels are interesting model systems for studies of the flow behavior of concentrated colloidal suspensions.[15,16] In this way core-shell microgels have become one of the best-studied class of polymer colloids.

In aqueous media, PNIPA exhibits a lower critical solution temperature (LCST) of about 32 °C.[17–21] Below this temperature the network is swollen by the solvent water whereas water is expelled from the microgel above the lower critical solution temperature. Hence, in the swollen state the PNIPA shell of the core-shell microgels is expected to have a rather soft character. This implies the presence of network breathing modes in this state. Up to now, there is evidence that the rheology of colloidal suspensions is strongly related to the dynamic properties of these often deformable objects. An important example in this context represents the flow of blood, containing deformable erythrocytes. Other important examples are liquid droplets, emulsions, and vesicles. While experimental and theoretical studies have been devoted to the understanding of the dynamics of bending modes,[22–27] the effect of shape fluctuations on the rotational diffusion coefficient of deformable objects has not been investigated yet despite the importance of the rotational degree of freedom for soft materials.[28–31] Possible reasons may be sought in the lack of well-defined monodisperse model systems that can be studied by suitable experimental techniques.

Here we study the translational and rotational motion of thermosensitive core-shell microgel particles by depolarized dynamic light scattering (DDLS).[32,33] The aim of the present work is a better understanding of the coupling of rotational motion and shape fluctuations. Microgels are highly suitable for the present study because these particles have been extensively studied by scattering methods such as small-angle neutron scattering, small-angle X-ray scattering, and light scattering.[6,34–41] It has been demonstrated that metal nanoparticles can be embedded in the network of the shell.[6,42,43] These composite

particles have a high catalytic activity that can be modulated by the volume transition of the network.[6,42] Moreover, recent work has shown that cryogenic transmission electron microscopy (Cryo-TEM) is well suited to study the structure and the shape of these particles in-situ:[44,45] A thin film of the fluid dispersion containing the particles is shock-frozen and subsequently analyzed by transmission electron microscopy (TEM), no staining or any other preparatory step is necessary. Figure 1 shows typical cryo-TEM micrographs of dilute suspensions of such core-shell particles. The core consisting of polystyrene and the shell of cross-linked PNIPA is clearly visible. Figures 1 (a) and (c) display the bare particles at different temperatures while Figure 1 (b) shows a core-shell system where palladium nanoparticles are embedded in the shell.[42,43] The shape of the core-shell microgels shown in Figures 1 (a) and (b) is slightly asymmetric. This asymmetry can be traced back to thermal fluctuations. Therefore, we expect the dynamic properties of the core-shell system to be influenced by the shape fluctuations of the shell.

Depolarized dynamic light scattering (DDLS) is the method of choice for studying the problem at hand since this technique simultaneously probes the translational and rotational diffusion coefficient of optically anisotropic particles.[32,33] DDLS has been applied to a number of anisometric particles in dilute solution.[46–49] In general, spherical particles should not exhibit a signal in DDLS. However, the shape fluctuations of the core-shell microgels that are visible as frozen anisometry in the Cryo-TEM micrographs (see Fig. 1) should lead to an optical anisotropy of sufficient magnitude to give a finite depolarized scattering signal in solution. In addition, even in the absence of these shape fluctuations network inhomogeneities due to an anisotropic distribution of crosslinking points will give rise to an additional contribution in the DDLS intensity autocorrelation function. This is observed indeed. On the other hand, the average shape of the particles is still spherical and rather simple models can still be applied. This conclusion can be derived from the fact that these particles have the phase diagram of hard spheres.[15,16]

The paper is organized as follows: After the section Experimental we first give a brief survey on the theory of DDLS and develop a general scheme for the evaluation of data. In a second step we discuss the intensity autocorrelation functions for the microgels above and below their transition temperature in terms of a slow and a fast relaxation rate, the latter being related to the coupling of shape fluctuations and rotational motion. In the last section

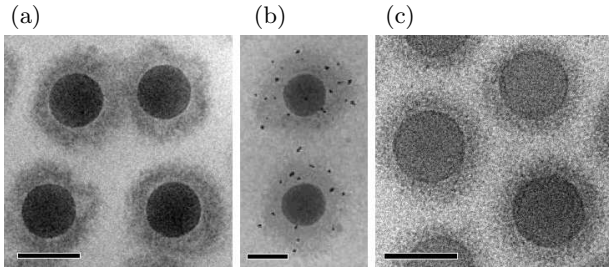

FIG. 1: CryoTEM micrographs of thermosensitive core-shell particles in aqueous solution. The samples were maintained at 25 °C in (a), (b) and at 45 °C in (c) before vitrification. The dark core consists of polystyrene and the corona of PNIPA cross-linked with N, N'-methylenebisacrylamide. In (b) palladium nanoparticles (black dots) are embedded in the PNIPA-shell.[42,43] The scale bars are 100 nm.

a simple statistical-mechanical model is presented that provides a qualitative explanation of the experimental data.

II. EXPERIMENTAL

The synthesis and the characterization of the particles has been described previously.[6,15,44] All solutions (0.05 wt %) were prepared in 0.05 M KCl to reduce electrostatic particle interactions[15,16] and filtered into dust free sample holders using 0.45 μm nylon filters.

All experiments were carried out using the ALV/DLS/SLS-5000 compact goniometer system equipped with a He-Ne laser ($\lambda = 632.8$ nm). The scattering cells (10 mm cylindric cuvettes, Hellma) were immersed in an index matching bath of cis-decaline which does not change the polarization plane of the laser light as e.g. toluene. For the DDLS experiment, the primary beam and the scattered light passed through a Glan-Thomson polarizer with an extinction coefficient better than 10^{-5}. The first polarizer guaranteed that mainly vertically polarized light impinges on the sample and the orientation of a second polarizer (analyzer) was carefully adjusted to a crossed position corresponding to the minimum scattered intensity. All radii a of the particles given in the text were obtained by DLS.

III. INTENSITY AUTOCORRELATION FUNCTION

The theory of dynamic light scattering has been presented in various treatises.[32,33] Hence, we only review the equations necessary for this study. For an incident light wave traveling in the x direction with a polarization vector in the z direction the intensity of the scattered electric field can be written as

$$I_s(\mathbf{q},t) = I_{VV}(\mathbf{q},t) + I_{VH}(\mathbf{q},t)\,, \tag{1}$$

where the absolute value of the scattering vector $\mathbf{q}$ is given by $q = |\mathbf{q}| = (4\pi n/\lambda)\sin(\theta/2)$ in which n is the refractive index of the medium. λ is the incident wavelength and θ is the scattering angle. Pecora[46,50] has given general expressions for $I_{VV}(\mathbf{q},t)$ and $I_{VH}(\mathbf{q},t)$ as

$$I_{VV}(\mathbf{q},t) \sim \int d\mathbf{r}\, d\mathbf{r}'\ \langle \alpha_{zz}(\mathbf{r}+\mathbf{r}',t)\alpha_{zz}(\mathbf{r}',0)\rangle\, e^{i\mathbf{q}\cdot\mathbf{r}}\,, \tag{2}$$

$$I_{VH}(\mathbf{q},t) \sim \int d\mathbf{r}\, d\mathbf{r}'\ \langle \alpha_{zy}(\mathbf{r}+\mathbf{r}',t)\alpha_{zy}(\mathbf{r}',0)\rangle\, e^{i\mathbf{q}\cdot\mathbf{r}}\,, \tag{3}$$

where $\alpha_{zz}(\mathbf{r},t)$ and $\alpha_{zy}(\mathbf{r},t)$ are the zz and zy elements of the fluid polarizability tensor. Experimentally accessible quantities are the intensity autocorrelation functions $g^{(2)}_{VV}(\mathbf{q},t)$ using dynamic light scattering (DLS) and $g^{(2)}_{VH}(\mathbf{q},t)$ using DDLS. For photon counts obeying Gaussian statistics, the intensity autocorrelation functions are related to the electric field autocorrelation functions $g^{(1)}_{VV}(\mathbf{q},t)$ and $g^{(1)}_{VH}(\mathbf{q},t)$ according to

$$g^{(2)}_{VV}(\mathbf{q},t) \;=\; 1 + f_{VV}\left(g^{(1)}_{VV}(\mathbf{q},t)\right)^2\,, \tag{4}$$

$$g^{(2)}_{VH}(\mathbf{q},t) \;=\; 1 + f_{VH}\left(g^{(1)}_{VH}(\mathbf{q},t)\right)^2\,, \tag{5}$$

where f_{VV} and f_{VH} are dependent on the scattering geometry and are usually treated as adjustable parameters. The electric field correlation functions can be calculated for various systems.

The core-shell particles in solution can change their position, orientation, and shape randomly by thermal agitation. For a dilute solution containing noninteracting monodisperse spherical particles of radius a the intensity autocorrelation functions are given by:

$$\sqrt{g^{(2)}_{VV}(q,t)-1} \;=\; e^{-q^2 D_T(a)t}, \tag{6}$$

$$\sqrt{g^{(2)}_{VH}(q,t)-1} \;=\; \frac{e^{-q^2 D_T(a)t}\left(B(q,a)+e^{-6D_R(a,\alpha)t}\right)}{B(q,a)+1}. \tag{7}$$

The translational and rotational diffusion coefficients read

$$D_T(a) = \frac{k_B T}{\eta} \frac{1}{6\pi a}, \tag{8}$$

$$D_R(a, \alpha) = \frac{k_B T}{\eta} \frac{1}{8\pi a^3} \alpha, \tag{9}$$

where the temperature T and viscosity η characterize the solvent and $\alpha = 1$ for hard spheres. The parameter $B(q, a)$ in eq 7 takes into account possible contributions of polarized components to the intensity of the scattered light in the DDLS experiment due to a limited extinction ratio of the polarizer as discussed below.

As a new feature of the present evaluation, we have introduced the parameter α in eq 9. This parameter describes the difference of the real system from the hard sphere model, that is, $\alpha = 1$: If $\alpha = 1$, the rotational diffusion as well as the translational diffusion is fully described by a single parameter, namely the hydrodynamic radius a. If $\alpha \neq 1$, the rotational diffusion is coupled to an additional degree of freedom of the particle. Since $D_R(a, \alpha)$ scales with a^{-3}, possible deviations may hence be determined by precise DDLS-measurements.

IV. RESULTS AND DISCUSSION

A. Microgels above the LCST

We first discuss the microgel particles at temperatures above the volume transition. Here we expect the dynamics of the core-shell particles at $T = 45\,^{\circ}\mathrm{C}$ to be the same as those of hard spheres because the shell is fully collapsed under these conditions and provides a rather tight envelope of the core as is apparent from Figure 1 (c).[44] The tight and nearly homogeneous shell visible above the transition temperature can be traced back to the fact that the particles are synthesized at high temperatures (80 °C).[10] It must be kept in mind that the interaction between the particles becomes attractive above the transition temperature and the particles may coagulate slowly.[15] However, the small concentrations used in the present DDLS experiments prevent this coagulation.

Figure 2 displays examples of measured and calculated intensity autocorrelation functions of the core-shell particles containing palladium nanoparticles at $T = 45\,^{\circ}\mathrm{C}$. In the calculations the model parameters $\eta = 0.601 \times 10^{-3}$ Ns/m^2, $a = 78$ nm, and $\alpha = 1$ have been used. From both the translational and the rotational diffusion coefficient the same hydrodynamic

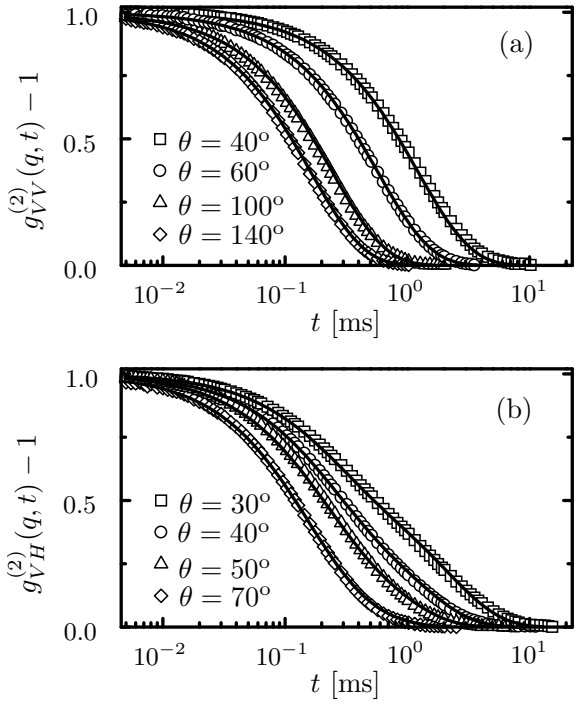

FIG. 2: (a) [(b)] DLS [DDLS] intensity autocorrelation functions $g^{(2)}_{VV}(q,t)$ [$g^{(2)}_{VH}(q,t)$] (symbols) of the core-shell particles containing palladium nanoparticles at $T = 45\,^{o}$C (see Figure 1 (c)) together with the calculated results for monodisperse hard spheres (lines) according to eqs 6 - 9 with $a = 78$ nm and $\alpha = 1$. In (a) and (b) the scattering angle θ increases from right to left.

radius of the microgel particles can be calculated (78 nm). The full agreement between the experimental data and the calculated results demonstrates that the theoretical approach according to eqs 6 - 9 for hard spheres is indeed appropriate for the microgel particles at high temperature. Moreover, it indicates that the residual polydispersity does not disturb the measurements.

B. Microgels below the transition

Figure 3 displays examples of measured and calculated intensity autocorrelation functions of the core-shell particles containing palladium nanoparticles at $T = 25\,^{o}$C. In the calculations the model parameters $\eta = 0.896 \times 10^{-3}$ Ns/m^2, $a = 115$ nm, and $\alpha = 1.6$ have been used. The radius agrees with the radius of the particles as obtained from the CryoTEM micrographs shown in Figures 1 (a) and (b). However, it turned out that a value of $\alpha = 1.6$

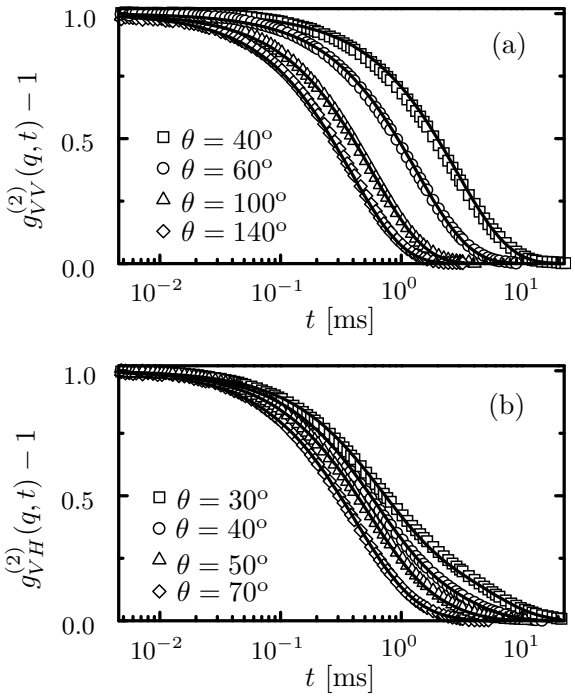

FIG. 3: (a) [(b)] DLS [DDLS] intensity autocorrelation functions $g^{(2)}_{VV}(q,t)$ [$g^{(2)}_{VH}(q,t)$] (symbols) of the core-shell particles containing palladium nanoparticles at $T = 25\,^{\circ}$C (see Figure 1 (b)) together with the theoretical results (lines) as obtained from eqs 6 - 9 with $a = 115$ nm and $\alpha = 1.6$. In (a) and (b) the scattering angle θ increases from right to left.

above unity had to be chosen in order to describe the experimental data. The value $\alpha = 1.6$ found here indicates that the core-shell particles exhibit additional dynamics resulting from the shape fluctuations shown in Figures 1 (a) and (b). The difference between the measured DDLS data and the ones calculated from the hard sphere model increase upon decreasing the temperature. This is illustrated in Table I, where the parameter α is presented for three temperatures.

We have found that embedding nanoparticles in the network of the shell only weakly influences the dynamics of the core-shell particles as is apparent from Fig. 4. In this figure examples of measured DLS and DDLS intensity autocorrelation functions of the core-shell particles without embedded palladium nanoparticles at $T = 25\,^{\circ}$C are shown together with the theoretical results (lines) already used in Fig. 3 that refer to core-shell particles containing palladium nanoparticles. Both measurements refer to the same temperature and the comparison demonstrates that the embedded nanoparticles do not disturb the volume

temperature T	45 °C	25 °C	15 °C
radius a [nm]	78	115	128
α	1	1.6	2.5
$D_R(a,\alpha)$ [s^{-1}]	611	192	168

TABLE I: The radius a of the core-shell particles containing palladium nanoparticles, the parameter α, and the diffusion coefficient $D_R(a,\alpha)$ as obtained from modelling experimental scattering data in terms of eqs 6 - 9. Above the transition temperature $T = 32\,^{\circ}\mathrm{C}$ the dynamics of the core-shell particles is the same as those for hard spheres ($\alpha = 1$) because the shell provides a rather tight envelope of the core (see Figure 1 (c)). Below the transition temperature the particles exhibit additional dynamics resulting from shape fluctuations ($\alpha > 1$ and see Figures 1 (a) and (b)).

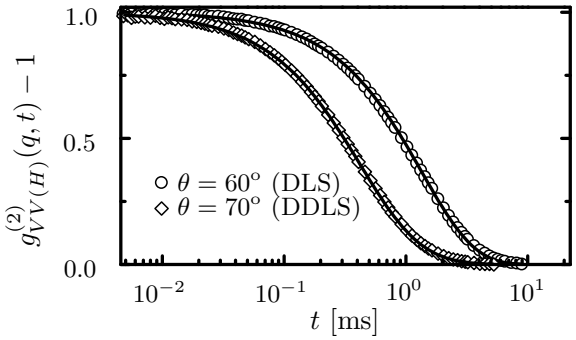

FIG. 4: Measured DLS (circles) and DDLS (diamonds) intensity autocorrelation functions $g^{(2)}_{VV}(q,t)$ and $g^{(2)}_{VH}(q,t)$ of the core-shell particles without embedded palladium nanoparticles at $T = 25\,^{\circ}\mathrm{C}$ (see Figure 1 (a)) together with the same theoretical results (lines) used in Fig. 3 for the core-shell particles containing palladium nanoparticles at $T = 25\,^{\circ}\mathrm{C}$.

transition of the thermosensitive network. No additional crosslinking or influence of the nanoparticles on the polymer chains in the network is seen in full accord with previous findings.[42,43]

C. Slow and fast mode

The autocorrelation function $\sqrt{g_{VH}^{(2)}(q,t)-1}$ in eq 7 is a sum of two discrete exponentially decaying functions, where the slow relaxation mode characterizes translational diffusion while the faster relaxation mode is related to rotational motion and shape fluctuations. Hence, one may describe the experimental data in terms of a slow (Γ_{slow}) and a fast relaxation rate (Γ_{fast}) according to

$$\Gamma_{slow}(q,a) \;=\; q^2 D_T(a)\,, \tag{10}$$

$$\Gamma_{fast}(q,a,\alpha) \;=\; q^2 D_T(a) + 6 D_R(a,\alpha)\,. \tag{11}$$

The slow mode is also characteristic for the single exponential decay of the autocorrelation function $\sqrt{g_{VV}^{(2)}(q,t)-1}$ in eq 6. Figure 5 shows the calculated relaxation rates as a function of q^2. The solid and dotted lines denote $\Gamma_{slow}(q,a)$ and $\Gamma_{fast}(q,a,\alpha=1)$, respectively, where $a = 78$ nm at $T = 45\,^{\circ}$C in (a) and $a = 115$ nm at $T = 25\,^{\circ}$C in (b). The hard sphere model, i.e., $\alpha = 1$, is indeed appropriate for the microgel particles at $T = 45\,^{\circ}$C as discussed above and apparent from a comparison of the calculated results (solid and dotted lines) with the experimental data (symbols) in Figure 5 (a). The pronounced differences between the calculated decay rates $\Gamma_{fast}(q,a,\alpha=1)$ (dotted line) and the experimental data (circles) in Figure 5 (b) are due to the shape fluctuations at $T = 25\,^{\circ}$C. Therefore, the value $\alpha = 1.6$ (see Table I) has been used in computing the dashed line displaying $\Gamma_{fast}(q,a,\alpha=1.6)$.

We emphasize that neither modeling the core-shell particles as hard nonspherical particles such as ellipsoids or dimers nor taking into account the small size polydispersity of the particles or intermolecular interactions lead to an agreement with the experimental data. For example, the corresponding diffusion coefficients of a hard dimer consisting of two identical hard spheres of radius a are given by $D_T^{(dim)}(a) = 0.718\,D_T(a)$ and $D_R^{(dim)}(a) = 0.265\,D_R(a)$, respectively.[51] Hence, the ratio of the rotational diffusion coefficient to the translational diffusion coefficient D_R/D_T is smaller for hard dimers than for hard spheres, while the opposite behavior has been found for the core-shell particles below the transition temperature.

Size polydispersity of the particles leads to a considerably slower decay of the intensity autocorrelation functions[52] in comparison with both the corresponding autocorrelation functions of a monodisperse system and the experimental data. Moreover, D_T and D_R decrease with increasing volume fraction of hard spheres.[49] Hence, this comparison demon-

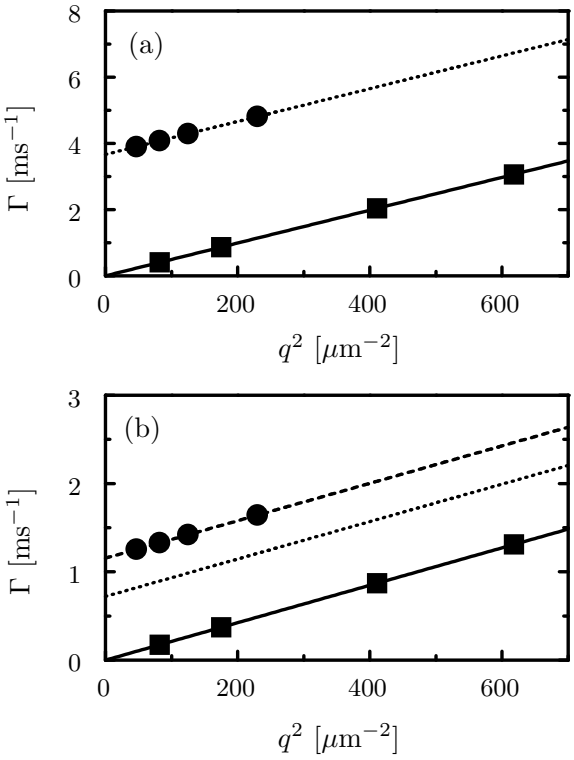

FIG. 5: Decay rates $\Gamma_{slow}(q,a)$ (solid lines), $\Gamma_{fast}(q,a,\alpha=1)$ (dotted lines), and $\Gamma_{fast}(q,a,\alpha=1.6)$ (dashed line) in (b) as calculated according to eqs 10 and 11. The squares and circles denote the slow and fast relaxation rate, respectively, used to describe the intensity autocorrelation functions of the core-shell particles containing palladium nanoparticles (see Figures 2 and 3) at $T = 45\,^{\circ}$C in (a) and $T = 25\,^{\circ}$C in (b). The absolute value of the scattering vector is given by $q = 26.45\,\sin(\theta/2)\,\mu\mathrm{m}^{-1}$, where θ is the scattering angle. Hence, $q^2 = 618\,\mu\mathrm{m}^{-2}$ corresponds to $\theta = 140\,^{\circ}$.

strates clearly that the dynamics of the core-shell particles below the transition temperature cannot be explained in terms of a hard particle model.

Furthermore, the experimental results cannot be explained by using slip boundary conditions (see, e.g., ref[53]) instead of the conventional stick boundary conditions which lead to eqs 8 an 9. The translational diffusion coefficient of a sphere with slip boundary conditions is increased by the factor 3/2 as compared to $D_T(a)$ in eq 8, while the rotational motion of such a sphere does not displace any fluid, implying that $D_R(a) \to \infty$. Both results do not agree with the experimental data.

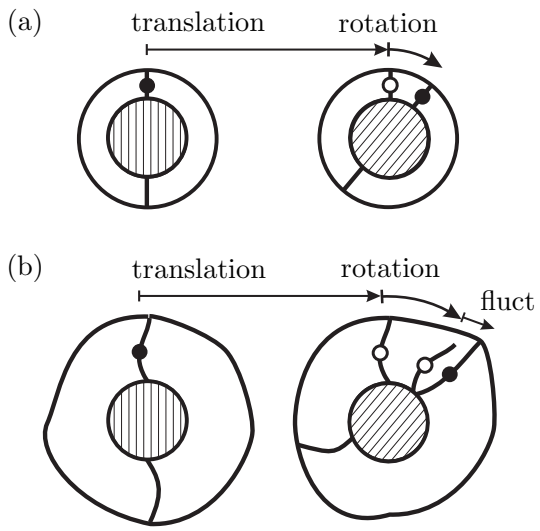

FIG. 6: Illustration of the motion of a scattering unit (filled circle) on a PNIPA chain within the shell of the core-shell particles, where the hatched region marks the core of the particles. The scattering unit exhibits translational motion and rotational motion around the center of mass of the particle in the case of a rather tight shell in (a), while there is an additional fluctuation dynamics (fluct) due to internal degrees of freedom of the PNIPA chain if the shell is rather soft in (b).

D. Coupling of the shape fluctuations with rotational motion

In the following, we present a model that takes into account the influence of shape fluctuations on the rotational motion of the particles. As is illustrated in Figure 6, the motion of a scattering unit (solid circle) on a PNIPA chain within the shell of the particles can be decomposed into various types of modes. If the shell provides a rather tight envelop of the core, the scattering unit will exhibit translational motion and rotational motion around the center of mass of the particle (Figure 6 (a)), that is, the particles will behave as hard spheres without internal degrees of freedom. So above the LCST the DDLS signal will be due to the inhomogeneity of the frozen polymer network. However, there is an additional fluctuation dynamic (fluct; see Figure 6) due to internal degrees of freedom of the PNIPA chain if the shell is rather soft (Figure 6 (b)).

In the following we shall discuss the coupling between the rotational dynamics and the internal modes of the particles that come into play below the transition temperature. The PNIPA chains are linear chain molecules which are described by a chain model for macro-

molecules of variable stiffness[54,55] that has been used earlier to discuss the dynamics of polymers under the influence of various forces (see, e.g., refs[56–59] and references therein). It has been shown that the dynamics of individual PNIPA chains in dilute solution can be interpreted in terms of a chain model of this type.[60] We consider a continuous, differentiable space curve $\mathbf{r}(s,t)$ inscribed into a sphere of radius a, where $s \in [-a,a]$ is a coordinate along the macromolecule and $\mathbf{r}(0,t)$ is the position vector of the center of the sphere (see Figure 6). The potential energy functional of the model reads[54,55]

$$\begin{aligned} U_{pot}[\mathbf{r}(s,t)] = & \\ & \int_{-a}^{a} ds \left[\nu p(s) \left(\frac{\partial \mathbf{r}(s,t)}{\partial s} \right)^2 + \frac{\epsilon}{p(s)} \left(\frac{\partial \mathbf{r}^2(s,t)}{\partial s^2} \right)^2 \right] \\ & + \nu_0 \left[\left(\frac{\partial \mathbf{r}(-a,t)}{\partial s} \right)^2 + \left(\frac{\partial \mathbf{r}(a,t)}{\partial s} \right)^2 \right] , \end{aligned} \tag{12}$$

where $1/p(s)$ is a local correlation length characterizing the stiffness of the space curve and ν_0, ν, ϵ are Lagrange multipliers. In the limit $p(s) \to 0$, the space curve describes a rigid vector inscribed into a hard sphere which exhibits translational and pure rotational Brownian motion. Internal fluctuation of the PNIPA chains are taken into account in terms of $p(s) \neq 0$ for values of s inside the shell. The term with the first derivative in $\mathbf{r}(s,t)$ captures the chain flexibility, i.e., it takes chain entropy into account. The term with the second derivative accounts for bending stiffness and the last two terms are due to the broken symmetry at the chain ends[54]. In order to gain analytical insight we consider the case that the flexibility parameter $p(s)$ does not depend on s, that is, $p(s) = p$. Applying Hamilton's principle we find the Langevin equation of motion along with the boundary conditions for free ends,

$$3\pi\eta \frac{\partial}{\partial t}\mathbf{r}(s,t) - 2\nu p \frac{\partial^2}{\partial s^2}\mathbf{r}(s,t) + \frac{\epsilon}{p}\frac{\partial^4}{\partial s^4}\mathbf{r}(s,t) = \mathbf{f}(s,t)\,, \tag{13}$$

$$\left[2\nu p \frac{\partial}{\partial s}\mathbf{r}(s,t) - \frac{\epsilon}{p}\frac{\partial^3}{\partial s^3}\mathbf{r}(s,t) \right]_{\pm a} = 0\,, \tag{14}$$

$$\left[2\nu_0 \frac{\partial}{\partial s}\mathbf{r}(s,t) + \frac{\epsilon}{p}\frac{\partial^2}{\partial s^2}\mathbf{r}(s,t) \right]_{a} = 0\,, \tag{15}$$

$$\left[2\nu_0 \frac{\partial}{\partial s}\mathbf{r}(s,t) - \frac{\epsilon}{p}\frac{\partial^2}{\partial s^2}\mathbf{r}(s,t) \right]_{-a} = 0\,, \tag{16}$$

where $\mathbf{f}(s,t)$ is the stochastic force. The first term in eq 13 represents the frictional force. Equation 13 is a fourth-order, linear partial differential equation which can be solved by

means of a normal mode analysis. The eigenvalue problem including the boundary conditions is hermitian. Therefore, the eigenfunctions $\psi_l(s)$ are orthogonal and form a complete set. An expansion of the position vector and of the stochastic force in terms of the eigenfunctions and the time-dependent amplitudes $\boldsymbol{\chi}_l(t)$, $\mathbf{f}_l(t)$ according to $\mathbf{r}(s,t) = \sum_{l=0}^{\infty} \psi_l(s)\boldsymbol{\chi}_l(t)$ and $\mathbf{f}(s,t) = \sum_{l=0}^{\infty} \psi_l(s)\mathbf{f}_l(t)$ yields

$$\mathbf{r}(s,t) \;=\; \sum_{l=1}^{\infty} \frac{\psi_l(s)}{3\pi\eta} \int_{-\infty}^{t} dt'\, \mathbf{f}_l(t') e^{-(t-t')/\tau_l} + \frac{\psi_0}{3\pi\eta} \int_{-\infty}^{t} dt'\, \mathbf{f}_0(t')\,. \tag{17}$$

Here $3\pi\eta/\tau_l$ is the eigenvalue corresponding to the eigenfunction $\psi_l(s)$. The eigenfunction $\psi_0 = 1/\sqrt{2a}$ belongs to the eigenvalue $3\pi\eta/\tau_0 = 0$ and corresponds to the translational motion of the center of mass

$$\mathbf{r}_{cm}(t) \;\equiv\; \frac{1}{2a} \int_{-a}^{a} ds\, \mathbf{r}(s,t) = \frac{\psi_0}{3\pi\eta} \int_{-\infty}^{t} dt'\, \mathbf{f}_0(t')\,, \tag{18}$$

because $\int_{-a}^{a} ds\, \psi_l(s) = 0 \;, \forall\; l \neq 0$. Assuming Gaussian distributed random forces $\mathbf{f}(s,t)$ characterized by the thermal average $\langle f_n(s,t)\rangle = 0$ and

$$\langle f_n(s,t) f_m(s',t')\rangle \;=\; 6\pi\eta k_B T \delta_{nm} \delta(s-s')\delta(t-t')\,, \quad n,m \in \{x,y,z\} \tag{19}$$

the translational diffusion coefficient $D_T(a)$ is of the form of eq 8:

$$D_T(a) \;\equiv\; \lim_{t\to\infty} \frac{1}{6t} \left\langle (\mathbf{r}_{cm}(t) - \mathbf{r}_{cm}(0))^2 \right\rangle = \frac{k_B T}{\eta} \frac{1}{6\pi a}\,. \tag{20}$$

Hence $D_T(a)$ is independent of the local correlation length $1/p$ which is valid in the so-called free-draining limit for dense polymer systems such as microgels.[54,56,57] On the other hand, intramolecular hydrodynamic interactions lead to a dependence of $D_T(a)$ on $1/p$ in the case of dilute[52,55,58] or semi-dilute[61,62] polymer solutions.

The first internal mode ($l = 1$) exhibits the largest relaxation time and the rotational-fluctuation diffusion coefficient $\tilde{D}_R(a) = 1/(3\tau_1)$ can be derived as

$$\tilde{D}_R(a) \;=\; \frac{k_B T}{\eta} \frac{\alpha_1^4 + 4\alpha_1^2 p^2}{48\pi p} \tag{21}$$

$$\approx \begin{cases} \frac{k_B T}{\eta} \frac{1}{8\pi a^3} & , \quad pa \lesssim 0.02 \\ \frac{k_B T}{\eta} \frac{\pi p}{48 a^2} & , \quad pa \gtrsim 2 \end{cases}\,, \tag{22}$$

where α_1 follows from the transcendental equation

$$\alpha_1^3 \sin(\alpha_1 a)\, \cosh(\beta_1 a) - \beta_1^3 \cos(\alpha_1 a)\, \sinh(\beta_1 a) - 2p(\alpha_1^2 + \beta_1^2) \cos(\alpha_1 a)\, \cosh(\beta_1 a) = 0 \quad (23)$$

together with $\beta_1^2 - \alpha_1^2 = 4p^2$ and $\nu_0 = 3/(16k_BT)$, $\nu = 3/(8k_BT)$, $\epsilon_0 = 3/(16k_BT)$. The normalized rotational-fluctuation diffusion coefficient $\tilde{D}_R(a)/D_R(a, \alpha = 1)$ is plotted in Figure 7 as function of pa. In the stiff limit $pa \to 0$ the diffusion coefficient $\tilde{D}_R(a)$ agrees exactly with the rotational diffusion coefficient $D_R(a, \alpha = 1)$ of hard spheres. With decreasing stiffness (increasing values of pa) the ratio $\tilde{D}_R(a)/D_R(a, \alpha = 1)$ increases similar to the experimental findings presented in Table I. Hence shape fluctuations do indeed lead to a considerable increase of the diffusion coefficient $\tilde{D}_R(a)$.

Of course, the results shown in Figure 7 can only be considered to be of qualitative significance for the core-shell particles under consideration. However, these results clearly point to the importance of the coupling of rotational and internal modes in the case of soft materials. We emphasize that the core-shell particles maintain on average a spherical shape because $g^{(2)}_{VV}(q,t) - 1$ can be described by a single exponential function according to eq 6. Any permanent deviation from a spherical shape would lead to an additional term in eq 6 due to rotational motion.

Finally, it is worthwhile to compare the results of the present investigation with earlier studies of properties of microgels. A key feature of the static scattering intensity of both uniform microgel particles and core-shell microgel particles below the transition temperature is a strong scattering signal that is due to collective fluctuations of the polymer gel.[10,13,21] It has been demonstrated that the contribution of this internal dynamics to the static scattering intensity vanishes for temperatures above the transition temperature T=32 °C (see Figure 4 in ref[21]). The corresponding collective dynamic fluctuations of the PNIPA network below the LCST have been measured using DLS[60,63] and neutron spin-echo spectroscopy.[64] Despite the different q range of the two methods, the found collective diffusion coefficient of the network has a similar order of magnitude. This most likely indicates that the network motion is always observable independent of the characteristic length scale of the experiment. Hence, the deviations from the hard sphere model observed in the present study by means of DDLS can be considered as a manifestation of these fluctuations. Very recently it has been demonstrated experimentally that the softness of microgel particles has also a pronounced influence on the dynamics in concentrated microgel suspensions.[65]

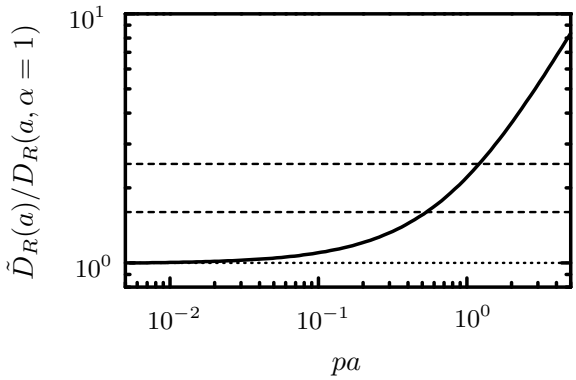

FIG. 7: The reduced rotational-fluctuation diffusion coefficient $\tilde{D}_R(a)/D_R(a,\alpha=1)$ according to eqs 21 and 9 as a function of pa characterizing the stiffness of the model described in the main text. In the stiff limit $pa \to 0$ the rotational-fluctuation diffusion coefficient $\tilde{D}_R(a)$ reduces to the rotational diffusion coefficient $D_R(a,\alpha=1)$ of hard spheres. The deviations of $\tilde{D}_R(a)/D_R(a,\alpha=1)$ from the value 1 increase with decreasing stiffness, i.e., increasing values of pa, due to additional internal dynamics. The dashed lines mark the values $\alpha = 1.6$ and $\alpha = 2.5$ as obtained from the experimental data at $T = 25\,^{\circ}\mathrm{C}$ and $T = 15\,^{\circ}\mathrm{C}$ (see Table I).

V. CONCLUSION

In conclusion, our findings elucidate an important and interesting interplay between shape fluctuations and rotational motion of deformable objects which profoundly affects their dynamics. The control over the degree of deformations offered by varying the temperature should make the core-shell microgels useful for fundamental studies in statistical physics. We anticipate that the results obtained for the present system is of general importance for a better understanding for more complicated systems related to biophysics as e.g. vesicles.

VI. ACKNOWLEDGMENT

Financial support by the Deutsche Forschungsgemeinschaft, SFB 481, Bayreuth, and by the Schwerpunktprogramm Hydrogele is gratefully acknowledged.

---

[1] Hu, Z.; Chen, Y.; Wang, C.; Zheng, Y.; Li, Y. *Nature* **1998**, 393, 149-152.

[2] Juodkazis, S.; Mukai, N.; Wakaki, R.; Yamaguchi, A.; Matsuo, S.; Misawa, H. *Nature* **2000**, 408, 178-181.

[3] Nayak, S.; Lyon, L. A. *Angew. Chem. Int. Ed.* **2005**, 44, 7686-7708.

[4] Dong, L.; Agarwal, A. K.; Beebe, D. J.; Jiang, H. *Nature* **2006**, 442, 551-554.

[5] Chu, L.-Y.; Kim, J.-W.; Shah, R. K.; Weitz, D. A. *Adv. Funct. Mater.* **2007**, 17, 3499-3504.

[6] Ballauff, M.; Lu, Y. *Polymer* **2007**, 48, 1815-1823.

[7] Contreras-Cáceres, R.; Sánchez-Iglesia, A.; Karg, M.; Pastoriza-Santos, I.; Pérez-Juste, J.; Pacifico, J.; Hellweg, Th.; Fernández-Barbero, A.; Liz-Marzán, L. M. *Advanced Mater.* **2008**, 20, 1666-1670.

[8] Karg, M.; Pastoriza-Santos, I.; Pérez-Juste, J.; Hellweg, Th.; Liz-Marzán, L. M. *Small*, **2007**, 3, 1222-1229.

[9] Schmidt, S.; Motschmann, H.; Hellweg, Th.; von Klitzing, R. *Polymer* **2008**, 49, 749-756.

[10] Dingenouts, N.; Norhausen, Ch.; Ballauff, M. *Macromolecules* **1998**, 31, 8912-8917.

[11] Duracher, D.; Sauzedde, F.; Elaissari, A.; Perrin, A.; Pichot, C. *Coll. Polym. Sci.*, **1998**, 276, 219-231.

[12] Duracher, D.; Sauzedde, F.; Elaissari, A.; Pichot, C.; Nabzar, K. *Coll. Polym. Sci.*, **1998**, 276, 920-929.

[13] Seelenmeyer, S.; Deike, I.; Rosenfeldt, S.; Norhausen, Ch.; Dingenouts, N.; Ballauff, M.; Narayanan, T.; Lindner, P. *J. Chem. Phys.* **2001**, 114, 10471-10478.

[14] Hellweg, Th.; Dewhurst, C. D.; Eimer, W.; Kratz, K. *Langmuir*, **2004**, 20, 4330-4335.

[15] Crassous, J.; Siebenbürger, M.; Ballauff, M.; Drechsler, M.; Henrich, O.; Fuchs, M. *J. Chem. Phys.* **2006**, 125, 204906-1–11.

[16] Crassous, J.; Siebenbürger, M.; Ballauff, M.; Drechsler, M.; Hajnal, D.; Henrich, O.; Fuchs, M. *J. Chem. Phys.* **2008**, 128, 204902-1–16.

[17] Shibayama, M.; Tanaka, T.; Han, C. C. *J. Chem. Phys.* **1992**, 97, 6829-6841.

[18] Pelton, R. *Adv. Colloid Interf. Sci.* **2000**, 85, 1-33.

[19] Tanaka, T.; Sato, E.; Hirokawa, Y.; Hirotsu, S.; Peetermans, J. *Phys. Rev. Lett.* **1985**, 55, 2455-2458.

[20] Wu, J. Z.; Zhou B.; Hu, Z. B. *Phys. Rev. Lett.* **2003**, 90, 048304-1–4.

[21] Kratz, K.; Hellweg, Th.; Eimer, W. *Polymer* **2001**, 42, 6631-6639.

[22] Huang, J. S.; Milner, S. T.; Farago, B; Richter, D. *Phys. Rev. Lett.* **1987**, 59, 2600-2603.

[23] Farago, B; Richter, D.; Huang, J. S.; Safran, S. A.; Milner, S. T. *Phys. Rev. Lett.* **1990**, 65, 3348-3351.

[24] Gang, H.; Krall, A. H.; Weitz, D. A. *Phys. Rev. Lett.* **1994**, 73, 3435-3438.

[25] Hellweg, Th.; Langevin, D. *Phys. Rev. E* **1998**, 57, 6825-6834.

[26] Kantsler, V; Segre, E.; Steinberg, V. *Phys. Rev. Lett.* **2007**, 99, 178102-1–4.

[27] Turitsyn, K. S.; Vergeles, S. S. *Phys. Rev. Lett.* **2008**, 100, 028103-1–4.

[28] Abkarian, M.; Lartigue, C.; Viallat, A. *Phys. Rev. Lett.* **2002**, 88, 068103-1–4.

[29] Kantsler V.; Steinberg V. *Phys. Rev. Lett.* **2005**, 95, 258101-1–4.

[30] Noguchi H.; Gompper, G. *Phys. Rev. Lett.* **2007**, 98, 128103-1–4.

[31] Lebedev, V. V.; Turitsyn, K. S.; Vergeles, S. S. *Phys. Rev. Lett.* **2007**, 99, 218101-1–4.

[32] Berne, B.; Pecora, R. *Dynamic Light Scattering*, Wiley: New York, 1976.

[33] Schmitz, K. S. *An Introduction to Dynamic Light Scattering by Macromolecules*, Academic Press: London, 1990.

[34] Crowther, H. M.; Saunders, B. R.; Mears, S. J.; Cosgrove, T.; Vincent, B.; King, S. M.; Yu, G. E. *Colloids Surf. A.*, **1999**, 152, 327-333.

[35] Wu, J. Z.; Huang, G.; Hu, Z. *Macromolecules* **2003**, 36, 440-448.

[36] Berndt, I.; Richtering, W. *Macromolecules* **2003**, 36, 8780-8785.

[37] Stieger, M.; Richtering, W.; Pedersen, J. S.; Linder., P. *J. Chem. Phys.* **2004**, 120, 6197-6206.

[38] Mason, T. G.; Lin, M. Y. *Phys. Rev. E* **2005**, 71, 040801-1-4.

[39] Berndt, I.; Pedersen, J. S.; Linder, P.; Richtering, W. *Langmuir* **2006**, 22, 459-468.

[40] Berndt, I.; Pedersen, J. S.; Richtering, W. *Ang. Chem. Int. Ed.* **2006**, 45, 1737-1741.

[41] Zhao, X.; Hong, W.; Suo, Z; *Appl. Phys. Lett.* **2008**, 92, 051904-051907.

[42] Lu, Y.; Mei, Y.; Drechsler, M.; Ballauff, M. *Ang. Chem. Int. Ed* **2006**, 45, 813-816.

[43] Mei, Y.; Lu, Y.; Polzer, F.; Ballauff, M.; Drechsler, M. *Chem. Mater.* **2007**, 19, 1062-1069.

[44] Crassous, J.; Ballauff, M.; Drechsler, M.; Schmidt, J.; Talmon, Y. *Langmuir* **2006**, 22, 2403-2406.

[45] Crassous, J.; Wittemann, A.; Siebenbürger, M.; Schrinner, M.; Drechsler, M.; Ballauff, M. *Colloid Polym. Sci.* **2008**, 286, 805-812.

[46] Pecora R. *J. Chem. Phys.* **1968**, 49, 1036-1043.

[47] Koenderink, G. H.; Philipse, A. P. *Langmuir* **2000**, 16, 5631-5638.

[48] Eimer, W.; Dorfmüller, T. *J. Phys. Chem.* **1992**, 96, 6790-6800.

[49] Degiorgio, V.; Piazza, R.; Corti, M.; Stavans, J. *J. Chem. Soc. Faraday Trans.* **1991**, 87, 431-434.

[50] Pecora R.; Steele W. A. *J. Chem. Phys.* **1965**, 42, 1872-1879.

[51] Carrasco, B; Garcia de la Torre, J. *Biophys. J.* **1999**, 75, 3044-3057.

[52] Harnau, L.; Winkler, R. G.; Reineker, P. *Macromolecules* **1999**, 32, 5956-5960.

[53] Hu, C.-M.; Zwanzig, R. *J. Chem. Phys.* **1974**, 60, 4354-4357.

[54] Harnau, L.; Winkler, R. G.; Reineker, P. *J. Chem. Phys.* **1995**, 102, 7750-7757.

[55] Harnau, L.; Winkler, R. G.; Reineker, P. *J. Chem. Phys.* **1996**, 104, 6355-6368.

[56] Harnau, L.; Winkler, R. G.; Reineker, P. *Europhys. Lett.* **1999**, 45, 488-494.

[57] Harnau, L.; Winkler, R. G.; Reineker, P. *Phys. Rev. Lett.* **1999**, 82, 2408-2408.

[58] Harnau, L.; Reineker, P. *New J. Phys.* **1999**, 1, 3.1-3.6.

[59] Winkler, R. G. *Phys. Rev. Lett.* **2006**, 97, 128301-1–4.

[60] Wu, C.; Zhou, S. *Macromolecules* **1996**, 29, 1574-1578

[61] Harnau, L. *J. Chem. Phys.* **2001**, 115, 1943-1945.

[62] Bolisetty, S.; Airaud, C.; Xu, Y.; Müller, A. H. E.; Harnau, L.; Rosenfeldt, S.; Lindner, P.; Ballauff, M. *Phys. Rev. E* **2007**, 75, 040803(R)-1–4.

[63] Yang, C.; Kizhakkedathu, J. N.; Brooks, D. E.; Jin, F.; Wu, C. *J. Phys. Chem. B* **2004**, 108, 18479-18484.

[64] Hellweg, Th.; Kratz, K.; Pouget, S.; Eimer, W. *Colloids Surf. A.* **2002**, 202, 223-232.

[65] Eckert, T.; Richtering, W. *J. Chem. Phys.* **2008**, 129, 124902-1–6.

VII. GRAPHIC FOR THE TABLE OF CONTENTS

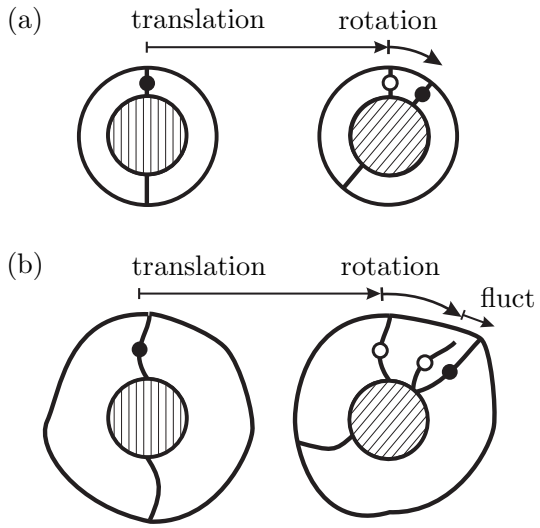

4. Summary

The structure and dynamics of the flexible cylindrical polymer brushes as well as spherical microgel systems are studied by using the scattering techniques. Different flexible cylindrical brushes of neutral charged cylindrical brushes and cylindrical dendronized polymers were investigated. The complete analysis of the cylindrical polymer brush consisting of a poly(2- hydroxyethylmethacrylate) (*p*-HEMA) backbone and poly(*t*-butyl acrylate) (*p*-TBA) side chains in the dilute and semi-dilute regime was investigated by a combination of small-angle neutron scattering, static and dynamic light scattering. The form factor is calculated by extrapolating to the infinite dilution concentration and compared with the theoretical models describe the polymer brush as worm like flexible cylindrical structure having structural parameters of contour length of 380 nm, persistence length of 17.5 nm. The interaction between the cylindrical brushes at semidilute concentration was evaluated by investigating the structure factors modelled with the Polymer reference interaction site model (PRISM). It reveals the softening of the polymer brush due to the interaction with the surrounding polymer brush demonstrating with the decreasing in persistence length from 17.5 nm (infinite dilution) to 5.3 nm at ca. 4 wt- %. The finding result was further clarified with the dynamics of the polymer brush at different concentration regime investigated by dynamic light scattering. Literature also confirms the decrease of this quantity for the linear polyelectrolyte cylindrical brushes at the same concentration regime.

The solution properties of thermoresponsive flexible cylindrical ethoxy-terminated oligoethyleneoxide (OEO) dendrons and their kinetics to formation of mesoglobule aggregates at different temperature conditions were investigated by using the dynamic light scattering and time resolved dynamic light scattering. The collapse transition as well as formation of mesoglobules at high temperature conditions was investigated with time by monitoring the hydrodynamic radius R_h using dynamic light scattering. The kinetics of formation of mesoglobules was approximate by cluster-cluster aggregation model as devised by Wagner and coworkers. The construction of the master curve determines the aggregation time required forming the mesogluboles at different temperature conditions. The master curve also exhibits three different stages during the formation of mesoglobules: 1. single chains aggregate to form clusters, 2. cluster-cluster aggregation, 3. the formation of the single stable mesoglobules.

The solution dynamics especially translational and rotational dynamics of the thermosensitive microgel of poly (N-isopropylacrylamide) (PNIPA) without and with embedded palladium nanoparticles were investigated by using the dynamic light scattering and the depolarized dynamic light scattering. By embedding the palladium nanoparticles to the microgel shell weakly influence the dynamics of the microgel. The interplay of rotational dynamics on shape fluctuations at different temperature conditions was calculated.

Zusammenfassung

Mit Hilfe von verschiedenen Streutechniken wurde die Struktur und die Dynamik von flexiblen zylindrischen Polymerbürsten und sphärischen Mikrogelsystemen studiert. Es wurden ungeladene zylindrische Bürsten und zylindrische dendronisierte Poylmerbürsten untersucht. Die vollständige Charakterisierung mit einer Kombination aus Neutronenkleinwinkelstreuung, statischer und dynamischer Lichtstreuung wurde für die zylindrische Polymerbürsten bestehend aus einem Poly(2-hydroxyethylmethacrylat) (p-HEMA) Rückrat mit Poly(t-butylacrlyat) (p-TBA) Seitenketten im verdünnten und semi-verdünnten Bereich durchgeführt.

Der Formfaktor wurde durch eine Extrapolation zu unendlicher Verdünnung ermittelt und mit theoretischen Modellen verglichen, die die Polymerbürste als flexiblen Zylinder mit einer Konturlänge von 380 nm und einer Persistenzlänge von 17,5 nm beschreiben. Die interpartikuläre Wechselwirkung der Zylinderbürsten im semi-verdünnten Konzentrationsbereich wurde durch eine Modellierung der Strukturfaktoren mit dem Polymer reference interaction site Modell (polymer reference interatction site model, PRISM) bestimmt.

Das Modell zeigt, dass die zunehmende Weichheit der Polymerbürste in der Wechselwirkung mit den umgebeneden Polymerbürsten begründet ist, was sich in der verminderten Persitenzlänge von 5,3 nm bei 4 Gewichtsprozent im Vergleich zu 17,5 nm bei unendlicher Verdünnung bemerkbar macht. Dieses Ergebnis wurde ebenfalls durch die Polymerbürstendynamik in verschiedenen Konzentrationsbereichen mit Hilfe

der Dynamischen Lichtstreuung (DLS) verdeutlicht und in der Literatur für den gleichen Konzentrationsbereich für lineare zylindrische Polyelektrolytbürsten bestätigt.

Die Lösungseigenschaften von thermosensitiven flexiblen zylindrischen ethoxy-terminierten Oligoetylenoxid (OEO) - Dendrons und deren Bildungskinetik zu mesoglobulären Aggregaten bei verschiedenen Temperaturen wurde mittels DLS und zeitaufgelöster DLS untersucht.

Der Übergang zu einem kollabierten Zustand und die Bildung von mesoglobulären Aggregaten bei hohen Temperaturen wurden anhand des hydrodynamischen Radius R_h verfolgt. Die Bildungskinetik der mesoglobulären Aggregate wurde mit dem Cluster-Cluster Aggregationsmodell von Wagner et al. angenähert. Bei Erstellung der Masterkurve wurde die Aggregationszeit für die Bildung der mesoglobulären Aggregate bei verschiedenen Temperaturen erhalten. Die Masterkurver zeigt drei unterschiedliche Stadien der Bildung dieser Aggregate auf: 1. Einzelketten aggregieren zu Clustern. 2. Cluster-Cluster-Aggregation 3. Bildung von separierten stabilen Mesoglubobularen Aggregate.

Die Lösungsdynamik, im sonderen die translative und rotative Dynamik der Kern-Schale-Partikel bestehend aus Polystyrol als Kern und aus einer thermosensitiven Poly(N-isopropylacrylamid) (PNIPA) Mikrogelschale, mit oder ohne eingebettete Palladiumnanopartikel wurde mit Hilfe der DLS und der depolarisierten DLS untersucht. Bei Latices mit in der Mikrogel-Schale eingebetteten Palladiumnanopartikel wurde eine schwache Beeinflussung der Lösungsdynamik der Mikrogel-Schale gemessen. Es wurde das Wechselspiel von Rotationsdynamik und Partikelformfluktuationen bei verschiedenen Temperaturen berechnet.

List of publications

- **"Softening of the Bottle brush polymers by mutual Interaction".**

  Bolisetty, S.; Airaud, C.; Xu, Y.; Müller, A.H.E.; Harnau, L.; Rosenfeldt, S.; Lindner, P.; Ballauff, M.;

  Phys. Rev. E. 2007, *75*, 040803.

- **"Interaction of the Cylindrical Bottlebrush polymers in dilute and semidilute solution**"

  Bolisetty, S.; Rosenfeldt, S.; Rochette, C.; Harnau, L ; Lindner, P.; Xu, Y.; Müller, A.H.E.; Ballauff, M.:

  Colloid and Polymer science **2009**, *287*, 129.

- **"Coupling of the rotational motion and the shape fluctuations of the tunable core-shell microgels"**

  Bolisetty, S.; Hoffmann, M.; Hellweg, T.; Harnau, L.; Ballauff, M.

  Submitted to ***Macromolecules*** **2009**, *42*, 1264.

- **"Water-Soluble Organo-Silica Hybrid nanowires"**

  Yuan, J.; Xu, Y.; Walther, A.; Bolisetty, S.; Schumacher, M.; Schmalz, H.; Ballauff, M.; Muller, A.H.E.;

  Nature materials, 2008, *7*, 679.

- **"pH and Salt Responsive Poly(N,N-dimethylaminoethyl methacrylate) Cylindrical Brushes and their Quaternized Derivatives "**

  Xu, Y.; Bolisetty, S.; Drechsler, M.; Yuan, J.; Ballauff, M.; Müller, A.H.E,; **Polymer**, 2008, *49*, 3957.

- **"Correlation of the counterions to flexible cylindrical bottlebrush macromolecules studied by using the anomalous small angle X-ray scattering"**

  Bolisetty, S.; Rosenfeldt, S.; Xu, Y.; Bösecke, P.; Müller, A.H.E., Ballauff, M.: in preparation

- **"Manipulating cylindrical polyelectrolyte brushes on the nanoscale by counterions Collapse transition to helical structures"**

  Xu, Y.; Bolisetty, S.; Drechsler, M.; Yuan, J.; Ballauff, M.; Müller, A.H.E.; **Softmatter**, 2009, *5*, 379

- **"Formation of the stable Mesoglobules by thermosensitive Dendronized polymers"**

  Bolisetty, S.; Schneider, C.; Zhang, A.; Li, W.; Schlüter, D.; Ballauff, M.;
  in preparation

- **"Switching the Morphologies of cylindrical Polycataion brushes by Ionic and Supramolecular Inclusion Complexs"**

  Xu, Y.; Bolisetty, S.; Ballauff, M.; Müller, A.H.E.;
  J. Am. Chem. Soc. 2009, *131*, 1640

- **"Salt –induced Aggregation of Polyelectrolyte-amphiphilic Dendron Complexes in THF Solutions"**

  Zhang, X.; Bolisetty, S.; Wang, Y.; Lu, Y.; Ballauff, M.; Wang. W.;
  Langmuir 2009, *25*, 2075.

- **"Interparticlespacing for the surface modified gold nanoparticle aggregates"**

  Basu, S.; Pande, S.; Jana, S.; Bolisetty, S. ; Pal, T. ; **Langmuir** , 2008**,** *24***,** 5562**.**

- **"Double Grafted Cylindrical Brushes: Synthesis and Characterization of Poly(lauryl methacrylate) Brushes "**

  Xu, Y; Becker, H; Yuan, J; Burkhardt, M; Zhang, Y; Walther, A; Bolisetty, S; Ballauff, M; Müller, A.H.E.: **Macromol. Chem. Phys.,** 2007, *208*, 1666.

Acknowledgements

This thesis work was accomplished at the Physical chemistry I, University of Bayreuth, Bayreuth, Germany from October 2005 to November 2008. I take the opportunity to thank all those who have helped me in completion of my thesis and I would like to show my gratitude towards them.

First and foremost, I would like to express my sincere thanks to Prof. Dr. Matthias Ballauff for providing an interesting theme for my PhD thesis at Physical Chemistry I department; his valuable great ideas, guidance, constant encouragement, and laboratory are the heart of my dissertation. But what measure exists for the gratitude, apprehensive student posses for a good and patient teacher.

I would like to express my gratitude to Dr. Sabine Rosenfeldt for her immense help in the field of small angle scattering, acquisition of scattering data, interpretation and various scientific discussions. I am highly thankful to Dr. Ludger Harnau for his outstanding contribution of simulation and theoretical analysis.

I would like to thank Youyong Xu, Jiayin Yuan, Dr. Afang Zhang and Dr. Yan Lu for providing me the samples of well synthesized hybrid cylindrical brush polymers, thermosensitive Dendron's and microgels. I am very thankful to Prof. Dr. Axel H. E. Müller, Prof. Thomas Hellweg, University of Bayreuth and Prof. Dieter Schlüter, ETH Zurich for collaboration and contribution of their valuable time. I am also thankful to Dr. Peter Lindner, Dr. Peter Boesecke, who has been of immense help at ILL and ESRF, Grenoble.

My special thanks to all the colleagues, technical and administrative staff of the Physical Chemistry-l for their kind cooperation, assistance, encouragement, successful discussions, technical help and lively working atmosphere during the period of my PhD. Especially I thank my colleagues Miriam Siebenbürger, Jerome Crassous, Alexander Wittemann, Christian Schneider, Marc Schriner, Martin Hoffmann, Christophe Rochette, Frank Polzer, Björn Haupt, Katja Henzler, Yu Mei, Mushtaq Patel and Karlheinz Lauterbach.

I must say many thanks to Mrs. Elisabeth Düngfelder for her great help in many bureaucratic works, without her help and kindness I would have run into many troubles in the sea of bureaucracies.

Many thanks for the financial support from the Deutsche Forschungs Gemeinschaft (DFG), (SFB-481).

I also want to express my gratitude to Indian colleagues: Dr. Mushtaq Patel, Dr. Geeta Sharma, Swapna Lekkala, Dr. John Bosco, Ram Sai Yelamanchili, Dr. Giriraj Amarnath, Shilpa Babar and other Indian friends. With them around life is more homely, easier and enjoyable.

It gives me great pleasure to thank my parents, brother and family for their love, tremendous support and encouragement they have shown in their own way during my long period of career.

Erklärung

Hiermit versichere ich, die vorliegende Arbeit selbstständig verfasst und keine anderen als die von mir angegebenen Quellen und Hilfsmittel benutzt zu haben.

Ferner erkläre ich, dass ich weder an der Universität Bayreuth, noch an einer anderen Hochschule versucht habe, eine Dissertation einzureichen, oder mich einer Promotionsprüfung zu unterziehen.

Sreenath Bolisetty **(23-12-2008)**
Bayreuth